POLYACRYLIC ACID AND POLYVINYLPYRROLIDONE STABILISED TERNARY NANOALLOYS OF PLATINUM GROUP METALS FOR THE ELECTROCHEMICAL PRODUCTION OF HYDROGEN FROM AMMONIA.

UNIVERSITY *of the*
WESTERN CAPE

BY

LERATO YVONNE MOLEFE

B.Sc Chemical Science, B.Sc Honours Chemistry Cum Laude (UWC)

A thesis submitted in partial fulfilment of the requirement for the Degree of Magister Scientiae in Nanoscience in the Department of Chemistry, University of the Western Cape, South Africa.

Supervisor

Professor Emmanuel I. Iwuoha

Co-supervisors

Doctor Edith Antunes and Professor Nazeem Jahed

February, 2016

KEYWORDS

Polyacrylic Acid and Polyvinylpyrrolidone Stabilised Ternary Nanoalloys of Platinum Group Metals for the Electrochemical Production of Hydrogen from Ammonia.

Keywords

Fuel cells

Hydrogen

Ammonia electro-oxidation

Electrocatalyst

Platinum group metals

Nanoalloys

ABSTRACT

Polyacrylic Acid and Polyvinylpyrrolidone Stabilised Ternary Nanoalloys of Platinum Group Metals for the Electrochemical Production of Hydrogen from Ammonia.

L.Y. Molefe

MSc Thesis, Department of Chemistry, University of the Western Cape, February 2016.

The electrochemical oxidation of ammonia has attracted much attention as an efficient green method for application in direct ammonia fuel cells (DAFCs) and the production of high purity hydrogen. However, the insufficient performance and high costs of platinum has hindered the large scale application of ammonia (NH_3) electro-oxidation technologies. Therefore, there is a need for the fabrication of efficient electrocatalysts for NH_3 electro-oxidation with improved activity and lower Pt loading. Owing to their unique catalytic properties, nanoalloys of platinum group metals (PGMs) are being designated as possible electrocatalysts for NH_3 oxidation.

This study presents for the first time a chemical synthesis of unsupported ternary PGM based nanoalloys such as Cu@Pt@Ir with multi-shell structures and Cu-Pt-Ir mixed nanoalloys for electro-catalysis of NH_3 oxidation. The nanoalloys were stabilised with polyvinylpyrrolidone (PVP) as the capping agent. The structural properties of the nanoalloys were studied using ultraviolet-visible (UV-Vis) and fourier transform infra-red (FTIR) spectroscopic techniques. The elemental composition, average particle size and morphology of the materials were evaluated by high resolution transmission electron microscopy (HRTEM) coupled to energy dispersive X-ray (EDX) spectroscopy. High resolution scanning electron microscopy (HRSEM) was used for morphological characterisation. Additionally, scanning auger nanoprobe microscopy (NanoSAM) was employed to provide high performance auger (AES) spectral analysis and auger imaging of complex multi-layered Cu@Pt@Ir nanoalloy surface. X-ray diffraction (XRD) spectroscopy was used to investigate the crystallinity of the nanoalloys. The electrochemistry of the nanoalloy materials was interrogated with cyclic

voltammetry (CV) and square wave voltammetry (SWV). The electrocatalytic activity of novel Cu-Pt-Ir trimetallic nanoalloys for the oxidation of ammonia was tested using CV.

UV-Vis spectroscopy confirmed the complete reduction of the metal precursors to the respective nanoparticles. FTIR spectroscopy confirmed the presence of the PVP polymer as well as formation of a bond between the polymer (PVP) chains and the metal surface for all nanoparticles (NPs). Furthermore, HRTEM confirmed that the small irregular interconnected PVP stabilised Cu@Pt@Ir NPs were about 5 nm in size. The elemental composition of the alloy nanoparticles measured using EDX also confirmed the presence of Cu, Pt and Ir. Cyclic voltammetry indicated that both the GCE|Cu-Pt-Ir NPs and GCE|Cu@Pt@Ir NPs are active electrocatalysts for NH_3 oxidation as witnessed by the formation of a well-defined anodic peak around -0.298 V (vs. Ag/AgCl). Thus the GCE|Cu-Pt-Ir NPs was found to be a suitable electrocatalyst that enhances the kinetics of oxidation of ammonia at reduced overpotential and high peak current in comparison with GCE|Cu@Pt@Ir NPs, GCE|Pt NPs, GCE|Ir NPs and GCE|Cu NPs electrocatalysts. The presence of the crystalline phases in each sample was confirmed by XRD analysis. The surface analysis of Cu@Pt@Ir nanoalloy with AES surveys revealed the presence of Pt, Ir and Cu elements in all probed spots suggesting some mixing between the layers of the nanoalloy. Yet, analysis of nanoalloys by CV and XRD confirmed the presence of Cu-Pt and Pt-Ir solid solutions in the Cu-Pt-Ir and Cu@Pt@Ir nanoalloys respectively.

DECLARATION

I declare that this thesis *"Polyacrylic acid and polyvinylpyrrolidone stabilised ternary nanoalloys of platinum group metals for electrochemical production of hydrogen from ammonia"* is a presentation of my original research work and it has not been submitted for any degree or examination in any other university. Wherever contributions of others are involved, every effort is made to indicate this clearly, with due reference to the literature and acknowledgement of collaborative research and discussions.

The work was done under the guidance of Professor Emmanuel I. Iwuoha, at the University of the Western Cape, South Africa.

Lerato Yvonne Molefe   ………   ……………………..

In my capacity as supervisor of the candidate's thesis, I certify that the above statements are true to the best of my knowledge.

Prof Emmanuel I. Iwuoha …………………………………

Date:

ACKNOWLEDGEMENT

I would like to extend my sincere gratitude and thanks to:

God Almighty for giving me patience and strength to endure all the difficulties and distress encountered through the process of completing this work.

Prof Emmanuel I. Iwuoha for his guidance, positive criticism and allowing me to grow as a researcher. I believe that his wealth of experience and knowledge has steered me on the path to achieve even greater heights.

Many thanks to my co-supervisors: Dr Edith Antunes and Dr Nazeem Jahed for their continuous assistance, encouragement and support.

I appreciate and thank all the SensorLab members and researchers for your input and being the best colleagues ever to date. I also cherish the good moments shared in the lab.

Dr Wafeeq of South African Institute for Advanced materials (SAIAMC) for making time to help with FTIR analysis out of his tight schedule.

I would like to thank Dr Cummings and Mr Adrian (Scanning Electron Microscopy Unit, Department of Physics at University of the Western Cape), for assistance with the HRTEM/SEM. I would also like to acknowledge Dr Liza Coetsee-Hugo and Prof Hendrik Swart at the Physics Department (University of the Free State), for assistance with the NanoSAM.

My thanks also go to my dearest family and friends for all their help, prayers and support throughout my studies. My beloved fiancé, Mr Tokelo Masokela, for his love, support, patience and always encouraging me to believe in myself and achieve more in life.

DEDICATION

I dedicate this thesis to

My loving dad, Mr Mohapi David Molefe for all the sacrifices, giving me the opportunity to pursue my degree, believing in me and inspiring me to achieve more.

&

My caring mom, Mrs Mamatshela Emily Molefe for her never-ending love, motivation and support. throughout the storms of life.

ACADEMIC OUTPUT

The following section lists technology transfer activities (posters, conference) derived from the results obtained from this research work.

Conferences

- Lerato Molefe, Miranda Ndipingwi, Edith Antunes, Nazeem Jahed and Emmanuel Iwuoha, Polyvinylpyrrolidone Stabilised Ternary Platinum Group Metals Nanoalloys for Electrochemical Production of Hydrogen from Ammonia, International Symposium on Electrochemistry under the theme "Materials, Analytical and Physical Electrochemistry Today" (MAPET'15), University of the Western Cape (Bellville, South Africa); 26-28 May 2015. Poster presentation.

- Lerato Molefe, Edith Antunes, Nazeem Jahed and Emmanuel Iwuoha, Design, Characterization and Application of Trimetallic Platinum Group Metal based Electrocatalysts for Ammonia oxidation, Second International Conference on Composites, Biocomposites and Nanocomposites (ICCBN), Durban University of Technology (Durban, South Africa); 28-30 October 2015. Oral presentation.

TABLE OF CONTENTS

x

xi

TABLE OF FIGURES

between PVP and metal ions.

xvi

UNIVERSITY *of the*

WESTERN CAPE

LIST OF TABLES

UNIVERSITY of the
WESTERN CAPE

xix

LIST OF SCHEMES

LIST OF ABBREVIATIONS AND SYMBOLS

I	Current
ΔE_{p}	Difference in peak potentials
E^0	Formal potential
E^{θ}	Standard potential
$E_{\mathrm{p,a}}$	Peak anodic potential
$E_{\mathrm{p,c}}$	Peak cathodic potential
$I_{\mathrm{p,a}}$	Peak anodic current
$I_{\mathrm{p,c}}$	Peak cathodic current
DAFC	Direct Ammonia Fuel Cell
DMFC	Direct Methanol Fuel Cell
AFC	Alkaline Fuel Cell
PEMFC	Polymer Electrolyte Membrane Fuel Cell
PAFC	Phosphoric Acid Fuel Cell
MCFC	Molten Carbonate Fuel Cell
SOFC	Solid Oxide Fuel cell
NanoSAM	Scanning Auger Nanoprobe Microscopy
EDX	Energy Dispersive X-ray
HRTEM	High Resolution Transmission Electron Microscopy
FTIR	Fourier Transform Infra-Red
AES	Auger Electron Spectroscopy
XRD	X-Ray Diffraction
SAED	Selected Area Electron Diffraction
HRSEM	High Resolution Scanning Electron Microscopy
SAM	Scanning Auger Microscopy

CV	Cyclic Voltammetry
SWV	Square Wave Voltammetry
UV-Vis	UltraViolet Visible
GCE	Glassy Carbon Electrode
NPs	Nanoparticles
PVP	Polyvinylpyrrolidone
NMs	Nanomaterials
HNCs	Hybrid nanocrystals
Cu-Pt-Ir NPs	Copper-platinum-iridium nanoparticles
Cu NPs	Copper nanoparticles
Ir NPs	Iridium nanoparticles
Pt NPs	Platinum nanoparticles
PGMs	Platinum Group Metals
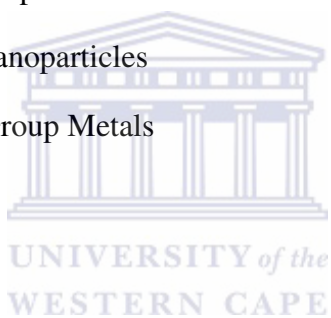
CHAPTER 1

INTRODUCTION

Summary

This chapter presents a brief background to the study which highlights, amongst other items, the importance of a transition from non-renewable to renewable energy sources (hydrogen fuel cells) and the substitution of direct-use hydrogen as a fuel by less hazardous chemical compounds as hydrogen carriers. The emphasis is more pronounced on the application of nanoalloys as electrocatalysts for the oxidation of ammonia to enable direct use of ammonia as a fuel. The problem and its significance, scope and delimitations, the research's aim, objectives and framework, as well as the thesis outline are further discussed.
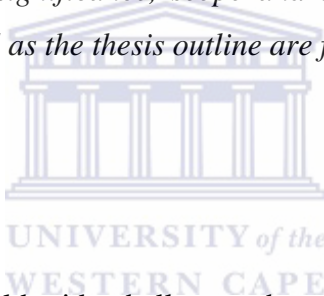
1.1. Background

Some of the most significant world-wide challenges that we are currently facing are energy production and combating climate change. Energy production from the combustion of fossil fuels has severely impacted on the future world economy and environment [1]. Even though the introduction of a hydrogen economy is one of the best strategies to reduce harmful emissions, hydrogen storage is still a barrier for the global distribution of hydrogen fuel cells [2]. Recently, electrochemical energy production has been considered to be an alternative energy source provided that it is cleaner, sustainable and economically viable [1]. Thus, the electro-oxidation of ammonia has attracted much attention owing to its ability to provide clean energy as well as in keeping the environment clean. The only problem holding the application of ammonia electro-oxidation for the evolution of hydrogen back is the inherently slow kinetics of this reaction [2, 3]. Consequently, research has been on going in trying to improve the performance of less expensive electrocatalysts. The usage of low Pt loadings and Pt-free electrocatalysts is encouraged understandably so as to lower the implicated costs. The role of nanotechnology makes it possible to achieve the goals of investigating novel, highly

1

catalytic nanomaterials (NMs) which can reduce, or even completely replace, the use of precious metals.

As previously mentioned, the replacement of existing energy systems in South Africa has been one of the greatest scientific challenges. This is predominantly related to current energy systems such as natural oil from fossil fuels. Non- renewable energy sources such as coal, which South Africa relies on mostly, will soon run out due to over dependence as well as a limited life span because the reserves are finite [4]. In addition, the industrial application of coal is accompanied by the release of toxic inorganic pollutants such as greenhouse gases like carbon dioxide and nitrogen oxides (CO_2 and NO_x where x=1 and 2) into the atmosphere resulting in climate change, causing global warming [4-5]. These will later lead to public health challenges, poor agricultural production and hence severe food crises. Therefore, in order to address these aforementioned problems, scientists have to develop the use of alternative energy sources that favours green, sustainable fuels. Examples of such energy sources include fuel cells, wind turbines and solar technologies (photovoltaic cells).

To recall, a fuel cell is an electrochemical cell that converts chemical energy directly into electrical energy in the presence of hydrogen, producing water and heat as by-products [6-7]. The majority of low-temperature fuel cells are based on new hydrogen fuel cell technologies which have been considered as promising future energy substitutes [6-8]. The hydrogen fuel cell exhibits the ideal properties of high power density and clean oxidation yielding no carbon-containing products [8]. The main obstacle hindering the widespread utilization of hydrogen fuel cells is the expense of hydrogen fuel. Other commonly used fuels in fuel cells are ethanol and methanol. In addition, platinum metal has also been found to be the key catalytic material used in hydrogen fuel cell technology. Since South Africa has more than 75% of the world's platinum reserves [9], development of hydrogen fuel cell technologies could therefore be an encouraging process to meet the energy demand. Furthermore fuel cells are energy efficient, clean and fuel-flexible because they only produce water as the by product and the waste heat released from a fuel cell can be used to provide hot water [6].

The use of hydrogen as an energy carrier could reduce the country's dependence on imported oil and petroleum for daily energy production. However, storage and transportation of light hydrogen is critical because the condensed hydrogen is heavy and, due to its properties,

hydrogen is highly flammable **[8]**. Following that, there has been extensive on-going research into overcoming compression and storage problems of hydrogen by finding alternative hydrogen storage or carrier compounds that can replace the direct use of hydrogen - but still maintaining high performance **[2, 4, 8]**. Thus various chemical compounds have been tested as hydrogen carriers. These include; water, alcohols, hydrocarbons, nitrogen hydrides, hydrazine and ammonia **[8]**. However, the extraction of hydrogen from some of these compounds is not efficient. For instance, the combustion of hydrocarbons and alcohols release polluting gases like carbon dioxide, carbon monoxide and ozone to the atmosphere thus contributing to the environmental pollution; unlike the clean electro-oxidation of ammonia **[2, 8]**. Hence, among these competing candidates, liquid ammonia, nitrogen hydrides and hydrazine have been shown to be the best hydrogen carriers because they can be easily handled and transported. Moreover, since they are nitrogen containing fuels their oxidation commonly yields dinitrogen (N_2) and hydrogen (H_2), thus they can be used as direct fuels for commercial, high performance, clean portable fuel cells **[8]**.

Ammonia is one of the most common pollutants in water bodies due to surface run-off from the agricultural sites. This is because ammonia is largely produced around the globe as it is widely used as fertiliser in agriculture **[10]**. Thus, studying its electrochemical behaviour plays a vital role in both energy and environmental sustainability. Ammonia can be oxidised to produce various products like nitrogen and hydrogen; this being one of the ways in which ammonia can be electrochemically destroyed with no harmful side-effects **[11]**. It contains 1.7 times the amount of hydrogen found in the same volume of liquid hydrogen and boasts a specific energy density 50% higher than liquid hydrogen for a given volume **[10].**

However, the oxidation of ammonia into hydrogen and nitrogen is a very slow process and for this reason, platinum, which is expensive, has been used as a catalyst for the reaction. Consequently new efficient electrocatalysts are required to improve the kinetics of this reaction **[12]**. Therefore, in order to reduce the impact of ammonia on environmental pollution and employ ammonia as a hydrogen carrier, it is very important to study the thermodynamics mechanism and kinetics of its oxidation **[10]**. In order to understand the factors affecting the poisoning of electrode surfaces by intermediates, Gerisher and Mauerer proposed a general mechanism of ammonia oxidation in alkaline solution on a Pt electrode in

3

1970 [13]. The mechanism entails dehydrogenation of absorbed ammonia and formation of nitrogen gas which is outlined below:

$$NH_3\ (aq) \rightarrow NH_{3,ads} \tag{1}$$

$$NH_{3,ads} \underset{\rightarrow}{\rightarrow} NH_{2,ads}\ +\ H^+\ +\ e^- \tag{2}$$

$$NH_{2,ads} \leftrightarrow NH_{ads}\ +\ H^+\ +\ e^- \tag{3}$$

$$NH_{x,ads}\ +\ NH_{y,ads} \rightarrow N_2\ (x\ +\ y)H^+\ +\ (x\ +\ y)e^- \tag{4}$$

$$NH_{ads} \rightarrow N_{ads}\ +\ H^+\ +\ e^- \tag{5}$$
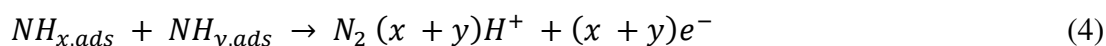
Where x, y = 1 or 2.

From the above mechanism step (1) – (3) is the formation of an active, weakly bound adsorbates NH_x (x =0, 1, or 2) intermediates at the surface of Pt catalyst. Unfortunately, these adsorbates species lead to the deactivation of the platinum during the oxidation of ammonia. This is due to the fact that the adsorption energy of N_{ads} on the Pt electrode surface is too high and it therefore hinders the formation of N_2 as it does not allow the recombination of two N adatoms [13]. Even though platinum has been proven to be the best catalyst for oxidation of ammonia in alkaline media, the poisoning incurred by the N_{ads} and its expense remain unresolved problems in using Pt as an electrode. Many researchers have contributed to developing binary and ternary catalysts that can be used to minimize the aforementioned problems. The carbon-supported monometallic Pd, Pt, Ir as well as bimetallic Pt-M (M= Ir, Pd, SnO_x) nanoalloys has been investigated and their performance was compared to that of pure Pt nanoparticles [13]. Similar studies were further conducted wherein the electrochemical behaviour of PGMs nanoalloys were tested, coupled with highlighting the surface structural sensitivity of Pt towards this reaction [12].

This is where nanotechnology takes part in solving the problem. Nanotechnology is a new, emerging science which entails the design, characterisation, production and application of systems, structures and devices which have one or more dimensions of about 1 - 100 nanometres (nm) [14]. These are widely known as nanomaterials (NMs) [14]. Moreover, the nanomaterials exhibit properties different to their bulk counterparts. Needless to say, the ability to modify NMs by controlling their size and shape at nano-scale has made these

materials to be of great importance for their wide application in various scientific fields. The most fascinating characteristics on the nanoscale include: the small size of the particles, which, owing to prevailing quantum confinement effects, results in increased surface area to volume ratio, further leading to an increase in the dominance of the surface atoms of the nanoparticles over those in its interior **[14]**. This is further substantiated by other previous studies **[12-15]** that wide applications of nanomaterials are due to their unique, enhanced, physicochemical properties which are distinct to their bulk counterparts.

The platinum group metals (PGMs) such as platinum (Pt), palladium (Pd), rhodium (Rh), iridium (Ir), osmium (Os) and ruthenium (Ru) are also convenient to use as electrocatalysts, owing to their nobility and high catalytic activity towards many reactions **[3, 12, 15]**. The most economically significant of the PGMs are Pt, Pd and Rh and these are found in the largest quantities, while Ru, Ir and Os are less prevalent and less in demand **[16]**. They are expensive, however with nanotechnology, scientists are cutting costs by synthesizing core-shell nano-catalysts where the core metal is non-noble, less catalytically active and less expensive while the shell is more expensive (PGMs) and more catalytically active **[14]**.

A great deal of work has been carried out and there is still more on-going research for an effective electrocatalyst of reasonable cost, high activity, minimum ohmic loss and long-term stability which sometimes may be in conflict with each other **[15]**. Since the main target is to reduce the amount of Pt loading, the following developments have been accomplished so far. Alloying Pt with other cheaper metals that exhibit a synergistic effect, increasing the electrochemically active sites and controlling the surface structure (shape, morphology and preferential orientation) of the electrocatalyst, thereby enhancing the mass activity of the Pt-based electrocatalyst, developing well performing Pt-free electrocatalysts and also investigating suitable support materials which improves the performance of the electrocatalyst **[13, 15, 17, 18, 19]**. Therefore in overcoming this obstacle, PGM based nanomaterials such as Pt-Ir, Pt-Rh, Pt-Pd, Pt-Ru and many other mono, binary and ternary metallic nanoparticles found in literature have been used to produce electrocatalysts which will improve the kinetics of the ammonia electrochemical-oxidation reaction **[12-19]**.

This study investigates the integrated functionalities between the modified structure of the outer shell of surface PGM and the stabilizing effect of a subsurface; second noble metal through interaction with a core of non-noble atoms. Moreover, the synthesised novel PGMs

based, triple layered, multi-shell nanostructures will be interrogated as advanced electrocatalysts towards the electrochemical production of hydrogen from ammonia for fuel cell applications.

1.2.   Problem statement

Energy utilisation and production from the combustion of coal has resulted in significant environmental issues (harmful emissions) which have led to the implementation of energy policies for sustainable development in South Africa. One of the major policy mandates, strategies and the corresponding objectives for energy policy of the Department of Science and Technology (DST) was documented on the White Paper on Science and Technology (1996) **[20-21]**. Some of the main objectives of the policy are focused on achieving increased access to affordable energy services, improving energy governance, stimulating economic development, managing energy related environmental impacts and security supply through diversity **[20-22]**. Securing energy supply is the goal that relates mostly to renewable energy sources for a more diverse energy supply. However, the focus of diversification has been more on other sources of renewable energy than hydrogen fuel systems. Thus more focus has to be shifted on hydrogen and fuel cell technologies as clean, sustainable energy suppliers. The main challenge so far with hydrogen and fuel cell technologies is making this technology completely green and clean.

Our country is famous world-wide for its abundance of mining and minerals and hence the mineral beneficiation policy has become one of the major strategies and key forces in advancing PGMs products. The national mineral beneficiation strategy, or value added processing, entails transformation of primary materials specifically from mining processes into advanced final products, which has a high export sales value. This policy involves a variety of activities such as large scale smelting, refining plants, capital and labour intensive processes **[23]**. Each successive stage of processing involved allows the final product to be sold at a higher price than intermediates and starting raw materials, thus adding more value to each level. These local benefits would include economic benefits, through job, wealth and industry creation; the development of appropriate skills and human resources capital; and an improved quality of life for all South Africans. Therefore, the proposed study supports and

6

directly addresses the need for the local utilisation of PGMs in a more value added manner, because the final product produced (PGMs nanoalloy electrocatalyst) exhibits enhanced properties compared to the raw, bulk elemental counterparts, conferring greater value to them. The benefits included have the potential to increase international markets as this study seeks to address the problems associated with large scale application of ammonia electro-oxidation technologies.

The majority of low temperature fuel cells are based on hydrogen fuel, with its ideal properties of high power density and clean oxidation, to yield no carbon containing products. Hence the issues related to compression, storage and distribution of hydrogen needs to be resolved by finding alternative hydrogen carriers that can replace a direct use of hydrogen but still maintaining high performance [6]. Therefore, the proposed study involves the electro-oxidation of ammonia as an on board production of high purity hydrogen in DAFCs. Amongst other conventional candidate chemicals, ammonia stands a good chance of being applied as hydrogen storage medium in addition to direct fuel cell applications because its oxidation is said to be carbon free so it provides clean and sustainable energy which is in compliance with the DST's energy policy. This study further addresses the objectives of the policy by providing affordable energy production. However, the only problem impeding its large scale applications is the insufficient performance and high cost of the electrocatalysts related to the usage of high platinum loadings as its reaction kinetics are so sluggish. The reaction below, according to investigations so far, appears to be fastest in the presence of expensive platinum catalysts [12, 13, 15].

$$2NH_3(g) \rightarrow N_2(g) + 3H_2(g) \qquad\qquad (6)$$

So far, substantial advancements have been made in the area of electrocatalysts designed at the nanoscale level, where the control of structure, size and composition play a crucial role to achieve enhanced activity. Subsequently, the design of a less expensive, but high performing electrocatalysts, is of extreme importance. The ability to modify the size, shape and composition of Pt-based nano crystals can help to lower the Pt loading, providing a large surface area, more active sites and thus improving the catalytic performance [3].

Considerable efforts have been dedicated to developing economically affordable electrocatalysts for ammonia electro-oxidation with enhanced activity and lower Pt loading.

Some of the previous studies were based on bulk noble Pt and Pt–Me (Me = Ni, Ir, Ru, Cu) binary alloys, while others focused on comparing the activities of Pt (100) with Pt (111) surfaces [11-12]. To date, successful replacement of Pt with other low cost electrocatalysts has not yet been achieved, thus there is still a high demand for scientists to develop the best electro-catalyst, since PGMs are known for their high catalytic activity and high resistance to corrosion and oxidation. Hence, in this study, glassy carbon electrodes modified with mono-metallic and novel ternary nanoalloys were used as new electrocatalysts for the oxidation of ammonia.

1.3.   Rationale and motivation

The research interests for this study have been encouraged by a need to speed up the transition to sustainable renewable energy systems in order to keep up with the drastically increasing energy demands directly related to the annual population growth. South Africa is at the stage whereby investment in renewable energies and energy efficiencies is a crucial strategy to eliminate negative social, economic and environmental impacts of non-renewable energy production and consumption [22].

It is well-known that ammonia is one of the more abundantly produced inorganic chemicals in the world and that is also found as a major pollutant in animal agricultural operations and industrial production. Subsequently, development of electro-catalytic techniques for ammonia oxidation has attracted much attention since it addresses both environmental sustainability and alternative energy supplies [12]. Since hydrogen is the main fuel source for power generation in fuel cells, its storage and transportation still remain challenging [4]. Thus ammonia has been found to be an excellent alternative hydrogen carrier. Although it is toxic, liquid ammonia contains 1.7 times more hydrogen than that contained in the same volume of liquid hydrogen [10, 12]. It also boasts a specific energy density (kWhl^{-1}) - 50% higher than liquefied hydrogen for a given volume [12]. However, the electro-oxidation reaction of ammonia to yield hydrogen is very slow, requiring elevated temperatures and purification of products, together with low efficiency in practice [13]. Conversely, this reaction is 100% efficient and produces pure products at ambient temperature in the presence of platinum catalysts [14]. Nonetheless, although platinum has been proven to be the best catalyst for

8

oxidation of ammonia in alkaline media, it is also susceptible to poisoning by N_{ads} [13]. Since bulk platinum catalysts are expensive, nanostructured materials are therefore used for better reaction kinetics [6].

In solving these problems, the research will then focus on the production of novel electro-catalysts in form of nanomaterials with high surface areas. The nanomaterials will consist of ultrasensitive, nanostructured ternary alloys of PGMs, with some incorporating non-noble metals as the core of the nanostructure. The main driving force behind the use of PGMs based electrocatalysts is that South Africa is the world's leading producer of platinum and rhodium and the second largest palladium producer after Russia. It has more than 75% of the world's platinum reserves which is the key catalytic material used in hydrogen fuel cell technology [9]. South Africa can therefore benefit from this technology to reducing the related costs by utilizing locally produced PGMs technologies.

The study was motivated by concerns and questions arising from the use of electrocatalysts with high Pt-loading. Furthermore, this area of study has become very interesting simply by looking at the fact that the cost of bulk Pt is too expensive and its limited supply in other parts of the world hinders its widespread utilization in fuel cells [2]. Consequently, it is advisable to investigate the synergistic effect of multi-shell multimetallic nano structures consisting of non-noble core and noble shell layers in targeting reduced costs coupled with excellent catalytic enhancements.

1.4.   Scope and delimitations

It is advantageous that South Africa is also exploring other energy options and it is intended to reduce the harmful emissions and environmental effects from non-renewable energy sources. For instance Hydrogen South Africa (HySA) aims to demonstrate hydrogen production by splitting water at a pilot scale, using nuclear or solar power as the primary power source. This kind of development will help drive the country in its transition into the use of renewable resources.

 In recent studies, bimetallic catalysts show greater catalytic properties than their monometallic counterparts, thus providing more opportunities to explore a variety of

combinations of metal nanoparticles for the essential enhancement of catalytic activity [10]. The manipulation of structure and compositions of core-shell nanostructures also possess an interesting, highly catalytic class of catalysts [3]. Despite the extensive research work which has been devoted to the electro-oxidation of ammonia, the fabrication of binary and ternary core-shell nanostructures with the nanoporous shell regions so as to enable easy access of the quest species has not been scrutinized enough in the past. Instead, investigating the structural sensitivity of Pt has been done over and over which does not add much new knowledge to the field; besides most of the electrocatalysts investigated was on bulk alloys. Therefore, it is reasonable to value the advantages of the core-shell architectures by enabling the interaction of the guest species with the interlayer of the trimetallic nanoalloy.

This study aims specifically on addressing this problem by making use of a glassy carbon electrode modified with a novel trimetallic core-shell nanoalloy. Such types of nanoalloys are called multi-shell nanoalloys since they consist of more than one shell (core, inner shell and outer shell). The study of ternary nanoalloys are of interest owing to their novelty, as previous efforts have been dedicated to the design of various combinations of binary nanoalloys with very few ternary nanoalloys being investigated. From the studies covered so far, in some cases the ternary nanoalloys show higher catalytic activity than those of the respective mono and binary nanoalloys due to the synergistic effects between the three metals [3, 15, 20].

The nanoalloys will be applied to the electrocatalytic oxidation of ammonia towards the evolution of hydrogen that can be captured for its use in hydrogen fuel cells or in DAFCs. The study is limited to the design of novel polyvinylpyrrolidone stabilised mixed Cu-Pt-Ir and multi-shell Cu@Pt@Ir nanoalloy systems. Here, the non-noble metal will act as the core, while the noble nanoporous PGMs will be present-as the shell layers. This will be followed by their characterisation and application in ammonia oxidation. The study therefore does not cover the application of these electrocatalysts to other reactions or for their use in other fuel cells except for DAFC.

1.5.   The aims and objectives of the research

The emphasis of this thesis is mainly to improve the kinetics of the electrochemical oxidation of ammonia. Specifically, this study aims to examine and enhance the kinetics of electro oxidation of ammonia when carried out in presence of novel PGMs based nanoalloys as electrocatalysts towards hydrogen evolution.

The objectives of this research include;

- To carry out chemical synthesis of novel nanoalloys (Cu@Pt@Ir multi-shell and Cu-Pt-Ir mixed)

- To interrogate the structural, spectroscopic and electrochemical properties of the nanoalloys using techniques such as HRSEM, HRTEM, EDX, SAED, XRD, NanoSAM, UV-Vis, FTIR, CV and SWV.

- To study and evaluate the electro-catalytic effect of glassy carbon electrode modified with the synthesised nanoalloys towards the catalytic oxidation of ammonia.
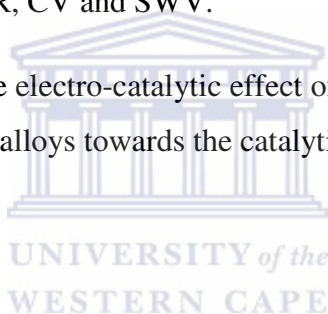
1.6.   Research questions

- Why multi-shell ternary nanoalloys?

- What is the role of non-noble metals as the core structure?

- Which factors affect the formation of core-shell nanoalloys?

- How do you prove successful formation of a nanoalloy structure?

- How can the activity of the electrocatalyst be further improved?

- How do you control the proper formation of nanoalloys?

- How unique or novel is this nanostructure compared to previous studies?

11

1.7.   Research Framework

Based on the study objectives, the research framework is presented on the scheme below.
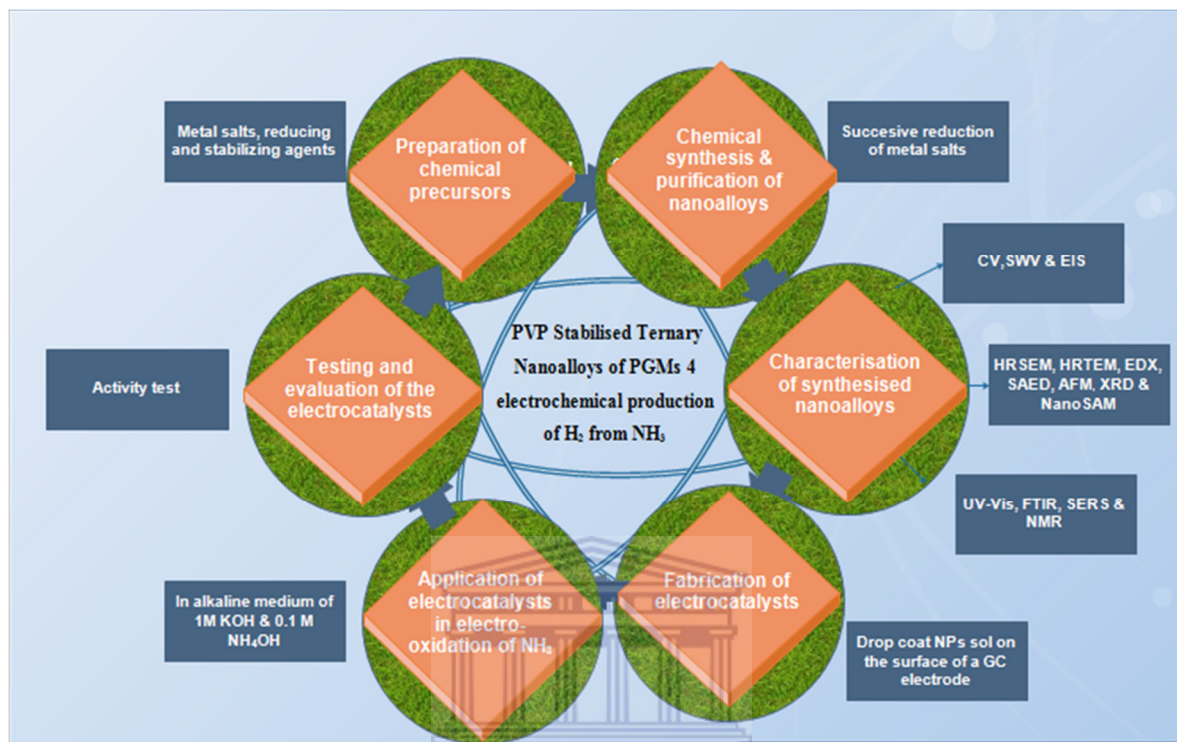
Scheme 1: Research framework.

1.8.   Outline of the thesis

Chapter 1: This chapter presents a brief background of the main aspects of the study, that is: hydrogen fuel cells, hydrogen carriers, with more emphasis on the use of nanoalloys as electrocatalysts for ammonia oxidation. The problem and its significance, scope and delimitations, the research's aim and objectives are also discussed.

Chapter 2: This chapter entails an extensive literature review of the concepts of the study which were briefly introduced in the previous chapter. The concepts, discussed amongst others, include: the working principles and classification of different types of fuel cells, forms of hydrogen carriers. This is followed by the thermodynamics of ammonia oxidation reaction and the use of various electrocatalysts. Nanotechnology and applications of nanomaterials are

further described with the background of characterisation techniques applied in this study finalising the scope of discussion for this chapter.

Chapter 3: This chapter provides the detailed experimental procedures, the chemical reagents, materials and instruments which facilitated the successful synthesis, characterisation and finally applications of desired nanostructures

Chapter 4: This chapter is a discussion of the results from various characterisation techniques employed to validate the formation of core-shell nanoalloys structures.

Chapter 5: This chapter discusses the application and testing of the electrocatalyst for electro-oxidation of ammonia.

Chapter 6: This chapter summarises the main points and findings of the study with final conclusion, future work and recommendations.

References: This is a list all the references cited in this work.

CHAPTER 2

LITERATURE REVIEW

Summary

This chapter presents an extensive literature review of the concepts of the study which were briefly introduced in the previous chapter. The concepts, discussed amongst others, include: the working principles and classification of different types of fuel cells and forms of hydrogen carriers. This is followed by the thermodynamics of ammonia oxidation reaction and the use of various electrocatalysts. Nanotechnology and applications of nanomaterials are further described with the background of characterisation techniques applied in this study finalising the scope of discussion for this chapter.

2.1. Energy

2.1.1. The energy challenge

The global energy demand is growing at an alarming rate and, alarmingly, is expected to further increase by as much as an order of magnitude by 2050, while primary-energy demands are expected to increase by 1.5 to 3 times **[24]**. The increased energy demand in developing countries like South Africa is met by burning limited fossil fuels that emit pollutants and greenhouse gases. Concurrently, this concern will also lead to an increase in energy-related environmental problems such as stratospheric ozone depletion, acid precipitation and global climate change in the future **[24-25]**. Additionally, there is already an expectation that by 2030, CO_2 emissions from developing countries could be more than 50% of the world CO_2 emissions **[26]**. Thus, a transformation from non-renewable energy to renewable energy is inevitable. Currently, South Africa is struggling to deal with an energy crisis and that was observed by Eskom cutting power supplies for 99 days this year as a strategy to ease an already strained grid. Ever since then, the energy department is evaluating the power-generation mix which includes renewable resources as a way to combat energy

shortages. Not only is the energy department coming with power plans, but scientists too are finding means to set out a vision for hydrogen and fuel cell technologies for future sustainable energy systems. These technologies can improve energy supply security and reduce air pollutants whilst mitigating climate change.

2.1.2. Need for clean energy technologies

Energy lies at the heart of all countries' core interests because it is a primary human need. Everyone requires energy for transportation, warming buildings, for operating machines and for other various operations. The department of energy in collaboration with the department of science and technology are investing in clean energy technologies by supporting research and development in coming up with clean and sustainable energy technologies to improve the economy and reduce dependence on foreign oil and combustion of coal. This serves as an approach to solve the energy challenges facing the country. At the moment hydrogen and fuel cell technology are very promising as part of clean energy plan. Hydrogen is an energy carrier and is used to store and distribute energy **[27]**. Fuel cell technologies can generate electricity efficiently from a number of fuels, including natural gas, biogas, methanol, propane, diesel and hydrogen.

2.1.3. Forms of energy

Nowadays, our lives are totally dependent on electrical energy and that can be witnessed by the effect that a 24 - 48 hours load shedding has on essential daily activities. This is due to the fact that without energy, life becomes exceedingly challenging as all advanced automated technological systems cease functioning, while the lights go out and the quality of hospital services also declines. All of the disturbances caused by power-cuts make daily activities very difficult and, at times, impossible.

There are different types of power plants which are used currently around the world to provide energy. Those include, thermal, nuclear, hydroelectric, wind, solar and geo-thermal power plants. The problem is that all of these power plants are dependent on a primary fuel to

produce electric power. In most cases, the fuels used in power plants are coal, natural gas and oil, while uranium and stored water are used in nuclear and hydroelectric power plants respectively. Thus the hydroelectric, thermal and nuclear power plants derive energy from non-renewable fuels, whereas wind, solar and geo-thermal power plants are based on renewable sources such as the wind, the sun and hot geysers, respectively **[28].** Nonetheless, worldwide, the present energy systems are primarily dependent on combustion of fossil fuels like oil, natural gas and coal **[24]**. These fuels are non-renewable and therefore unsustainable but they provide high net energy or net emergy **[28]**. This is due to the fact that they need comparatively little power and energy to be extracted from their primary industry (mines), to process them through secondary industry and to finally be transported to the end-users (tertiary industry) as illustrated in **Scheme 2** below.
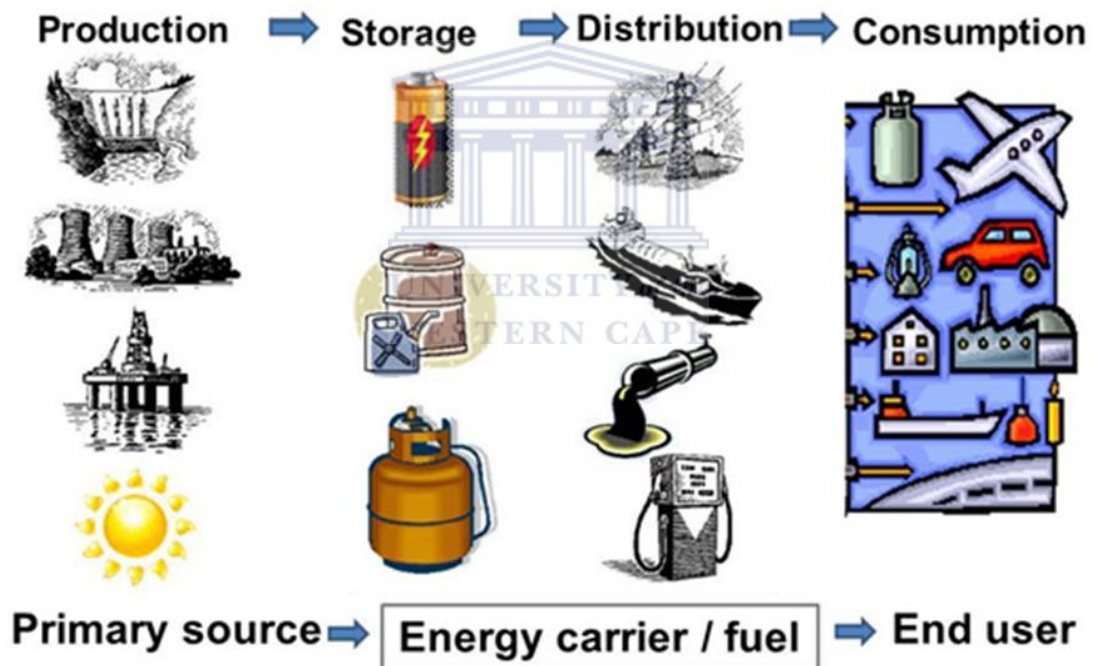
Scheme 2: The energy value chain showing processes involved in producing energy from its primary source to storage and distribution as fuel or an energy carrier to end users for consumption.

Hence, there is no doubt that non-renewable sources have been providing extraordinary economic development where they are used ever since the industrial revolution. Net energy is described as a difference between the energy content of a fuel and the energy required to

extract, process and deliver that fuel. On the other side, emergy is defined as the amount of available energy of one kind that is required to produce something and is used up in a transformation process. Therefore, net emergy is a difference between emergy of a given fuel and emergy of all energies used directly and indirectly for materials, goods and human services in extraction, processing and delivery of that fuel **[4]**. Therefore, in general the renewable energy sources have less emergy than non-renewable energy fuels, resulting in their carriers to have even lower net emergy **[4, 28]**. For that reason, renewable energy sources cannot support continuous economic growth and the end result will be a steady-state economy.

There are several problems with present global energy systems and this will become more evident with time. The most frightening problem being that the reserves of fossil fuels are limited and research on new innovations for energy sources cannot keep up with the drastically increasing energy demand; thus it clearly shows that the world will soon run out of fossil fuels **[4]**. The exploitation of non-renewable energy supplies is related not only to global warming, but also to environmental pollutions such as deforestation, air pollution, acid rain and emission of radioactive substances **[24]**.

In developing countries the energy demand is even worse owing to rapid industrialization, economic development and maintaining enhanced lifestyles which consume extremely large amount of world's energy sources. On the other hand, in developed countries energy consumption is decreasing because of transferring businesses and industries which require high energy to undeveloped countries **[4]**. This fast growing energy demand put pressure on finding alternative energy production sources and it also leads to high oil prices. Furthermore, the reserves of fossil fuels are not equally distributed across the world. For instance, oil and gas reserves are mostly found in the Middle East and Arabic countries which are in politically unstable geographic areas. Therefore this will further lead to political wars over the remaining available reserves **[4]**. It is obvious that if these issues are not addressed on time, then future consequences will be harsh. The only solution to these obstacles is an implementation of a transition to sustainable renewable energy systems.
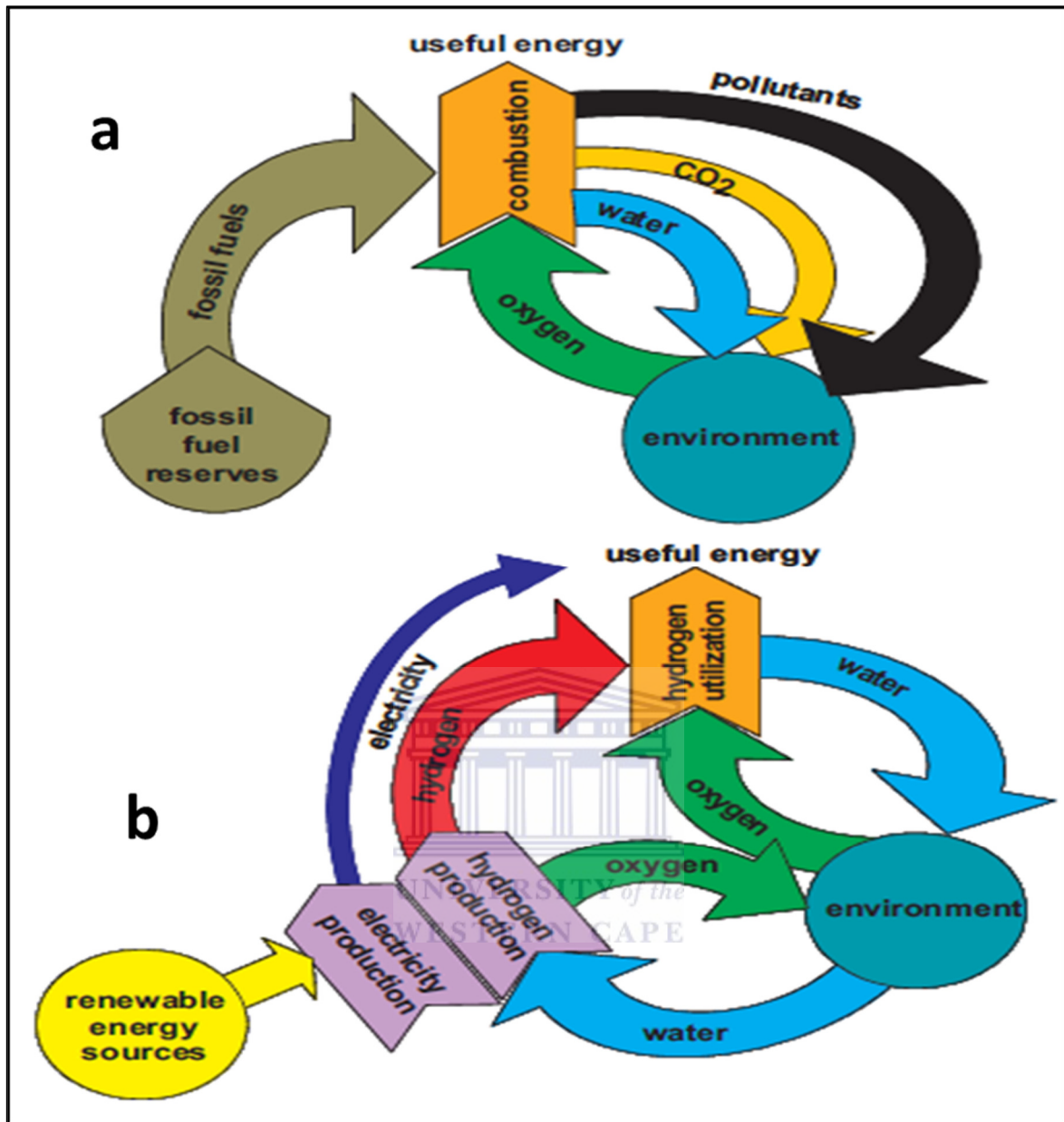
Scheme 3: Representation of the present unsustainable energy system based on fossil fuels (**a**) and a future sustainable energy system based on renewable energy sources with hydrogen and electricity as energy carriers (**b**) (extracted from ref [**4**]).

As illustrated in **Scheme 3** the non-renewable energy sources are unsustainable in comparison to renewable energy sources. Renewable energy systems offer sustainability and recyclability of water and oxygen obtained from the environment, whereas for non-renewable resources fuels get used up as fossil fuel reserves are finite. Moreover, during the process of combustion of fossil fuels, oxygen is being taken from the environment while pollutants are released as by-products to the environment making the whole process unclean. Thus there is a

need for a transition to renewable energy sources such as solar, wind, water and biomass with infinite reserves to ensure sustainable global energy supply. These renewable energy sources can easily be converted to heat, hydrogen, electricity and biofuels in large quantities so as to replace fossil fuels utterly **[4]**. The use of renewable energy sources which are more evenly distributed around the world will help in reducing air pollution as well as global wars over the remaining fossil fuel reserves. Therefore the utilization of renewable energy systems appears to be a promising solution to the current energy crisis.

Just to emphasise, the renewable energy sources are of great importance in reducing pollution and preserving the environment. Among the fuels used to generate electricity in power plants, fossil fuels are considered destructive in a sense that they emit green-house gases upon their combustion which poses threat to the environment as presented in **Scheme 3**. Moreover, fossil fuels will soon run out because their sources are limited **[25]**. These make renewable energy sources and fuels like solar, wind, biofuels and biomass to be in high demand. Nonetheless, as previously mentioned, the power efficiency from renewable sources is lower in comparison to that of non-renewable conventional power plants. Moreover, some of these renewable sources are periodic because they depend on the availability of sunlight and wind. Thus, fuel cells can be used to provide energy when periodic sources are not available **[28]**.

2.2. Fuel cells

2.2.1. Introduction

Sir William Robert Groove and Prof Christian Friedrich Schoenbein were the first scientists to demonstrate the fuel cell in 1839; however it took more than a century for fuel cells to be approved as a genuine power unit **[6]**. Their extraordinary invention was first known as the gas battery which is now called the fuel cell **[29]**. Grove constructed a cell consisting of two platinum electrodes placed in two separate tubes, one filled with oxygen and other with hydrogen, immersed in water, while the other end of the electrode were placed in sulphuric acid. He realised that the cell does not produce sufficient electricity to useful work and that led him into connecting several sets of electrodes in series to obtain the "gas battery" **[30]**.

The flow of current was measured to be proportional to the increase in water level in the tubes and heat was produced as a by-product. However, he could not quantify the reaction

products and study his system in more detail due to the lack of a comprehensive theory and adequate equipment in the 1840s **[29]**. The main founder of physical chemistry, the Russian-German Friedrich Ostwald made a significant contribution to the theoretical and experimental fundamentals of fuel cell reactions in the 1880s. He did not only explain how components of the fuel cells operate, but he further determined their kinetically- and thermodynamically-driven interactions at the electrode-electrolyte interface in presence of a fuel. Around 1890, Lang, Mond and Jacques were the first to introduce the term "fuel cell", becoming the first fuel-cell system builders **[29-30]**.

The advantages of using fuel cells among the various renewable energy sources available are that they have higher efficiencies and do not produce any polluting gases during operation; so they are very clean **[30-32]**. However, at this moment key challenge impeding the world-wide commercialisation of fuel cells is due to the high cost of the required loadings of precious metal used as electrode catalyst. Other barriers include the source and infrastructure of hydrogen supply as well as the system complexity when it comes to management or control of temperature, hydration and cold climates **[28]**. Consequently, these problems will need to be addressed to make this technology competitive. South Africa has an advantage and a strong potential to achieve this cost reduction through development of local PGM-based technology.

Table 1 presented below, shows a comparison of different generation systems **[33]**. It can be observed that among conventional systems and other distributed generation systems, fuel cells are the only ones with a high efficiency. The overall efficiency in fuel cells to produce profitable energy is almost twice that obtained by means of conventional combustion engines. This is because the thermal–mechanical–electric sequence with Carnot's cycle limitations used in the conventional indirect technology is avoided in fuel cells **[32]**. Additionally, as they do not have mobile parts, they do not produce noise, so as a result, fuel cells offer more advantages such as high energy conversion efficiency, modularity, zero emission, scalability, quick installation as well as in giving good opportunities for cogeneration operations as compared to other distributed generation technologies **[7, 28, 33]**.

Table 1: Comparison of different generation systems

	Reciprocating engine: diesel	Turbine generator	Photo voltaics	Wind turbines	Fuel cells
Capacity Range (kW)	500 - 5000	500 - 25000	1 - 1000	10 - 1000	200 - 2000
Efficiency (%)	35	29 - 42	6 - 19	25	40 - 60
Capital Cost ($/kW)	200 - 350	450 - 870	6600	1000	1500 - 3000
O & M Cost ($/kW)	0.005 - 0.015	0.005 - 0.0065	0.001 - 0.004	0.01	0.0019 - 0.0153

Data obtained from ref **[33]**. O & M: operation and maintenance

2.2.2. Working principles of fuel cells

Fuel cells are electrochemical devices that continuously and directly convert chemical energy into electrical energy for as long as fuels and oxidants are being supplied **[7]**. The only by products produced are pure water and heat when hydrogen is used as a fuel. The overall process can also be referred to as reverse water electrolysis **[29]**. A fuel cell is very much like a battery that can produce electricity while being recharged continuously. However, unlike internal combustion engines which develop mechanical work by the combustion of fossil fuel derivatives, fuel cells rely on a chemical reaction involving fuel instead of its combustion **[6, 31, 33]**.

The internal combustion engine is an affordable and effective way of generating mechanical work from a fuel. On the other hand, because most of these engines are powered by a hydrocarbon fossil fuel, their combustion emits carbon dioxide into the atmosphere contributing to a "greenhouse effect" which will lead to global warming **[28]**. The hydrogen fuel cell produces electricity through the electrochemical reaction of hydrogen and oxygen, with only water as a reaction product. Thus, they are seen as advantageous because their operation produces no carbon dioxide **[32]**.

A single fuel cell consists of an electrolyte sandwiched between two catalyst-coated electrodes (a porous anode and cathode). While there are different fuel cell types, all fuel cells have similar working principles [6]. During operation of a fuel cell (**Scheme 4**), a hydrogen fuel pumped in the anode compartment reacts with oxygen which is an oxidant supplied at the cathode compartment to produce electricity and water [29]. At the anode terminal, a platinum catalyst causes the hydrogen to split into positive ions and negative ions. The electrolyte membrane found between the electrodes permits only the positive ions to flow from anode to cathode side and acts as an insulator for electrons. The electrons travel along an external circuit to the cathode side, creating an electrical current. At the cathode, the positive and negative ions combine with oxygen to form pure water which flow out of the cell with unused gases [33]. The structure of a simplified fuel cell operation is shown in **Scheme 4.** For as long as hydrogen and oxygen gas are supplied to the fuel cell, then a direct current can be generated. In most of the fuel cell applications, air is used instead of oxygen, since air is composed of about 21% oxygen [28]. Therefore, the electrochemical reactions that occur in the anode and cathode are as follows:

Anode: $H_2 \rightarrow 2H^+ + 2e^-$ $\hspace{4cm}$ (7)

Cathode: $\frac{1}{2}O_2 + 2H^+ + 2e^- \rightarrow H_2O$ $\hspace{3cm}$ (8)

Overall reaction: $\frac{1}{2}O_2 + H_2 \rightarrow H_2O$ $\hspace{3.5cm}$ (9)
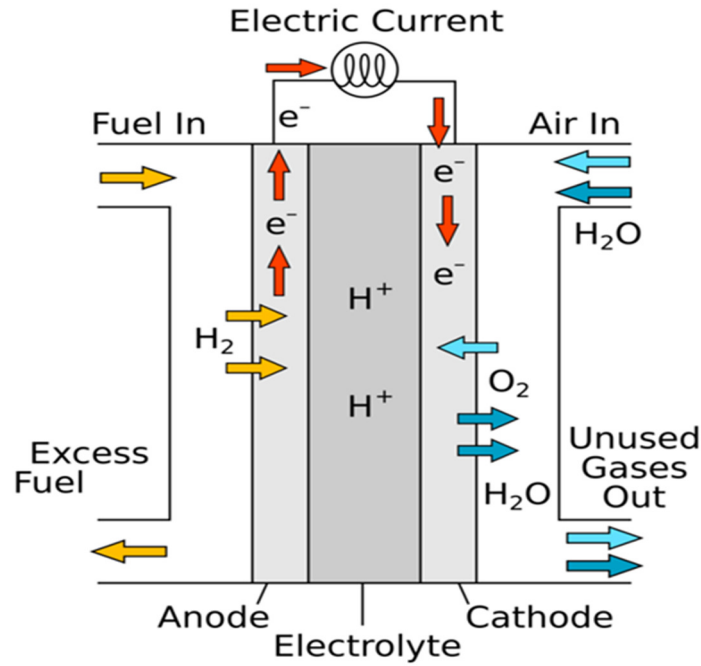
Scheme 4: Fuel cell operation diagram.
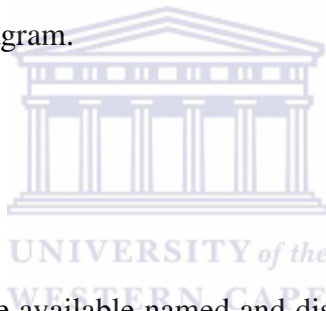
2.2.3. Types of fuel cells

The various types of fuel cells are available named and distinguished based on the operating temperatures and the type of the electrolyte used as summarised in **Table 2**. Below is the full discussion of the six main types of fuel cells.

2.2.3.1. Alkaline Fuel Cell (AFC)

The alkaline fuel cell is also known as Bacon fuel cell named after its British inventor. It uses an aqueous solution of potassium hydroxide (KOH) as an electrolyte and it operates at low temperature around 100 ºC. Furthermore, it can reach efficiency levels of 50-70% **[33]**. During its operation, the negative ions, instead of the positive ions, travel through the electrolyte to the cathode where they combine with hydrogen to generate water as by product. One of its advantages is that it gives quick start. However, its major drawbacks include being very sensitive towards CO_2 because it takes a long time to react, consuming the alkalis in the

23

electrolyte in so doing it reduces the concentration of hydroxide ion during chemical reactions **[30]**. For that reason AFC needs a separate system to remove the CO_2 from the air. The other disadvantage is the use of a corrosive electrolyte owing to its short life span and these factors limits its commercial applications. AFCs are therefore applicable in transportations and space shuttles. Proton ceramic fuel cells (PCFCs) and direct borohydride fuel cells (DBFCs) are subcategory of AFCs.

2.2.3.2.   Polymer Electrolyte Membrane Fuel Cell (PEMFC)

Polymer electrolyte membrane (PEM) fuel cell also called proton exchange membrane fuel cell uses a solid polymer electrolyte (Teflon-like membrane) to allow exchange of ions between two porous electrodes. The solid electrolyte also helps in preventing gas cross-over **[6]**. This membrane serves as an excellent proton conductor and electron insulator. It operates at relatively low temperatures of around 100 ºC allowing it to start quickly (less warm-up time) making it ideal for use in automotive vehicles and commercial applications like laptop computers, mobile phones and bicycles. Moreover, the PEM fuel cell delivers high power density and offers the advantages of low weight and volume compared to other fuel cells. The major disadvantages of the PEM fuel cell are its lower operating efficiency (40-45%), use of an expensive platinum catalyst and it is also intolerant to carbon monoxide **[6, 33]**. Direct formic acid fuel cell (DFAFC) and direct ethanol fuel cell (DEFC) come under the subcategory of PEMFC.

2.2.3.3.   Direct Methanol Fuel Cell (DMFC)

The direct methanol fuel cells (DMFCs) are a relatively new fuel cell type in comparison to others. The DMFC uses polymer electrolyte just like PEM fuel cell, but instead of using reformed hydrogen fuel it uses liquid alcohol such as methanol **[33]**. During its operation, at the anode side the methanol (CH_3OH) dissolves in water to produce hydrogen without the use of an external reformer. At the cathode side, the recombination of protons and electrons from anode through external circuit with oxidised air take place to produce water as the by product. One of the main advantages of DMFC is that the anode catalyst itself draws hydrogen from

methanol thereby eliminating the need of a reformer reducing the overall cost. It operates in a very similar manner to the PEM fuel cell, however its performance is limited by the slow kinetics of the electrochemical oxidation of methanol at the anode and the crossover of methanol from anode to cathode lowers the efficiency of DMFC **[34]**. Since a single DMFC is capable of supplying 0.3-0.5 V under loaded conditions, it is mainly used to replace batteries for notebook computers, cameras and other portable electronic devices in the range of 1 W to 1 kW capacity.

2.2.3.4. Phosphoric Acid Fuel Cell (PAFC)

The phosphoric acid fuel cell (PAFCs) utilizes liquid phosphoric acid as an electrolyte; the acid is contained in a Teflon-bonded silicon carbide matrix while the porous carbon electrode contains a platinum catalyst. The operation temperature of PAFC is around 175-200 ℃, almost double that of PEM fuel cell. Unlike PEMFC and AFC, it is more tolerant of impurities in fossil fuels (hydrocarbons) that have been reformed into hydrogen **[33]**. Owing to its high operating temperature, PAFC is more than 85% efficient when used for the co-generation of electricity and heat but is less efficient at generating electricity alone (37%–42%). This efficiency is only slightly more than that of combustion-based power plants, which typically operate at around 33% efficiency. It operates like PEM fuel where pure hydrogen is used as the input fuel so they have the same chemical reactions **[34]**. The drawback of PAFC is same as for PEM fuel cell; it is also expensive due to the use of high loadings of expensive platinum catalyst. This type of fuel cell is typically used for stationary power generation, but some PAFCs can be used to power large vehicles like city buses.

2.2.3.5. Molten Carbonate Fuel Cell (MCFC)

MCFC is a high-temperature fuel cell that uses an electrolyte composed of a molten carbonate salt mixture suspended in a porous, chemically inert ceramic lithium aluminium oxide matrix **[6]**. It operates at high temperatures of 600-700°C. Unlike alkaline, phosphoric acid and PEM fuel cells, MCFC does not require an external reformer to convert fuels such as natural gas and biogas to hydrogen. At the high temperatures due to its internal reforming

capability, it separates hydrogen from carbon monoxide fuel, while hydrogen is produced through the water shift reaction. Thus the resultant reaction is taken the same as PEM fuel cell to generate electricity. The major advantages of MCFC include high efficiency of 50-60%, no need of precious metal catalyst and external reformer due to its high operating temperature [37]. The primary disadvantages of the current MCFC technology are its intolerance towards sulphur and slow start up [33]. It is mainly used for medium and large power applications.

2.2.3.6. Solid Oxide Fuel cell (SOFC)

The SOFCs are basically high temperature fuel cells. They utilize hard yttria stabilised zirconia, non-porous ceramic compounds as the electrolyte. Since SOFC is a solid state device, it therefore shares some properties and fabrication techniques with semiconductor devices [34]. During its operation oxygen O^- reacts with hydrogen H^+ to produce water and heat. SOFCs operate at very high temperatures - as high as 1000 °C. The main advantage of SOFCs is that they are around 50-60% efficient at converting fuel to electricity. Furthermore, the high-temperature operation allows them to reform fuels internally, so a separate reformer is not required to extract hydrogen from the fuel [30]. The system's waste heat can be captured, recycled and utilized to make additional electricity by co-generation operation [35]. Operation up to 1000 °C allows more flexibility in the choice of fuels and it exhibits enhanced performance in combined-cycle applications [6]. Some of its drawbacks include, slow start up, high cost and an intolerance to sulphur contents in the fuel cell. It is not suitable for larger fluctuations in load demand [33]. Therefore, just like MCFC, the SOFC is mainly utilized for medium and large power applications.

2.2.3.7. Summary

In general PEMFC, AFC and PAFC have the low operating temperature in the range of (50–250) ºC and MCFC and SOFC have high operating temperature in the range of (650–1000) ºC. The summary of electrolyte type, operating conditions, applications and limitations of various major types of fuel cells is presented on **Table 2 [28]**.

26

Table 2: Types of fuel cells

Fuel cell type	Mobile ion	Operating temperature (ºC)	Limitations	Applications
AFC	OH^-	50 - 200	Air and fuel should be free from CO_2 to avoid carbonate formation in the electrolyte. Expensive catalysts are required.	Used in space (Apollo Shuttle)
PEMFC	H^+	30 - 100	Pure hydrogen and expensive catalysts are required.	Vehicles and mobile applications and for low power CHP systems.
DMFC	H^+	20 - 90	Slow methanol oxidation rate, low power output and fuel crossover problems.	Suitable for portable electronics systems of low power, running for long times.
PAFC	H^+	~220	Fuel reformers needed: complex system and high cost.	Large numbers of 200 kW CHP systems in use.
MCFC	CO_3^{2-}	~650	Requires molten electrolyte: hot and corrosive mixtures of lithium, potassium and sodium carbonate.	Suitable for medium-to-large scale CHP systems, up to MW capacity.
SOFC	O^{2-}	500 - 1000	Ceramic electrolyte, complex and expensive accessory equipment.	Suitable for all sizes of CHP systems, 2 kW to multi-MW

Data extracted from ref **[28]**. CHP: combined heat and power

Research in the field of fuel cell systems has been dedicated to areas such as cell design, electro-catalyst materials for anode and cathode, electrodes, hydrogen production and storage, flow field plates and direct fuel supply systems **[28]**. It is crucial to investigate electro-catalyst materials and cell design of fuel cells so as to reduce their overall expense/cost. Fuel cells are more expensive than internal combustion engines and currently used power generators. On the other hand, there is a critical problem with obtaining the source of fuel (hydrogen), its storage and transportation. Therefore, research is on-going in finding efficient transportation networks and storage systems for hydrogen. The major

sources of hydrogen production are fossil fuels and water, which are described in the next section below.

2.3. Hydrogen production methods

The common major sources for hydrogen production are water and fossil fuels, other chemical compounds like alcohols and hydrocarbons are also used as hydrogen carriers. Ammonia electrolysis was introduced as a novel approach to hydrogen production, whereby ammonia is electrochemically cracked into hydrogen and nitrogen gas. Ammonia has more advantages over other chemical compounds to be used as a hydrogen carrier. As previously mentioned, the operation of an efficient fuel cell needs a reliable supply of a pure hydrogen gas as fuel. Hydrogen is abundantly available in the world, however it can only be obtained in the form of various compounds not as a pure hydrogen gas. Hence, the compounds which contain a high content of hydrogen are currently being used as hydrogen carriers and these include: alcohols, ammonia, water and hydrocarbons like oil, coal, gas and methane [28]. Fuel processing is the only way of harvesting hydrogen gas from different compounds. Below is a description of the most common and widely used fuel processing techniques for generating hydrogen gas from hydrocarbons.

2.3.1. Steam Reforming

Steam reforming is one of the well-known techniques for producing hydrogen gas. In a reformer, hydrocarbons denoted as (C_nH_m), undergoes the following chemical reaction summarised below:

$$C_n H_m + n H_2O \rightarrow n CO + (\frac{m}{2} + n) H_2 \tag{10}$$

$$CO + H_2O \rightarrow CO_2 + H_2 \tag{11}$$

The reaction (11) is known as the water gas shift reaction, wherein hydrogen and carbon dioxide are being formed from the reaction of steam mixed with hydrocarbons and carbon monoxide in presence of a nickel catalyst at high temperatures, normally above 500 ºC [36].

The hydrocarbons which can be used in steam reforming processes include methane, methanol and natural gas.

$$CH_4 + H_2O \rightarrow CO + 3H_2 \tag{12}$$

$$CH_3OH + H_2O \rightarrow CO_2 + 3H_2 \tag{13}$$

In order to obtain clean hydrogen from this process, the reformed gas has to be purified by removing all gas products other than hydrogen before it can be sent for use in fuel cells. The disadvantage of this method is that all the reforming reactions are endothermic, that is they need energy to produce hydrogen gas. Additionally, hydrogen still has to be purified prior to its application in fuel cells [28]. Lately, with new developments, methanol can be used directly as a fuel in the fuel cells, thereby both reforming and electrochemical conversion of hydrogen to water and electrical energy is taking place. Such types of setups are referred to as a direct methanol fuel cell (DMFC). It should be noted that not only methanol can be used for fuel reforming in fuel cells, but other fossil fuels can be used as well. The general name for this process is known as internal reforming.
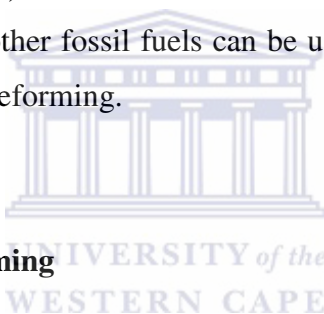
2.3.2. Partial Oxidation Reforming

Another way of extracting hydrogen gas from methane and other hydrocarbons is via partial oxidation reforming. This method does not require the use of a catalyst due to high operating temperatures (of 1200 to 1500 ℃) used in presence of oxygen to ensure complete conversion [37]. The partial oxidation reaction for the conversion of methane to hydrogen and carbon monoxide presented below is an exothermic process:

$$CH_4 + \frac{1}{2}O_2 \rightarrow CO + 2H_2 \tag{14}$$

In comparison with reaction (12), it can be observed that fewer molecules of hydrogen are produced by the partial oxidation method than the steam reforming methods, signifying that the partial oxidation process is less efficient. However, the high operating temperature for partial oxidation allows for the easy handling of heavier petroleum fractions such as diesels and residual fractions.

2.3.3. Coal gasification

Gasification is another technology commonly used for large scale conversion of complex hydrocarbons into various products, which are further processed to enrich the hydrogen fraction. This technology can use all types of carbon-based feedstock such as biomass, coal, petroleum residues and municipal wastes and can be used to produce a range of commodity products. The process of coal gasification reactions operates at high temperatures (1040-1540 ºC) at moderate pressures (5-10 bar) [28]. Steam and oxygen are therefore used to produce gas products containing CO, CO_2, CH_4, H_2, N_2 and H_2S in varying proportions.

2.3.4. Water electrolysis

Water electrolysis is a quite old technology started around two centuries back, but very promising technology for hydrogen production. This process has its various merits like very simple process with plenty of resource and is a pollution free process if renewable energy sources use purity of high degree. In water electrolysis water molecule passes through electrochemical process and they spilt into hydrogen and oxygen gases. Since electric current is used for the splitting of water, sometimes water electrolysis is seen as a better way of producing hydrogen for fuel cell applications as there is no purification step required [38]. Combining the process of water electrolysis and fuel cells would mean that the electricity and water produced from the fuel cell might be used in the electrolyser to from hydrogen and oxygen and this is not considered power efficient.

At room temperature the splitting of water is very small, approximately 10 moles/litre owing to poor electric conductivity of pure water. In order to solve this problem, acid or base is used to improve the conductivity. Hence, water electrolysis technology can be sub-divided into three main classifications based on the electrolyte used in the electrolysis cell. The electrolysers available include; alkaline electrolyser, PEM electrolyser and solid oxide electrolyser [39-40]. In an alkaline electrolyser, a liquid electrolyte such as potassium hydroxide (KOH), sodium hydroxide (NaOH) and sulphuric acid (H_2SO_4) solutions are used with water. During this process the solution splits into positive and negative ions which readily conduct electricity in a water solution by flowing from one electrode to the other [38].

On the other hand, the electrolysis process in a PEM electrolyser is carried out in acid ionomer environment, whereas a solid oxide electrolyser makes use of a solid oxide electrolyte at high temperatures [38-42]. A minimum voltage of 1.23 V, which is required to dissociate water to hydrogen and oxygen under normal room temperature and atmospheric pressure, results in a lower hydrogen gas evolution rate and low current density. Thus at present, the current efficiency of hydrogen production by water electrolysis is too low to be economically competitive. In addition, the high energy consumption is a serious problem for water electrolysis, as on average 4.5–5.0 kWh/$m^3$$H_2$ energy is needed for a conventional industrial electrolyser [28].

2.3.5. Efficiency of hydrogen production methods

The importance of all the previously discussed hydrogen production methods is that the obtained hydrogen will be applied in fuel cell to generate power. Usually, the efficiency for hydrogen production method is described as the ratio of energy derived from hydrogen over the energy contained in the raw material. However, the calculation should also include other energies involved in combustion, i.e. cooling, electrical heating and purification steps, so as to obtain the actual efficiency for converting the raw material to final product (pure hydrogen gas) [28]. The efficiencies of the various hydrogen production methods are listed in **Table 3** using the values provided in a report by the National Research Council [28].

Table 3: Hydrogen production efficiency

Methods	Efficiency (%)
Steam methane reforming	63
Coal gasification	64
Water electrolysis	67

Data obtained from ref [28].

Upon comparing these three hydrogen production methods, it can be observed that electrolysis of water seems to have a slight advantage over steam reforming and coal gasification.

2.4.   Ammonia and related chemicals as potential hydrogen carriers

As previously mentioned, ammonia is a potential hydrogen carrier that can provide an *in-situ* method for the production of hydrogen. However, not only ammonia can achieve this as other chemicals related to ammonia may also provide an alternative energy supply. Materials such as hydrazine, ammonia carbonate, ammonia bicarbonate, ammonia borane, nitrogen hydrides and urea have the potential to be used as hydrogen carrier chemicals **[2, 10]**. Like hydrogen, ammonia, hydrazine and ammonia borane also are carbon-free, which means no CO_x emissions are expected upon their oxidation. The catalytic decomposition of ammonia and these nitrogen-based chemicals for their application in fuel cells towards *in-situ* hydrogen production is a promising approach to attaining higher efficiencies **[2]**.

Ammonia reforming has been mainly proposed for use with fuel cells for portable power applications **[10, 36, 43-45]**. It is regarded as an inexpensive largely produced inorganic fuel and due to its use in fertilizer production it has an extensive distribution system **[36, 46]**. Pure ammonia has an energy density of 8.9 kWh/kg, which is higher than methanol (6.2 kWh/kg), but less than diesel (13.2 kWh/kg) **[43]**. One mole of ammonia contains 1.5 mol of hydrogen and is equivalent to 17.8% by weight or 108 kg H_2/m^3 embedded in liquid ammonia at 20 °C and 8.6 bars. It is essential to note that this density is about 4 times higher than that of the most advanced storage methods in metal hydrides **[48]**.

Although it is toxic, unlike odourless H_2, ammonia can be detected by its characteristic strong odour even at safe concentration levels (< 1 ppm) making leak detections simple, reducing some of the risk **[44, 46, 49]**. Additionally, ammonia has a narrower flammable range than hydrogen and is considered non-flammable when being transported, whereas hydrogen burns with an invisible flame **[46, 49]**. Furthermore, NH_3 has a high content of H_2 atoms per unit of volume, it is easy to transport and is considered to be less toxic in comparison to methanol **[47, 50]**. In comparison to other compounds ammonia is the best H_2 carrier because unlike alcohols and hydrocarbons, ammonia oxidation yields no carbon and nitrogen oxides (CO_x

and NO_x) containing products. So it is environmentally friendly thus compared to hydrogen it can be easily handled, stored and distributed as indicated in **Scheme 5.**

Scheme 5: Ammonia fuel cycle, (extracted from ref **[51]**).

2.5. Recent progress in direct ammonia fuel cells

Due to the excellent properties described above, ammonia has the potential to be used directly as a fuel in alkaline and solid oxide fuel-cells (SOFCs) to produce steam and some NO_x exhausts **[52]**. The first type of ammonia fuel cells were investigated in 1960s based on alkaline fuel cells (AFCs) with a typical operating temperature of 50–200 °C, using KOH as electrolyte **[53]**. It was reported that ammonia can also be used for molten hydroxide NaOH/KOH fuel cells at operational temperatures of 200–450 °C and when nickel was used as both cathode and anode material, a power density of 40 mW cm^{-2} at 450 °C was attained **[54, 55]**. Conversely, the durability of ammonia fuel cells operating with KOH-based electrolytes is an issue owing to the reaction between hydroxide electrolytes and CO_2 **[56]**.

In addition to AFCs, the low temperature proton exchange membrane fuel cells (PEMFCs) using hydrogen as the fuel have been developed for various applications such as electric

vehicles. It was found that ammonia is not a suitable fuel for PEMFCs as it may react with the acidic Nafion membrane and poison the Pt/C anode catalyst [57]. However, ammonia can solely be used to produce hydrogen which can then be captured and be fed into PEMFCs for power generation [58].

Up to date, the best choice for direct ammonia fuel cells is to operate at high temperatures using solid oxide fuel cell (SOFCs) because ammonia decomposes readily at these high temperatures and so far it has not been reported to poison the ceramic utilised in SOFCs [46, 58]. The ammonia based SOFCs can be divided into two categories, that is SOFC-O (oxygen ion conducting electrolytes) and SOFC-H (proton conducting electrolytes). SOFC-O entails an oxygen ion conducting electrolyte, such as samarium doped ceria (SDC) or yittria stabilised zirconia (YSZ) and water formation at the anode. On the other hand, SOFC-H entails a proton conducting ceramic electrolyte such as barium cerate and water formation at the cathode [46]. The earliest direct ammonia SOFC was reported by Vayenas and Farr in 1980 based on yttria stabilised zirconia (YSZ) electrolyte and platinum electrodes for the co-generation of electricity and nitric oxide [59-60].

Another challenge facing the development of these fuel cells is that in order to ensure a long life for PEM fuel cells, ammonia levels are required to be reduced to below ppb levels because exposure of ammonia to the acidic PEM electrolyte may cause a huge and irreversible loss in performance [36]. However, for SOFC, ammonia can be fed directly to the fuel cell without any reforming [44-45]. Therefore, in general, the main challenge for direct ammonia fuel cells is the fabrication of robust anode electrocatalysts because the accumulation of adsorbed nitrogen species on the catalyst surface has proven to be problematic as they cause catalyst degradation. Another shortcoming of these cells is the ammonia flux through the anion exchange membrane [61].

2.6.   Hydrogen production from ammonia

The production of hydrogen gas has been mostly based on reforming of hydrocarbons and sometimes water electrolysis has been considered. As it has been mentioned, the production, storage and transportation problems of hydrogen has led to research of finding novel hydrogen storage materials like metal hydride compounds to enable quick release of

hydrogen **[28]**. Thus, in overcoming the concerns of generating hydrogen with less energy consumption, the use of ammonia as a hydrogen carrier towards hydrogen production via ammonia electrolysis should be considered. The fuel cell technology is more efficient, compact, quieter and reliable, if and only if, the hydrogen used is from a renewable source, as "hydrogen is only as clean as it is made" **[27].** This will help in making the whole technology green, clean and better for the environment.

2.6.1. Ammonia cracking

Ammonia cracking is basically the thermal decomposition of ammonia into hydrogen and nitrogen at high temperatures (<500 ℃), thus it is an endothermic process and unlike ammonia synthesis, low pressures (250 atm) are preferred **[44]**. Ammonia cracking is regarded as the reverse of the synthesis reaction, where its synthesis is represented by the following reaction **[2, 44]**:

$$N_2(g) \ + \ 3H_2(g) \ \rightarrow \ 2NH_3\ (g) \qquad\qquad \Delta H \ = \ -92.4 \ kJmol^{-1} \qquad (15)$$

In contrast to steam reforming, partial oxidation and coal gasification, ammonia cracking is a CO_x free process. This advantage has motivated the indirect use of ammonia in an alkaline fuel cell. The research on ammonia cracking started when synthesis of ammonia was extensively investigated and then with the information developed on ammonia synthesis, various catalysts were also fabricated and tested for ammonia cracking **[28, 44]**. The catalysts tested for this reaction are metals, alloys and compounds of noble metals. In recent decades, Ni and Ru based catalysts supported on an activated carbon or porous alumina has been widely studied **[36, 44]**.

2.6.2. Ammonia electrolysis

A lot can be done with application of ammonia oxidation for hydrogen production. The ammonia electrolysis process where ammonia is broken electrochemically into hydrogen and nitrogen can be made green and more sustainable. The vital goal of this process is presented in **Scheme 6** where ammonia-waste can be pumped into an ammonia electrolyser that

operates with renewable energy sources towards hydrogen and clean water production **[10, 28]**. The ammonia used here can be obtained from waste, making it compatible with renewable energy sources. Indeed, this technology can be used as a breakthrough to the hydrogen storage and transportation challenges.

Scheme 6: Diagram showing how an ammonia electrolyser operating with renewable energy can produce hydrogen and clean water from livestock and industrial ammonia waste**,** (extracted from ref **[28]**).

2.6.3. Comparison of ammonia cracking and ammonia electrolysis

Both approaches discussed in the above section are used to break down ammonia into hydrogen and nitrogen, so their thermodynamic efficiencies are the same. Thermodynamic efficiencies were determined by calculating the ratio of the lower heating value of H_2 (242.7 kJ mol^{-1}) over the sum of ammonia lower heating value (320.1 kJ mol^{-1}) and either thermal energy (NH_3 cracking) or the electrical energy (NH_3 electrolysis) **[28]**. The efficiency of more than 100% in theoretical terms for these two technologies under various conditions, presented in **Table 4**, because the energy to produce ammonia has not been included in the

calculation. One of the advantages of ammonia electrolysis over thermal cracking is that ammonia electrolysis allows the direct conversion of ammonia from waste to hydrogen, whereas thermal cracking of ammonia needs pure ammonia [28]. It therefore means that for ammonia cracking the energy required to make NH_3 should be taken into consideration. Other than its poor conversion efficiency, ammonia cracking it requires a complex system. While ammonia electrolysis just uses renewable energy and is a less complex system.

Table 4: Efficiency data for ammonia cracking and electrolysis

Methods	Conditions	Efficiency (%)
Ammonia cracking and ammonia electrolysis	Thermodynamic at standard conditions	112.1
Ammonia cracking	Pure ammonia (exclude energy)	102.1
Ammonia electrolysis	Glass cell, one compartment with 1 M NH_3.	80
	Single cell electrolyser (with separator), 1 M NH_3.	104.5
	9-cell stack, 1 M NH_3.	98.2
	Low concentration electrolyser (20 mM NH_3): glass cell, one compartment.	95.1

Data obtained from ref [28].

2.7. The thermodynamics of the electro-oxidation of ammonia for hydrogen production

The electrolysis of ammonia is a new approach for hydrogen production recently proposed by Botte *et al*. [62]. It involves the use of an ammonia solution (NH_4OH) containing and potassium hydroxide. In a typical ammonia electro-oxidation reaction, electrolyte composition consists of 1 M NH_4OH in 5 M KOH [28]. Ammonia gets

oxidised in an alkaline medium to form nitrogen gas at the anode electrode, while on the cathode side of the electrolytic cell, water is reduced to hydrogen gas [63]. Hence, the overall ammonia electrolysis reaction for the cell involves dissociation of ammonia into hydrogen and nitrogen. The reactions at each electrode side and overall reaction are presented below [10, 63, 64]:

Anode reaction:

$$2NH_3 + 6OH^- \rightarrow N_2 + 6H_2O + 6e^- \tag{16}$$

$$E^0 = -0.77\ V\ vs.\ SHE$$

Cathode reaction:

$$2H_2O + 2e^- \rightarrow H_2 + 2OH^- \tag{17}$$

$$E^0 = -0.829\ V\ vs.\ SHE$$

Overall reaction:

$$2NH_3 \rightarrow N_2 + 3H_2 \tag{18}$$

$$E^0 = -0.059\ V$$

The processes which occur in an ammonia electrolytic cell are illustrated below in **Scheme 7**. In comparing ammonia with water electrolysis methods, thermodynamically there is a significant difference in potential between 0.059 V and 1.23 V of cell voltage for ammonia and water electrolysis, respectively [63]. Based on these thermodynamic cell voltages, theoretically the energy required to produce a gram of H_2 is 1.55 Wh for NH_3 and 33 Wh for H_2O electrolysis (assuming that there are not kinetics limitations for the reaction to take place at the thermodynamics conditions) [10, 63]. Therefore, the thermodynamic values favour the production of hydrogen coupled to the oxidation of ammonia over hydrogen production by water electrolysis [65]. Even though ammonia electrolysis is thermodynamically favourable, the reaction kinetics is slow [46]. The energy consumption and efficiency for different

38

ammonia electrolysis systems varies with different catalysts, support materials and electrolytic cell configurations. This are listed in **Table 4**. Furthermore, the cost and energy expenditure of H_2 production from ammonia electrolysis is almost 87% cheaper and 95% less energy consuming than water electrolysis **[28]**. The other advantages of this process is its ease of integration with renewable energy (electricity) sources (e.g., wind and solar energy) as well as its ability to provide hydrogen production on demand, thus minimising the need for hydrogen storage **[10]**. This alone shows the importance of ammonia electrolysis and its promising impact in the present hydrogen economy.

Scheme 7: Diagram of ammonia electrolysis with anode and cathode electrodes reactions producing nitrogen and hydrogen gas respectively, (obtained from ref **[28]**).

2.8. The ammonia electro-oxidation reaction mechanisms

The electrolysis of ammonia has evolved in recent years with an objective to clean wastewater. The electro-oxidation of ammonia is now seen as one of the best ways for

optimising H_2 production. There are two different reaction mechanisms which have been proposed for the electrochemical oxidation of ammonia in alkaline media, one by Oswin and Salomon (1963) [66] and one by Gerischer and Mauerer (1970) [63, 67]. Therefore, in this section, the mechanism of ammonia electro-oxidation is briefly discussed with particular attention drawn to latest findings on the active intermediates and poisonous species, which are highly significant for the fundamental understanding of the principles of enhancing the electrocatalyst performance. Below are the reaction steps proposed by Oswin and Salomon, in 1963, for the oxidation of ammonia [63]:

$$NH_3 + M \rightarrow MNH_3 \qquad (19)$$

$$MNH_3 + OH^- \rightarrow MNH_2 + H_2O + e^- \qquad (20)$$

$$MNH_2 + OH^- \rightarrow MNH + H_2O + e^- \qquad (21)$$

$$MNH + OH^- \rightarrow MN + H_2O + e^- \qquad (22)$$

$$MN + MN \rightarrow M_2N_2 \qquad (23)$$

$$M_2N_2 \rightarrow N_2 + 2M \qquad (24)$$

Where, M represents the catalyst material as the electrochemical reactions takes place on the catalyst surface.

Then in 1970, Gerischer and Mauerer proposed a reaction mechanism for the ammonia electro-oxidation with inclusion of extra reaction steps to those suggested by Oswin and Salomon [63]:

$$NH_3 + M \rightarrow MNH_3 \qquad (19)$$

$$MNH_3 + OH^- \rightarrow MNH_2 + H_2O + e^- \qquad (20)$$

$$MNH_2 + OH^- \rightarrow MNH + H_2O + e^- \qquad (21)$$

$$MNH + OH^- \rightarrow MN + H_2O + e^- \qquad (22)$$

$$MN + MN \rightarrow M_2N_2 \qquad (23)$$

$$MNH_x + MNH_y \rightarrow M_2N_2H_{(x+y)} \qquad (25)$$

$$M_2N_2H_{(x+y)} + (x + y)OH^- \rightarrow M_2N_2 + (x + y)H_2O + (x + y)e^- \qquad (26)$$

$$M_2N_2 \rightarrow N_2 + 2M \qquad (24)$$

The steps in the Gerischer and Mauerer reaction mechanism follow the same reactions listed by Oswin and Salomon except for those shown in reactions (25) and (26). Based on the Gerischer and Mauerer mechanism, there are additional re-actions and intermediates formed during the electrochemical oxidation of ammonia [63]. The secondary reactions involve other intermediates such as NH_x and NH_y (x and y = 1 or 2). These NH_x and NH_y intermediate molecules can combine to form N_2H_2, N_2H_3 and N_2H_4 molecules reaction (25), which eventually reacts with OH^- ions to form adsorbed N_2 and water molecules reaction (26).

Molecular modelling of the reactions steps gives information on the structural changes for each molecule with the catalyst surface. Furthermore, the reaction rates of the various reaction steps involved in both mechanisms can be calculated from molecular modelling [63]. Therefore, a thorough understanding of different steps mentioned in the mechanism is mandatory when it comes to the development of a highly efficient electrocatalyst for ammonia oxidation.

The same mechanism of Gerischer and Mauerer can also be represented as follows [28]:

$$NH_3 \; (aq) \rightarrow NH_{3,ads} \qquad (1)$$

$$NH_{3,ads} + OH^- \rightarrow NH_{2,ads} + H_2O + e^- \qquad (27)$$

$$NH_{2,ads} + OH^- \rightarrow NH_{ads} + H_2O + e^- \qquad (28)$$

$$NH_{x,ads} + NH_{y,ads} \rightarrow N_2H_{x+y,ads} \qquad (29)$$

$$NH_{x,ads} + (x + y)OH^- \rightarrow N_2 + (x + y)H_2O + (x + y)e^- \qquad (30)$$

$$NH_{ads} + OH^- \rightarrow N_{ads} + H_2O + e^- \qquad (31)$$

$$N_{ads} + N_{ads} \rightarrow N_{2,ads} \qquad (32)$$

$$N_{2,ads} \rightarrow N_2(aq) \qquad (33)$$
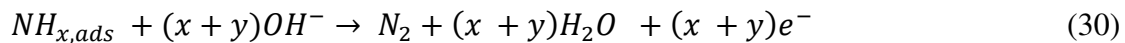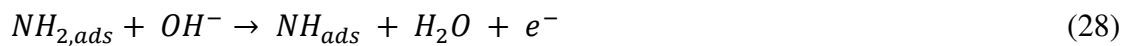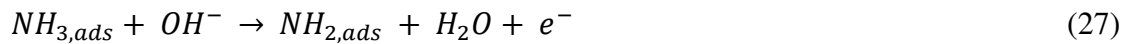
Where x, y = 1 or 2.

2.9.   Technological problems encountered during hydrogen production from ammonia

Various catalysts have been interrogated for improving the sluggish kinetics of the ammonia electro-oxidation reaction. Even though significant current densities are obtained on a platinum electrode surface, this electrode process is far less reversible owing to high anodic overpotentials compared to hydrogen oxidation [66, 67]. Moreover, the Pt catalyst, which is the best electrocatalyst for this reaction, gets easily deactivated at high current densities as it is susceptible to poisoning by the nitrogen adsorbate (N_{ads}) intermediates [68-70]. Consequently, hydrogen production from ammonia electrolysis needs the development of better catalysts for electro-oxidation of ammonia. In previous years, substantial efforts have been dedicated to testing several metals and alloys as potential catalysts. One of the studies was based on the use of bulk platinum and bulk iridium electrodes as electrocatalysts toward ammonia oxidation and their findings showed that these metals have best catalytic activity compared to noble and coinage metals [70, 71]. The only problem encountered was that the observed current densities for these catalysts were very low - less than 1 mA cm^{-2}. It was also proven that metal alloys, metal oxides and bimetallic electrocatalysts exhibit higher activity toward ammonia oxidation in comparison to monometallic catalysts. In this case the investigated alloys and oxides include, among others, Ag-Pb [71] alloys and Ru oxides [72], but this was only observed at very high overpotentials. Independent findings [11] have supported the fact that the Pt catalysts structure plays a vital role on the kinetics of ammonia electro-oxidation and have reported low overpotentials exclusively for Pt (100). However, the electro-oxidation of ammonia is strongly inhibited with Pt (111) and Pt (110) catalysts surfaces [11, 12, 73-79]. Furthermore, in a separate study, various bimetallic Pt-Me electrocatalysts (where Me is other PGMs e.g. Ir, Rh, Pd and Ru) and preferentially oriented Pt (100) nanoparticles were screened for ammonia oxidation [12]. The authors concluded that among all the bimetallic NPs tested, only $Pt_{75}Ir_{25}$ and $Pt_{75}Rh_{25}$ nanoalloys show an improved oxidation current density at the low potential range with respect to the activity found for pure Pt nanoparticles prepared by the same method. In addition, they reported that the Pt (100) preferentially oriented NPs exhibit higher current densities than polycrystalline Pt NPs owing to the structural sensitivity of ammonia oxidation towards the presence of surface sites with square symmetry [12].

42

The importance of using PGMs based multi-shell or core-shell, or even alloy electrocatalysts with cheaper base metals is to reduce the high cost of fuel cells by reducing the amount of Pt loading of the catalyst. Most of these experiments were carried out using bimetallic, bulk metal or metal oxide electrodes with high precious metal loading. In this study, the use of novel mixed and multi-shell PGMs-based electrocatalysts towards hydrogen production from ammonia electro-oxidation reaction will be investigated. Multi-shell nanoparticles will be constructed in such a way that the catalyst atoms are located on the shell region, while the core can be constituted by a cheap, catalytically inactive metal in order to develop efficient and economically viable electrocatalysts with low Pt- loading. This structure has the advantage in catalytic activity because the shell provides strongly catalytic sites and the synergistic effects also play a role. Thus, the core element does not play a significant role except for the shell growth and it also gives an electronic effect (a ligand effect) on the shell element because the surface atoms of the shell are coordinated to the core in their catalytic reactions **[80]**.

2.10.   Principles of electrocatalysis

Electrocatalysis is a distinct field in electrochemistry that has gained a special growth after the late eighties due to the application of new hybrid techniques **[81]**. Recently, the application of new concepts of electrocatalysis for industrial electrochemical processes has attracted a significant amount of attention for chemists and engineers. Electrocatalysis can be described as an electrochemical reaction with an adsorbed species, either as reactant and/or product, which can change the kinetics of the reaction and in some cases also the mechanism, selectively at electrode surfaces in electrochemical cells using materials exhibiting high catalytic activity towards the electrode processes **[82]**. Accordingly, electrocatalysts are a specific form of catalyst (substances that accelerate the rate of a chemical reaction without being transformed or consumed by the reaction) that functions at an electrode surface or it may be the electrode surface itself. So they act directly at the electrode/electrolyte interfaces to assist in transferring electrons between the electrode and reactants **[83]**. An electrocatalyst can be heterogeneous like platinum surface or nanoparticles, or homogeneous like enzyme or a coordination complex **[83]**.

43

Desirable electrocatalysts exhibit good corrosion stability over extended periods, good electrical conductivity, so as to minimise resistance loss and must be of low cost, while the activity, selectivity, yield and efficiency of electrochemical reactions are maximized. Nonetheless, it should be noted that the structure and performance of the electrocatalysts depend strongly on the preparation method **[84]**. Pt-catalysts, owing to its relatively high catalytic activity, it is the most commonly studied electrocatalyst. Moreover, it is used as the main component of a number of binary and ternary nanoalloys for ammonia electro-oxidation reaction. The sluggish reaction kinetics of ammonia electro-oxidation needs high Pt loading in the electrocatalysts in order to achieve acceptable reaction rates. However, because of its high cost and limited resources in some other parts of the world, Pt cannot be used for widespread applications **[85]**.

2.11. A variety of electrocatalysts for ammonia electro-oxidation

The primary purpose of using Pt-based core-shell, mixtures or even alloy nanocatalysts with cheaper base metals is to reduce the high costs of fuel cells **[86]**. Most importantly, when it comes to Pt-based alloys and core-shells, a very thin layer of Pt to form a shell can also help to reduce cost. The research is not only focusing on the low cost of Pt-based mixture, alloy and core-shell nanoparticles, but the increased catalytic activity, reliability, stability and durability are part of a package of benefits which comes with these materials **[86]**. Thus, these types of catalysts are promising to be a breakthrough in the hindered large-scale commercialization of direct ammonia fuel cells.

The demand for researchers to come up with new electrocatalysts which have similar or even higher catalytic activity than Pt, has been posed by avoiding the dependence of Pt metal catalysts in fuel cells. Since the properties of the catalyst surface are closely associated with the catalytic activities, catalyst surface modification with another component or changing the morphology could enable the controlled tuning of the catalytic properties. In light of that, a detailed description of the recent developments made towards improving ammonia electrolysis exclusively in anode electrode catalysts during the past few years are discussed in the following sub-sections.

These advances for ammonia electro-oxidation can be summarised as follows: firstly, the alloying of Pt with other cheaper metals that have a potential synergistic effect with Pt including other PGMs such as Ir, Ru and Rh; secondly, enhancing the mass activity of the Pt-based electrocatalysts by increasing the electrochemically active sites and/or controlling the surface structure of the electrocatalysts (shape, preferential orientation, morphology, etc.); thirdly, developing well-performing Pt-free electrocatalysts; and lastly, exploring appropriate support strategies which have a positive effect on improving the performance of the electrocatalysts **[15]**. An overview of the performance of the typical varieties of electrocatalysts used for ammonia electro-oxidation is given below:

2.11.1. Pure metal electrocatalysts

Even though Pt is expensive, it is still the most active metal catalyst used for enhancing the reaction rate of the ammonia electro-oxidation. Katan and Galiotto **[67]** explored the electro-oxidation of ammonia on a Pt black electrode, which was fabricated by spreading precipitated Pt black on sintered Ni plates in a solution of 3 M ammonia + 6.9 M KOH at 23 ℃. Their study gave an average current efficiency of 99.7±1.8% for N_2 production at current densities from 10 to 100 mA cm^2.

In other similar studies, electrocatalysts in which the noble metal is deposited on an inactive base substrate (e.g., Ni, Ti and carbon-based materials) were reported **[87, 88]**. For instance, the cyclic voltammetric studies on a RANEY Ni supported Pt in 1 M NH_3 + 1 M KOH solution showed a well-defined peak around 0.2 V (vs. Hg/HgO), confirming the activity of the electrocatalyst for ammonia electro-oxidation **[89]**. The electrochemical activity of Pt/RANEY Ni towards ammonia electro-oxidation was similar to that witnessed for a pure Pt, although it seemed to exhibit a much higher oxidation current density.

In many cases, Pt was able to support the electro-oxidation of ammonia at a reasonable rate. However, in addition to Pt, many other metals have been investigated for this reaction. De Vooys and co-workers carried out a detailed study on the electrocatalytic oxidation of ammonia in alkaline media focusing on a range of polycrystalline transition metal (Pt, Pd, Ru, Rh and Ir) and coinage metal (Cu, Ag and Au) electrodes using a combination of cyclic

voltammetry and online electrochemical mass spectrometry (DEMS) [69]. The authors discovered that the activity of the electrode towards the selective oxidation to N_2 was related directly to the type of the species at the surface, i.e. the electrode was active if NH_{ads} or $NH_{2,ads}$ was present and deactivated in the presence of N_{ads}. This was in agreement with the Gerischer-Mauerer mechanism. The potential at which NH_{ads} or N_{ads} was formed was metal dependent. The observed trend in the strength of adsorption of N_{ads} was Ru > Rh > Pd > Ir > Pt>>Au, Ag, Cu. The Sabatier principle [90] was employed to describe the relationship between the activities of different metals for the selective oxidation of ammonia to N_2. Coinage metals such as Cu, Ag and Au, have a low affinity for N_{ads} and are inactive in the selective oxidation to N_2 since the active intermediates (partially dehydrogenated ammonia species $NH_{2,ads}$ or NH_{ads}) are not formed. However, in the case of PGMs such as Ru, Rh and Pd with a high N_{ads} binding energy, ammonia is dehydrogenated at much lower potentials compared to Pt and Ir, leading to the formation of surface poisonous N_{ads} at much lower potentials than on Pt and Ir. Hence, Ru, Rh and Pd show little activity for ammonia electro-oxidation. Only Pt and Ir have been proven to have a good dehydrogenation capacity with a sufficiently low affinity for the formation of N_{ads}, leading to a steady-state production of the active intermediates needed to produce N_2. Endo *et al.* [91] reported a cyclic voltammetry study, wherein the main oxidation peak on Ir was observed at a lower potential than on Pt, showing that Ir probably had a lower overpotential for ammonia electro-oxidation than Pt. However, the peak current density on Ir was much lower than that on Pt.

2.11.2. Platinum (Pt) based binary or ternary electrocatalysts

The importance of ammonia oxidation has led to numerous investigations about metal catalysts like heterometallic nanoparticles. Heterometallic nanoparticles are emerging as an important type of catalyst. Bimetallic NPs with alloyed and core-shell structures are said to have higher catalytic activities than their monometallic counterparts due to the synergistic effects acting between the two metals [80]. In addition, synergistic catalysis of trimetallic and multimetallic NPs has also attracted considerable attention in recent years. Therefore, advances have been made to enhance the catalytic activity of pure Pt by fabricating Pt-based binary and ternary (reduced Pt loading) catalysts.

In general, developing Pt-based alloys causes a series of effects, like the surface segregation of one element [92], geometric change (decrease of the Pt–Pt bond distance) [93] and a change in electronic structure of Pt (increase of Pt d-electron vacancies) [94] , which might contribute to the enhanced electrocatalytic activity of Pt. Some of platinum group metals such as Ir and Ru are so far the most studied elements for alloying to Pt, even though their results concerning their effect on enhancing the electrocatalyst performance are controversial. It has been reported that the controversy for their alloying effect on the catalytic activity can be credited to the modifications in electrochemical test conditions and preparation methods [15].

The application of binary alloys for enhancing the electro-oxidation of ammonia was also described by Mishima *et al*. [95] who studied the electrochemical oxidation of ammonia in KOH solutions on a Pt and Ir black electrodes, with a mixture of both and a Pt–Ir alloy prepared by an electrodeposition method. The authors reported that both the mixture of Pt and Ir black powders and the electrodeposited Pt–Ir alloy displayed superior activity than that of Pt black or Ir black based on ammonia oxidation currents at E = +0.6 V (vs. RHE). In a similar study, Moran *et al*. [96] also proposed the application of Pt–Ir for ammonia electro-oxidation, also obtained by an electrodeposition method. The DEMS analysis results indicated that N_2 was the major product during ammonia electro-oxidation for both Pt and Pt–Ir at lower potentials. However, the yield of N_2 was higher for the Pt–Ir alloy, while lower poisoning levels of the surface with increasing ammonia concentration was also observed. In contrast, the onset potential for ammonia oxidation at Pt–Ir was slightly shifted to a more positive potential (ca. 0.05 V) compared to pure Pt.

Recently, Endo *et al*. [70] fabricated various $Pt_{1-x}M_x$ (M = Ir, Ru or Ni) bimetallic alloys on a glassy carbon (GC) substrate by a thermal decomposition method and interrogated their electrocatalytic activities for ammonia oxidation in presence of KOH. The authors found that the saturated current density at a low oxidation potential was higher on $Pt_{1-x}Ir$ ($x \leq 0.8$) or $Pt_{1-x}Ru_x$ ($x \leq 0.4$) than that on Pt, signifying a positive synergy of Ir and Ru with Pt in the ammonia electro-oxidation. Therefore Ir or Ru was able to dehydrogenate ammonia at a lower potential than Pt, contributing to the enhanced electrocatalytic activity for ammonia oxidation when alloyed with Pt, whereas alloying of Ni with Pt lowered the current density of Pt with x in $Pt_{1-x}Ni_x$ ($0.2 \leq x \leq 0.7$) and did not lower the onset potential of ammonia electro-oxidation. In another interrelated study [91], it was reported that both $Pt_{0.5}Cu_{0.33}$ and $Pt_{0.67}Cu_{0.33}$ alloys showed an electrocatalytic activity inferior to Pt. Therefore, according to

47

authors, alloying of Pt with Cu and Ni will lead to a decrease in the electrocatalytic activity for ammonia oxidation.

Bonnin and co-workers [97] conducted a similar study where a comparison between cyclic voltammetry and galvanostatic performance of various electrodes such as Pt-Ir, Pt-Rh, Pt-Ir-Rh and Pt was investigated for the electro-oxidation of ammonia at low concentrations. According to their results it was found that Pt-Ir-Rh showed the lowest onset potential, even though the peak current was highest for pure Pt. Furthermore, the Pt-Ir –Rh electrode exhibited the highest current density coupled with the lowest voltage for all tested currents during the galvanostatic experiments. The authors concluded that Pt-Ir-Rh and Pt-Ir supported on carbon fiber substrates were the most promising electrodes for ammonia electrolysis at low concentrations [97].

It is worth noting that the effect of alloying elements to Pt is strongly dependent on the electrochemical test conditions. Thus, in general, based on the review of literature data, it appears that the electrochemical tests based on the galvanostatic or potentiostatic measurements usually come to the conclusion that alloying of Pt with e.g. Ru or Ir has a positive effect on improving the activity whereas the cyclic voltammetry studies often lead to a contrary conclusion [15]. For instance, Vidal-Iglesias *et al*. [12] reported a negative effect for alloying Pt with other metals by using cyclic voltammetry measurements. The ammonia electro-oxidation on different Pt–M (M = Ir, Rh, Pd and Ru) binary nanoparticles was investigated. Their findings revealed that the incorporation of a second metal such as Ir, Pd, Rh and Ru, caused a significant loss on the peak current density (i.e. maximum activity) for ammonia electro-oxidation. According to the authors this significant drop in current density was attributed to a decrease of the density of Pt (100) surface sites that are particularly active for ammonia electro-oxidation. For the nanoparticles containing Ir or Rh with high Pt loadings (e.g., $Pt_{75}Ir_{25}$ and $Pt_{75}Rh_{25}$), the onset potential of the ammonia electro-oxidation process shifted towards less positive potentials producing higher current densities than pure Pt nanoparticles [12]. The authors then concluded that the use of these binary nanoalloys did not significantly improve the activity of pure Pt, emphasising that the alloying of Pt with Ir or Ru enhanced the ammonia electro-oxidation only in the low oxidation potential region. Consequently, when Pt alloys are used, caution should be paid to the operating conditions (e.g., working mode and electrode potential).

2.11.3. Platinum (Pt) free electrocatalysts

The fabrication of Pt-free electrocatalysts is another way of significantly reducing electrocatalysts cost. These non-Pt electrocatalysts include mostly metal oxides such as $Ni/Ni(OH)_2$, IrO_2 and RuO_2 and boron-doped diamond (BDD). The problem with these materials is that, in contrast to the amount of information available for Pt and Pt-based alloys, little is known about the mechanism of ammonia electro-oxidation on the surface of these catalysts [98]. In comparison to ammonia electro-oxidation on Pt-based anode materials, ammonia electro-oxidation on metal oxides and BDD usually occur at a high overpotential, leading to a low current efficiency. Furthermore, on a Pt-based electrocatalyst ammonia can be selectively oxidised to N_2 in the potential window where Pt is without adsorbed oxygen. Conversely, that is not the case for the majority of metal oxides and BDD electrodes as oxygenated nitrogen species (e.g., NO, N_2O, nitrite and nitrate), apart from N_2 have also been found during ammonia oxidation [15]. However, it is should be taken into consideration that in many applications, such as the remediation of ammonia-contaminated wastewaters and ammonia-based fuel cells, the preferred ammonia oxidation product is elemental nitrogen, rather than further oxidation products. Therefore, it is highly advisable to develop non-Pt electrocatalysts and electrolytic conditions which display maximum chemical and current efficiency towards electrochemical decomposition of ammonia to environmentally friendly nitrogen gas.

In a study conducted by Ge and Johnson, [99] they investigated ammonia oxidation in an alkaline solution at the surface of Ag-Pb eutectic alloy electrodes (2.4 wt% Ag), the anodic responses were observed at very high overpotentials compared to Pt-based electrodes. At a pH of < 8, the anodic signal faded due to the protonation of NH_3 to form NH_4^+. It was reported that protonation of NH_3 prevents adsorption of the NH_3 at Ag sites as the expected in the first step of ammonia electro-oxidation. According to their findings, authors concluded that NO_3^- was the final product in the electrolysis of ammonia, which is also different to the product observed in the case of Pt-based electrocatalysts.

In view of the electrochemical removal of ammonia from environmental wastewater, metal oxides such as IrO_2 and RuO_2 are used as dimensionally stable anodes (DSA) owing to their metal-like properties [100, 101]. Donten *et al*. [102] studied the electro-oxidation of ammonia

49

in a Na_2SO_4 solution at the surface of $Ti/TiO_2/RuO_2$ electrode. The ammonia oxidation response was identified as a well-defined anodic peak at 0.8 V (vs. SCE), with the major product formed being elementary nitrogen, while nitrate was formed as a minor product. Additionally, the pH optimisation study carried out indicated that the height of the anodic voltammetric peak of ammonia was found to be linearly dependent on the ammonia concentration in a millimolar range. In a similar study by Kim *et al*. [108] the effects of pH, the supporting electrolyte type and chloride ion on the decomposition rate of ammonia into N_2 and the by products produced in presence of the IrO_2 electrocatalyst, was investigated. It was found that in the basic solution, ammonia was oxidised mainly to N_2 with some small yield of nitrate and nitrite ions as by products through a direct electrolytic reaction in addition to adsorption at the electrode where the oxygen evolution rarely occurred. On the other hand, in neutral and acidic solutions, the ammonium ion was partly oxidised to N_2 by the OH radicals generated at the oxide surface under the oxygen evolution condition through an indirect electrode reaction. However, the decomposition rate in the neutral and acidic media was much lower than that in the basic condition. In contrast, the chloride ion coexisting with ammonia resulted in an increase in the decomposition yield of the ammonia by the active hypochlorite ion generated at the electrode. The conversion yields of ammonia to N_2 ranged from 6.8 % to 62.5% depending on the solution conditions. Hence, they concluded that the electrochemical decomposition path and products of the ammonia are strongly dependant on the conditions of the ammonia solution [103].

In a subsequent study, the same authors (Kim *et al*.) [104] improved the performance of the IrO_2 anodes for ammonia electrolysis by using a continuous multi-cell-stacked electrolyser consisting of an ion exchange membrane with a self-pH-adjustment function. The obtained current efficiency for the decomposition of ammonia to N_2 at a pH of 7 and a pH 13 was 32% and 52% respectively. When the concentration of ammonia was reduced in the effluent from successive cells, the overall current efficiency was stated to be 76% with a decreasing current efficiency from cell to cell.

2.12.   Factors affecting the performance of the electrocatalysts

The nature of the electrocatalysts and the operating conditions affects the performance of the electrocatalysts significantly. The design of the electrocatalysts towards ammonia electro-oxidation is all about creating a surface that balances the stabilization of active intermediates and the fast desorption of the oxidation products, whist simultaneously decreasing the activation energy of reactions [15]. Moreover, the performance of the electrocatalyst can be categorised by a series of parameters including (1) mass activity (MA, activity mass^{-1}): current density normalized by the mass of the electrocatalyst as measured at a specific potential, (2) specific activity (SA, activity area^{-1}): current density normalized by the electrochemically active surface area (ECSA) of the electrocatalyst, (3) specific, electrochemically active surface area (SSA, area mass^{-1}): ECSA normalized by the mass of the electrocatalyst and (4) durability: the ability of the electrocatalyst to resist permanent change in performance over time [15]. According to the above definitions, the MA, which is the most important parameter, can be generally expressed as follows:

$$MA = SSA \times SA \quad\quad\quad\quad\quad\quad\quad\quad\quad\quad (34)$$
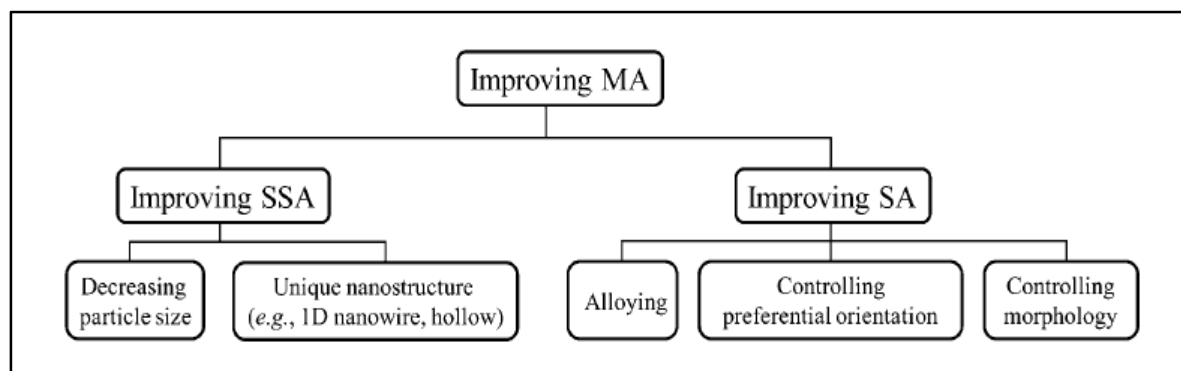
Scheme 8: Approaches for enhancing the mass activity (MA) of the electrocatalysts for ammonia electro-oxidation, (obtained from ref [15]).

As can be seen in equation (34), the electrochemically active surface area of the electrocatalysts can be enhanced by increasing MA (and thus the Pt loading can be lowered) while increasing the SSA of the catalysts. This can be easily accomplished by reducing the

particle size so as to increase the surface to volume ratio and thus increasing catalytically active sites per mass.

In addition to improving the SSA, SA can also be enhanced to increase the MA of the electrocatalysts. This can be attained by a variety of strategies, like alloying, controlling the surface structure, morphology and preferential orientation **[15]**. Thus in this subsection, a brief report on the highlights of the previous work where the authors investigated the effect that preferential orientation, morphology, support materials and electrochemical test conditions have on the performance of the electrocatalysts is discussed. This section is very important as it gives an insight into the optimisation of the electrocatalyst performance.

2.12.1. Preferential orientation effect

Pt and Pt-based materials are still considered to be the most effective electrocatalysts for ammonia electro-oxidation. However, the electro-oxidation of ammonia has been found to be highly structure sensitive. Hence, various crystal surfaces of Pt can display very different electronic structures and atomic arrangements, **[105, 106]** leading to unique reactivity towards ammonia electro-oxidation.

Vidal-Iglesias *et al*., **[107]** were the first to report on the effect that Pt surface structure have on ammonia electro-oxidation in basic media. This was investigated by carrying out the study of electro-oxidation of ammonia on a series of single crystal Pt electrodes. The results obtained proved that the ammonia electro-oxidation is extremely sensitive to both the domain size and type of site. Thus the reaction takes place exclusively on (100) sites **[77, 107, 108]**. In their subsequent study, they used stepped surfaces containing (100) terraces and (111) monoatomic steps and it was found that the electro-oxidation of ammonia was also dependent on the width of the (100) domains **[77]**. The authors concluded there is a possibility that the geometry of the surface may affect various stabilities of the formed reaction intermediates.

In an effort to explain the observed difference in activity between Pt (111) and Pt (100) surfaces, Rosca and Koper **[75]** carried out the electro-oxidation of ammonia on Pt (111) and Pt (100) using voltammetry, chronoamperometry and *in situ* infrared spectroscopy measurements. It was found that the catalytic difference is due to differences in their ability

to stabilize the adsorbed intermediates (NH$_2$ fragment) on the surface. Hence it was proposed that the high activity of Pt (100) could be ascribed to the ability of the Pt (100) surface to stabilize the adsorbed NH$_2$ intermediate on the Pt surface. In a similar study, Solla-Gull´on *et al*. [76, 109] also emphasised the importance of controlling the surface structure of both bulk electrodes and nanoparticles. They compared the catalytic activity of preferentially oriented Pt (100) nanoparticles with polycrystalline Pt nanoparticles on ammonia electro-oxidation.

2.12.2. Morphological effect

In addition to the preferred orientation effect, recent work showed that controlling the shape of Pt-based electrocatalysts to more complex morphologies (e.g., dendritic-like morphology) is another strategy to improving Pt activity (i.e., MA) towards ammonia electro-oxidation [110-112]. It was reported that by just increasing the deposition current density during the electrodeposition process, the morphology of the deposited Pt particles changed from smooth spherical particles to 3D flower-like and sheet-like particles [111]. The morphological change of the Pt particles was attributed to the change of the diffusion control degree during electrodeposition. The MA of the flower- and sheet-like Pt particles was found to be about 3 times higher than the smooth spherical Pt particles. Further analysis on the critical role of the morphological effect in the observed improvement of SA also confirmed that the presence of an open dendritic morphology in the surface of these Pt particles, results in enhanced catalytic performance owing to the high accessibility of guest species and the rich corner atoms of their surface [112, 113].

2.12.3. Electrocatalyst supports

In electrocatalysis, catalysts are usually dispersed on an appropriate support. The support material helps in improving the catalytic activity and durability of the electrocatalyst through the enhancement of dispersion degree, particle size, size distribution, morphology, alloyed degree, mass transport and electrical conductivity [15]. An ideal support material should meet the following requirements such as (1) high specific surface area, which is essential for

improving the dispersion of catalytic materials, (2) high electrical conductivity and (3) high electrochemical stability under ammonia electro-oxidation conditions. The commonly used support materials for ammonia electro-oxidation include carbon-based materials (e.g., carbon powders and carbon fibers), metallic materials (e.g., Ti and RANEY Ni) and metal oxides. Carbon black (e.g., Vulcan XC-72) is the most frequently used catalyst support due to its large specific surface area, good electrical conductivity, porosity and relative stability in both acidic and basic media **[13, 114, 115]**.

To justify the importance of electrocatalyst support, Bonnin *et al*. **[97]** carried out a comparison study between the use of RANEY nickel and carbon fiber as substrates for the electrodeposition of Pt-based alloys. The results obtained showed that electrodes prepared on a carbon fiber substrate exhibited higher activity towards the electro-oxidation of ammonia at low concentrations compared to the catalysts on a RANEY Ni. The authors concluded that carbon fiber was a better substrate than RANEY Ni for the electro-oxidation of ammonia owing to: (1) uniform coverage by noble metals, (2) minimal surface blockage effect and (3) light weight presented by carbon fiber. This behaviour was ascribed to an increase of the surface area. Boggs and Botte **[18]**, further developed optimization of the electrodeposition parameters for depositing Pt and Pt alloys on carbon fiber paper substrates.

2.12.4. Parametric influence of the electrochemical test conditions

Another crucial factor affecting the performance of the electrocatalyst is the electrochemical test conditions during operation of the electro-oxidation of ammonia. Therefore various electrochemical methods have been developed in order to restore the activity of the electrode during the oxidation of ammonia **[10, 116]**. In their previous work, Zhong and Cheng **[65]** studied the anodic ammonia oxidation reaction and the cathodic hydrogen evolution reaction systematically by cyclic voltammetry on Pt surface as electrocatalyst. The aim was to interrogate the effect of various electrolytic parameters and operation conditions, such as ammonia concentration, support electrolyte (KOH) concentration, electrode rotating speed, temperature, upper switch potential, potential sweep rate and cyclic number. The results showed that the oxidation of ammonia on a Pt electrode was controlled by a mass-transfer process of ammonia towards the electrode surface.

Through their optimization studies, optimal ammonia concentration and KOH concentration were obtained which maximize the ammonia oxidation and hydrogen evolution currents simultaneously. Furthermore, it was reported that the role of the solution alkalinity in ammonia electro-oxidation was essential for enhancing the oxidation of ammonia and decreasing both the oxidation reaction overpotential and hydrogen evolution. Thus, from their findings they concluded that an optimal KOH concentration is crucial to the ammonia electrolysis especially for hydrogen generation purposes [65].

2.13. Nanoalloys

In many cases, alloying tends to enhance certain properties of materials due to synergistic effects which come with mixing two or more metals of different properties together. Alloying metals further opens the opportunities for diverse structures, properties and compositions which lead to widespread applications in engineering, catalysis and electronics [117].

The ability to produce, modify and even control the properties of materials on the nanometer scale has attracted interest in bimetallic and trimetallic nanoclusters/nanoparticles which are also known as alloy nanoclusters or nanoalloys. Just like bulk alloys, nanoalloys also have a wide range of combinations and compositions depending on the applications they are meant for. The structures of nanoparticles and the degree of separation or mixing between two or more metals in bimetallic or trimetallic nanoclusters may depend on a few factors. The factors involved include method and conditions of cluster generation (i.e. temperature, pressure, type of cluster source, etc.) [117, 118]. All of these factors lead to a variety of nanoclusters of differing properties. Furthermore, nanoalloys can also be generated in either colloidal solution, cluster beams: they can be immobilized on surfaces, can be formed inside porous materials or by decomposing/dealloying bimetallic organometallic complexes [117].

At the moment, interest and efforts are being dedicated to the ability to tune the chemical and physical properties of the alloy nanoparticles by varying the atomic ordering, composition and size of the clusters because they are important in controlling and determining their catalytic activity [119]. The other main reason for interest in nanoalloys is that they exhibit improved unique structures and properties which are distinct from those of their pure bulk or

elemental cluster counterparts **[80, 120, 121]**. That is the structures, physical and chemical properties of bimetallic clusters may be different from the structures and properties of the pure cluster of the same type and size. Synergism is often observed in catalysis or electrocatalysis by binary nanoalloys. This extraordinary behaviour is attributed to finite or quantum size and surface effects **[80, 119]**. The fact that the individual metal atoms have different electronegativities and atomic electron configurations also adds to the distinctive properties observed.

2.13.1. Types of nanoalloys

Generally, nanoalloys can be categorised according to their chemical ordering/mixing patterns and geometric structure **[117]**.There are four main types of chemical ordering for nanoalloys **[117]** as illustrated in **Figure 1**.
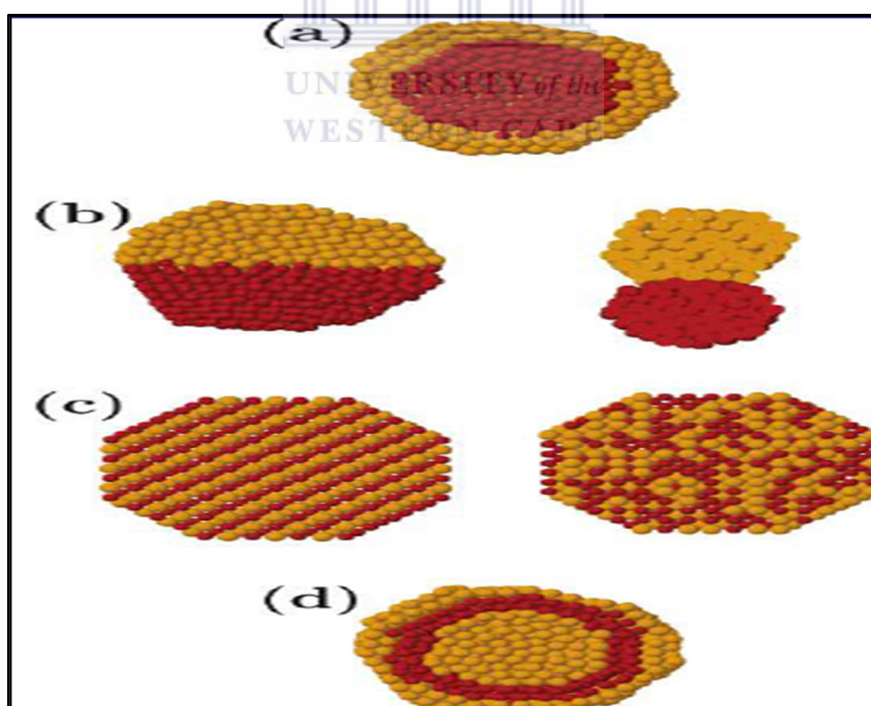
Figure 1: Schematic representation of the cross-sections of the main, possible mixing patterns: core-shell (**a**), sub cluster segregated (**b**), mixed (**c**), three shell (**d**) structures, (extracted from ref **[117]**).

56

Core-shell segregated nanoalloys (Figure 1a)

They consist of a core of one type of atom (A) surrounded by a shell of another (B) and are usually denoted as $A_{core}B_{shell}$. It is possible to have some mixing between shells.

Sub cluster segregated nanoalloys (Figure 1b)

This type consists of A and B sub clusters which may share a mixed interface (left) or may also have a small number of A-B bonds (right).

Mixed A-B nanoalloys (Figure 1c)

Here clusters may be either ordered (left) or randomly (right) mixed. Random mixed nanoalloys are referred to as "alloyed" nanoparticles.

Multi-shell nanoalloys (Figure 1d)

The pattern may present layered or onion-like alternating A-B-A shells.

2.13.2. Factors influencing segregation, mixing and ordering in nanoalloys
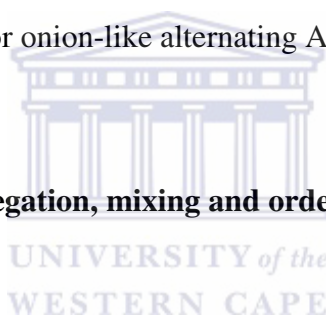
The degree of segregation/mixing and atomic ordering in A_mB_n nanoalloys depends on the balance of the following factors **[117, 122]**:

- Relative strengths of A-A, B-B and A-B bonds. For instance, if A-B bonds are strongest, this will favour mixing; otherwise if the bonds are weak, segregation will be favoured.

- Charge transfer, the electron transfer from less to more electronegative elements favours mixing.

- Specific electronic or magnetic effects. That is electronic shell structure or electron spin interactions may stabilize certain compositions, sizes and/or segregation arrangements.

- Surface energies of bulk elements A and B. The element with lowest surface energy tends to segregate to the surface.

- Relative atomic sizes. The smaller atoms prefer to occupy the more sterically confined core.

- Strength of binding to surface ligands (surfactants). For coated or supported clusters, the element that strongly binds to the support or ligands may be pulled out toward the surface.

The observed atomic arrangement for a particular nanoalloy depends critically on the balance of the factors outlined above, the preparation method and experimental conditions [117].

2.13.3. Preparation methods of nanoalloys

There are various methods for the preparation of nanoalloys such as in solution, in the gas phase, in a matrix or supported on the substrate; thus the method varies depending on the desired application of materials to be synthesised. The preparation methods play a crucial role in determining the final performance of the electrocatalysts particularly fabricated from nanoalloys since they affect a series of chemical and physical properties of the electrocatalysts such as the composition, alloying degree, particle size, surface structure and morphology [15]. Furthermore, the nanoalloys can be synthesised from concurrent or successive reduction of the metal salts. However, in most cases the simultaneous reduction of individual metal ions to form metal nanoalloys is challenging due to a huge difference in redox potentials of involved metals. Hence, redox potentials play a significant role in controlling the structure of the nanoalloy. Many of the methods for generating nanoalloys are the same as for pure monometallic clusters, although there may be additional complexities [117]. Common synthetic pathways for the preparation of nanoalloys are discussed below:

2.13.3.1. Electrochemical synthesis

Electrochemical synthesis is a very versatile and attractive method for generating nanoalloys in solution. The most common technique is electrochemical deposition (ECD) because it offers the possibility of controlling the process simply [118]. In electrochemical syntheses,

the current is applied at a certain potential in a solution containing metal salts in the presence of a suitable supporting electrolyte. During this process the NPs are deposited on the electrode surface. The advantages of this process include low cost, no contamination with by-products, it allows simple control of the metal content of bimetallic NPs and more reactive metals can act as the reducing agents for more noble metals. The only drawback is that it gives relatively low product yield **[117, 118]**.

2.13.3.2. Microwave synthesis

Microwave synthesis is a commonly employed method for the synthesis of a wide variety of inorganic (pure metallic and bimetallic alloy) NPs since it is facile, fast and energy-efficient as no high temperatures or high pressures are needed **[123]**. Microwaves are generally generated using a magnetron. The reactants absorb microwave energy, which is then converted to heat causing the rapid decomposition of the precursors and creating highly supersaturated solutions, whereby nucleation and growth occur to produce the desired nanocrystalline products **[124]**.

Furthermore, the advantage of microwave heating (irradiation) (MWI) is that it is very useful for controlled large-scale synthesis, since it minimizes the thermal gradient effects **[125]**. In addition, nanoparticle size can be controlled by changing the concentration of the precursor and the MWI duration, while the shape of formed nanostructures is controlled by varying the concentration and composition of the ligating solvents **[118]**.

2.13.3.3. Chemical reduction

This method is one of the most important methods, because of the simplicity and the possibility of its application in any chemical laboratory. Hence, many, various, nanoalloys are generated by the chemical reduction of metal salts dissolved in an appropriate solvent and surfactant such as citrate, thioethers, or alkylthiols) or polymeric ligands (e.g., polyvinylpyrrolidone, PVP), which passivates the nanoalloys surface **[117, 118]**. Colloid

preparation can be single phase or two phase, whereby colloids form at the interface between an aqueous layer (in which the metal salt is dissolved) and an organic layer (containing the surfactant and reducing agent). They can also be generated by using inverse micelles. The control of average particle size and size distribution can be achieved by tuning the preparation conditions (solvent, surfactant, reducing agent, etc.) or varying the size of the inverse micelles. The advantage of this method is that it gives a high yield, while the disadvantage is contamination from surfactants/capping agents and by-products [117].

Chemical reduction methods can be divided into two main strategies which are: co-reduction and successive reduction of metal salts. In a co-reduction method, bimetallic nanoalloys can readily be prepared by the simultaneous chemical reduction of the appropriate mixture of salts in the solution phase using reducing agents such as $NaBH_4$, N_2H_4 (hydrazine) and H_2 gas. Generally during co-reduction, the metal species with the highest redox potential precipitates first, forming a core on which the second component is deposited as a shell. The order of deposition can be changed by performing the reduction in the presence of a surfactant that bonds more strongly to the metal with the higher redox potential, stabilizing the inverse-core-shell arrangement. On the other hand, successive reduction is based on the reaction of preformed clusters whereby atoms of one metal can be deposited onto a preformed cluster of another metal via the "seed-germ" process wherein a cluster without passivating ligands, or with weakly bonded surfactant molecules, undergoes a second reduction step in the presence of salts of the other metal [117].

2.13.3.4. Thermal decomposition of transition-metal complexes

Thermal decomposition, which is also known as thermolysis, is defined as chemical reaction in which complexes containing two or more metals, break up into at least two elemental metals when heated. This process has been used to produce nanoalloys of the more noble metals. The use of stabilizing ligands like PVP helps in improving the quality of the obtained results. Precursors can be mixtures of metal-containing complexes. A series of nanoalloys was obtained via the thermolysis of compounds, which had low stability at elevated temperatures. The main advantage of this method is to eliminate phase separation and composition control issues [118].

2.13.3.5.   Radiolysis

Radiolysis of aqueous solutions is an efficient method for reducing metal ions in order to generate nanoalloys. In the radiolytic method, gamma-ray (ý-ray) irradiation of water leads to solvated electrons which subsequently reduce the metal ions **[117]**. Radiolysis of aqueous solutions of two metals, can lead to formation of core-shell or alloyed nanoparticles depending on the rate of radiolysis (which depends on the ý -ray dose), the relative concentrations of the two metals, the rate of interion electron transfer and the nature of ligands which are coordinated to the metal ions. This method has been used to synthesise (among others) Ag-Au, Cu-Ag, Pd-Ag, Pt-Ag, Pd-Au, Pt-Au, Cu-Pd and Ni-Pt nanoalloys. Higher ý-ray dose rates favour mixing over core-shell formation; though for some systems mixing can take place at moderately low dose rates **[126]**.

2.13.3.6.   Ion implantation

The implantation of metal salts is done on the insulating matrices generating a solid-solution of nanoalloys. Metal nanoalloys embedded in insulating matrices are of interest for magnetic, optical and catalytic properties. The sequential implantation of two different metal ions has been used to generate implanted binary nanoalloys. Examples of such nanoalloys include: Ag-Au, Cu-Pd and Cu-Au nanoalloys implanted on silica using beams with energies of approximately 100 keV **[127]**.

2.13.3.7.   Biosynthesis

It is known that certain microbes themselves can reduce metal salts to their zero-valent metallic states. The traditional and most widely used synthetic methods for metallic nanoparticles use wet-chemical procedures. However, their drawbacks include contamination from precursor chemicals, use of toxic solvents and generation of hazardous by-products **[128]**. Hence, the biological approach for synthesis of nanoparticles becomes important. Over

the past several years, plants, algae, fungi, bacteria and viruses have been used for production of low-cost, energy-efficient and nontoxic metallic nanoparticles [128, 129]. The advantage of biological synthesis of NPs is that the process is scalable, offers particle size and shape control and can even be coupled to the remediation of precious metal-containing wastes [130].

A common *Lactobacillus* strain present in buttermilk was exposed to large concentrations of metal ions to produce microscopic gold, silver and gold-silver alloy crystals of well-defined morphology [131]. Cyanobacteria have also been observed to produce AgNPs. Another example is a spontaneous biosynthesis of cadmium sulfide (CdS) semiconductor nanocrystals done by incubating *Escherichia coli* with cadmium chloride ($CdCl_2$) and sodium sulfide (Na_2S) [132].

2.13.3.8.   Sol-gel methods

The sol–gel method is mainly employed for the synthesis of metal oxide NPs and oxide nanocomposites. The sol–gel process involves the hydrolysis and condensation of metal precursors [133]. The sol–gel process can be either in aqueous or non-aqueous media. In the aqueous sol–gel process, water molecules serve as the source of oxygen for the formation of the oxide. Whereas, in the non-aqueous process, oxygen is provided by the solvent (ethers, alcohols, ketones, or aldehydes) or by an organic constituent of the precursor (alkoxides or acetylacetonates) [134]. The condensation process in non-aqueous sol–gel synthesis involves metal–oxygen–metal bonds formed either by alkyl halide elimination, ester elimination, ether elimination, or by aldol-like condensation [133].

2.13.3.9.   Hydrothermal and solvothermal synthesis

Hydrothermal–solvothermal synthesis is a common method employed to synthesise inorganic NPs. Properties of the reactants, such as their solubility and reactivity change in the solvent or water at elevated temperatures and pressures have to be taken into consideration. Thus by

taking advantage of the high reactivity of metal salts and complexes at elevated temperatures and pressures, inorganic nanomaterials are prepared at temperatures considerably lower than in solid-state reactions. Reaction parameters such as time, temperature, pressure, reactant concentration, pH, can be tuned to attain acceptable nucleation rates and particle size distribution. Both hydrothermal and solvothermal synthesis methods can be used to prepare NPs of metals, oxides, chalcogenides, pnictides and various materials **[133]**.

2.13.4. Applications of nanoalloys

Nanoalloys can be used in a number of technologically important areas such as catalysis, optoelectronics, magnetic and medical applications.

2.13.4.1.   Catalysis

Catalytic applications of nanoalloys are of great importance. It is known that classic noble-metal catalysts, such as palladium, platinum and ruthenium, are the most frequently used in synthesis. However, their industrial large-scale applications are certainly limited, because of their high cost. In this case, synthesis of nanoalloyed catalysts such as M_1M_2, where M_1 = Pd, Pt, Au and the less-expensive M_2 = Ni, Cu and Co, could decrease their cost without reduction in their high catalytic activity, due to the presence of M_1 **[118]**. The catalytic properties were found to be highly dependent on the preparation method **[135]**.

Nanoalloys have higher catalytic properties compared to monometallic nanoparticles. Based on their extraordinary catalytic properties nanoalloys have been applied in many areas of catalysis including in various types of fuel cells where nanoalloys are employed as electrocatalysts to decrease the overpotential of electrochemical reactions, in enzyme kinetic studies where conducting metal NPs are used as electron transfer "mediators" for enhancement of electron transfer and for electro-analysis in sensors and biosensors to improve mass transport, high effective surface area and catalytic properties **[136-139]**. In addition, large surface area and high surface energies enable NPs to adsorb biomolecules,

thus making immobilization and biocompatibility of biomolecules easy **[137]**. Other applications of nanoalloys are not as frequent as in the field of catalysis.

The catalytic properties of metals may be modified and fine-tuned by alloying, i.e., forming bimetallic solids. The same is true for small metal particles and nanoparticles and the field of alloy nanocatalysis is currently attracting a lot of attention **[117]**. According to the experts, in the field of catalysis, the mutual influence of different neighbouring atoms can lead to catalytic behaviour which is different (and often enhanced) than that of the monometallic clusters, i.e., "synergistic effects" are observed. The layered (core-shell) bimetallic nanoparticles offer even more fascinating prospects for the design of new catalysts **[117, 118, 128]**.

2.13.4.2. Optoelectronics

Some nanoalloys show strong absorption bands in the visible region caused by "surface plasmon" resonance effects **[143]**. The surface plasmon resonance effect is due to extensive electronic correlation and corresponds to a collective excitation of weakly bound electrons relative to the ionic cores, i.e., the correlated motion of the cluster's itinerant electrons in the attractive field due to the positively charged ionic cores **[117]**. Therefore, nanoalloys due to their unique optical properties, they have found great applications in optoelectronics.

2.13.4.3. Magnetic applications

Recently there has been much interest in granular materials formed by embedding nanoparticles in a solid host **[117]**. When magnetic 3d metal nanoparticles (e.g. of Cr, Fe, Co, Ni or mixtures of these metals) are embedded in nonmagnetic metals, or even insulators, they exhibit the phenomenon of giant magneto-resistance (GMR), with a change in resistance upon application of a magnetic field. Such GMR materials are promising for applications as magnetic sensors and magnetic recording. This has led to the study of bimetallic nanoalloys formed between magnetic 3d metals and nonmagnetic 4d (e.g. Rh, P and Ag) or 5d metals

(e.g. Pt, Au). The combination of 3d metals (e.g. Co and Ni) with large local magnetic moments and 4d metals (e.g. Rh) with strong spin-orbit coupling may be an effective way of obtaining a high magnetic moment and anisotropy which is required in high-density magnetic recording [117]. For example, 3d-5d Fe-Pt and Co-Pt nanoalloys are candidates for ultrahigh density magnetic recording media due to their high magnetic anisotropy with associated high magnetic susceptibility and coercively [140].

2.13.4.4. Medical applications (Biodiagnostics)

In the past decade, there has been tremendous growth in the use of nanoalloys in biodiagnostics such as for bioconjugation, as cellular labels and in assays for gases, metal ions and DNA/protein markers for diseases [141]. Nanoalloys offer the possibility of enhanced robustness, sensitivity and selectivity. So, based on their tunability, (in terms of composition and ordering as well as size and shape) nanoalloys show considerable promise as biodiagnostic agents [117]. For example, Mirkin and colleagues used $Ag_{core}Au_{shell}$ nanoparticles (50-100 nm diameter) as tunable colorimetric probes for DNA detection, making use of the variation of the surface plasmon resonance band with the composition and ordering and the sharp melting transitions of nanoparticle-labelled [142].

2.13.5. Platinum Group Metals (PGMs) nanoalloys

The platinum group metals (PGMs) are a family of six greyish to silver-white metals clustered together in the periodic table with related chemical and physical affinities as well as similar geochemical behaviour. The three heavier metals platinum (Pt), iridium (Ir) and osmium (Os), have densities of about 22 g/cm^3; and the three somewhat lighter metals palladium (Pd), rhodium (Rh) and ruthenium (Ru), have densities of about 12 g/cm^3. The PGMs belong to the transition metals of Group VIII in the Periodic Table, as do iron (Fe), cobalt (Co) and nickel (Ni) [16]. The position of the elements is shown in the periodic table below (**Figure 2**). Owing to their great scarcity they are classified as precious metals. The

PGMs, along with gold (Au) and silver (Ag), are classified as noble metals because of their high resistance to oxidation and corrosion.

IA	IIA	IIIA	IVA	VA	VIA	VIIA	VIII A	VIII A	VIII A	I B	II B	III B	IV B	V B	VI B	VII B	VIII B
1 H											Metals	Non metals					2 He
3 Li	4 Be			PERIODIC TABLE OF THE ELEMENTS								5 B	6 C	7 N	8 O	9 F	10 Ne
11 Na	12 Mg			d Transition Elements								13 Al	14 Si	15 P	16 S	17 Cl	18 Ar
19 K	20 Ca	21 Sc	22 Ti	23 V	24 Cr	25 Mn	26 Fe	27 Co	28 Ni	29 Cu	30 Zn	31 Ga	32 Ge	33 As	34 Se	35 Br	36 Kr
37 Rb	38 Sr	39 Y	40 Zr	41 Nb	42 Mo	43 Tc	44 Ru	45 Rh	46 Pd	47 Ag	48 Cd	49 In	50 Sn	51 Sb	52 Te	53 I	54 Xe
55 Cs	56 Ba	57 La*	72 Hf	73 Ta	74 W	75 Re	76 Os	77 Ir	78 Pt	79 Au	80 Hg	81 Tl	82 Pb	83 Bi	84 Po	85 At	86 Rn
87 Fr	88 Ra	89 Ac**	104 Unq	105 Unp	106 Uns		f Transition Elements										
		*Lanthanides		58 Ce	59 Pr	60 Nd	61 Pm	62 Sm	63 Eu	64 Gd	65 Tb	66 Dy	67 Ho	68 Er	69 Tm	70 Yb	71 Lu
		**Actinides		90 Th	91 Pa	92 U	93 Np	94 Pu	95 Am	96 Cm	97 Bk	98 Cf	99 Es	100 Fm	101 Md	102 No	103 Lr

Figure 2: The periodic table showing platinum group metals (highlighted in green), (reprinted from ref **[143]**).

PGMs based nanoalloys exhibit unique physical and chemical properties that have made them crucial to the modern industrial world. The PGMs have very high melting points and are chemically inert to a wide variety of substances (even at very high temperatures) thus resisting corrosion. Most importantly, they have excellent catalytic properties; hence they are widely used in chemical industries and in automobile catalytic converters. Commercial substitution of PGMs with cheaper metals has rarely been successful, but an individual platinum group metal may readily be replaced by another **[16, 143]**. Since it has been reported that binary and ternary nanoalloys based on Pt often enhance the catalytic activity of

Pt, PGM-based nanoalloys have found application in fuel cells, oxidation of methanol, hydrogen activation, biosensors and immunosensors [144,145].

2.13.6. Core-shell nanostructures

Core-shell nanoparticles are particles that contain an inner core covered by an outer shell, whereby the type of the material used for core can be different to the shell material.

2.13.6.1.   Why core shell?

These nanostructures exhibit enhanced extraordinary physical and chemical properties over their individual counterparts. For instance if a material has a core of material A and shell of material B, then the core-shell of A-B can have improved reactivity of the surface, enhanced stability and dispersibility of the colloidal core. Furthermore, these structures can be employed in many applications. There are diverse applications for these core-shell materials including drug delivery agents to control release of drugs in medicines, which can also protect materials from light and moisture for sensitive compounds. In the latter case, the light or moisture sensitive compound can be synthesised as a core and be covered with a shell which will prevent the reaction of atmospheric oxygen or moisture on the core, thus stabilizing a core material. Other applications include catalysis and coatings [146].

2.13.6.2.   Synthesis of core-shell

There are several factors affecting the formation of core-shell nanostructures as previously mentioned. Therefore, their synthesis can be followed using the basic principles which are;

- The miscibility and the interfacial energy of the two materials are very important when it comes to the formation of core-shell nanostructures.

- In terms of miscibility, if the two materials are immiscible there is a significant possibility of formation for the core-shell. However, if they are miscible, they may form a solid solution.

- On the other hand, in terms of interfacial energy, a large interfacial energy will lead to formation of individual particles and not core-shell nanostructures. If the interfacial energies between two materials is very high, then chances are core-shell nanostructures will not form; instead a nano composite of A and B will be formed.

- Lastly, lattice mismatch also plays a role. Lattice mismatch has to do with the lattice parameters of A and B. Consequently, if the lattice (unit cell) parameters are widely different, the interfacial energy will increase. Thus, it is crucial to choose materials which do not differ significantly in their lattice constants (usually within 1-3 %). A large lattice mismatch implies large interfacial energies which lead to composite formation, not a core-shell [146].

  Methods to achieve uniform core-shell involve:

- Slow addition of the shell forming agents at relatively low temperatures

- The correct sequence of mixing of the reactants, for example if the aim is to form A_{core} with B_{shell} therefore, the precursor of material A has to be added first followed by precursor of material B.

- Proper choice of the shell forming agent and a choice of appropriate reagent which will be related to the shell forming agent has to be taken into consideration.

- Control over the rate of addition of the shell forming agent for making a proper shell.

- Control of the temperature and the proper selection of organic ligands to be adhered to the surface of core [146].

Therefore, these are some of the key parameters that have to be taken into consideration in achieving a uniform core-shell nanostructure. There are kinetics and thermodynamics involved in making a stable core-shell structures and thus by changing key parameters, one can sometimes get meta-stable phases and one can stabilise those that normal thermodynamic

conditions do not favour more especially because the synthesis is carried out in the nano dimensions.

2.13.6.3. Mechanisms for the formation of core@shell hybrid nanocrystals (HNCs)
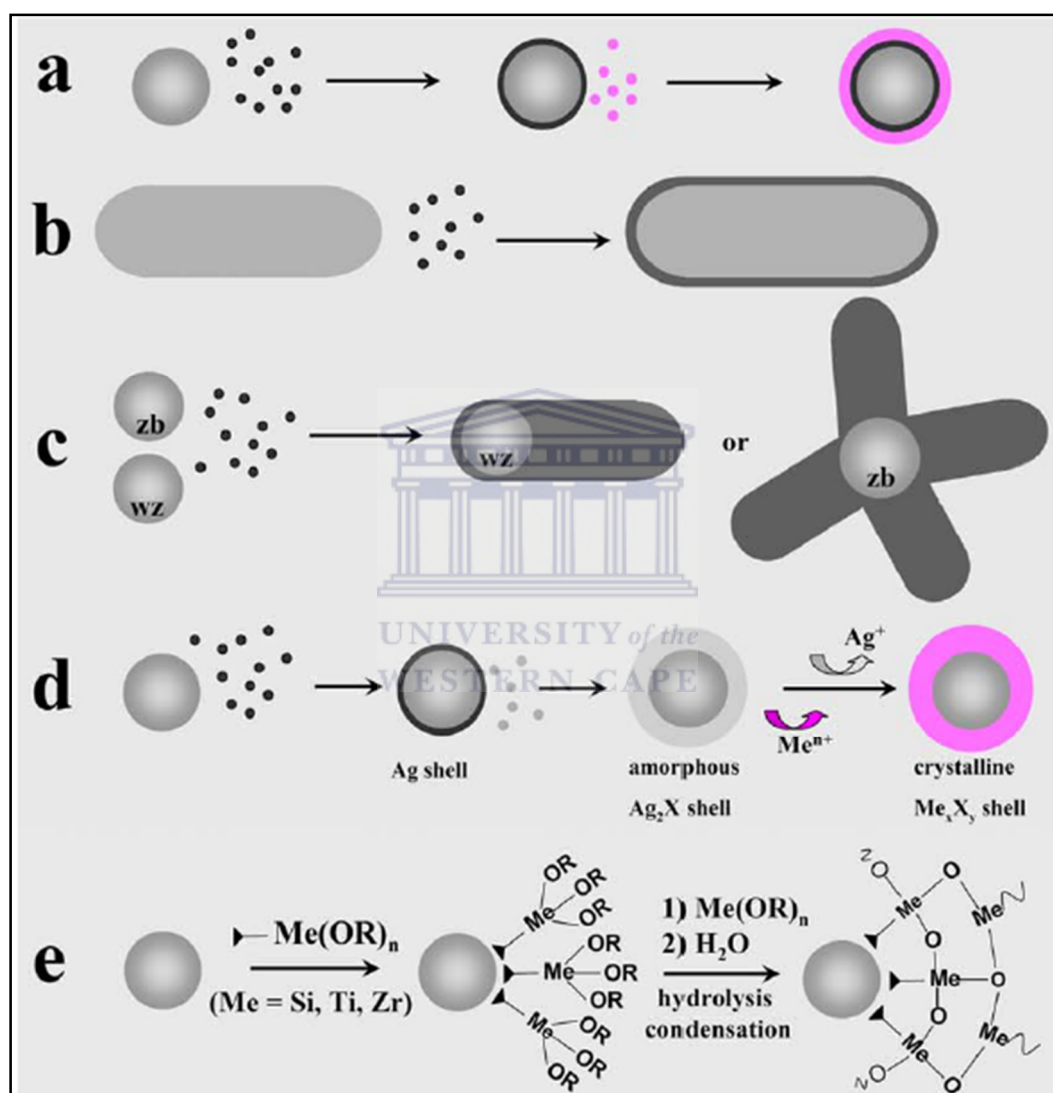
Scheme 9: Mechanisms for the formation of core@shell HNCs: **(a—c)** direct heterogeneous nucleation and growth of the shell material onto preformed nanocrystals seeds with controlled shape and crystal structure; **(d)** sequential heterogeneous nucleation and growth steps onto preformed seeds, involving deposition of an amorphous shell and its conversion to crystals upon cation exchange; **(e)** silica shell growth after chemical activation of the seed surface and subsequent polymerization; (obtained from ref **[147]**).

There can be several various mechanisms by which core@shell nanostructures can be formed; **Scheme 9 (a-c)** above shows a direct heterogeneous nucleation and growth of one or more secondary material layers onto the surface of preformed nanocrystals seeds serving as starting "cores". In general multi-layered nanostructures are being formed by first preparing nanoparticles of one material which are then used as nucleation seeds to deposit other materials on the surface **[147]**.

Therefore, it can be observed that the shell tends to adapt to the symmetry as well as the shape of the starting core (**Scheme 9 (b)** and **(c)**). This is where a rod-like particle gives rod-like shaped core-shell structures, with the same applying when different crystalline forms of zinc sulphide are used to form cores and the symmetry is taken into consideration. That is when hexagonal zinc wurtzite is used as a core; a rod-shaped shell will then form; whereas when cubic zinc blende is a core, a tetrapods shell will form on top because of the tetrahedral symmetry **[147]**. A three-step shell growth process, for example in organic media can also be achieved as illustrated in **Scheme 9 (d)** whereby a silver shell is formed on the particle by adding silver nitrate initially to form an amorphous shell layer which can be replaced by a cationic exchange process using some other alkylating agent **[148]**.

The initial step in a three-step growth involves the deposition of a Ag layer with a precisely tailored thickness onto the target core, followed by conversion of the latter to an amorphous Ag_xS shell upon sulfidation **[148]**. The last step is then the cation-exchange reaction leading to Ag^+ replacement by X^{n+} metal ions (favoured by the strong acid softness of Ag^+), which ultimately results in a single-crystalline Me_xY_y coverage **[147]**.

The core@shell structures can also be formed by controlled hydrolysis and condensation reactions in organic media, here you supply a desired metal alkoxide such as silica, titanium or zirconium alkoxide is supplied to form on top of a core particle **[149-152]**. This is then followed by a hydrolysis condensation step where the water molecules result in the built-up metal oxide network covering the starting seeds to form a shell as shown in **Scheme 9 (e)**.
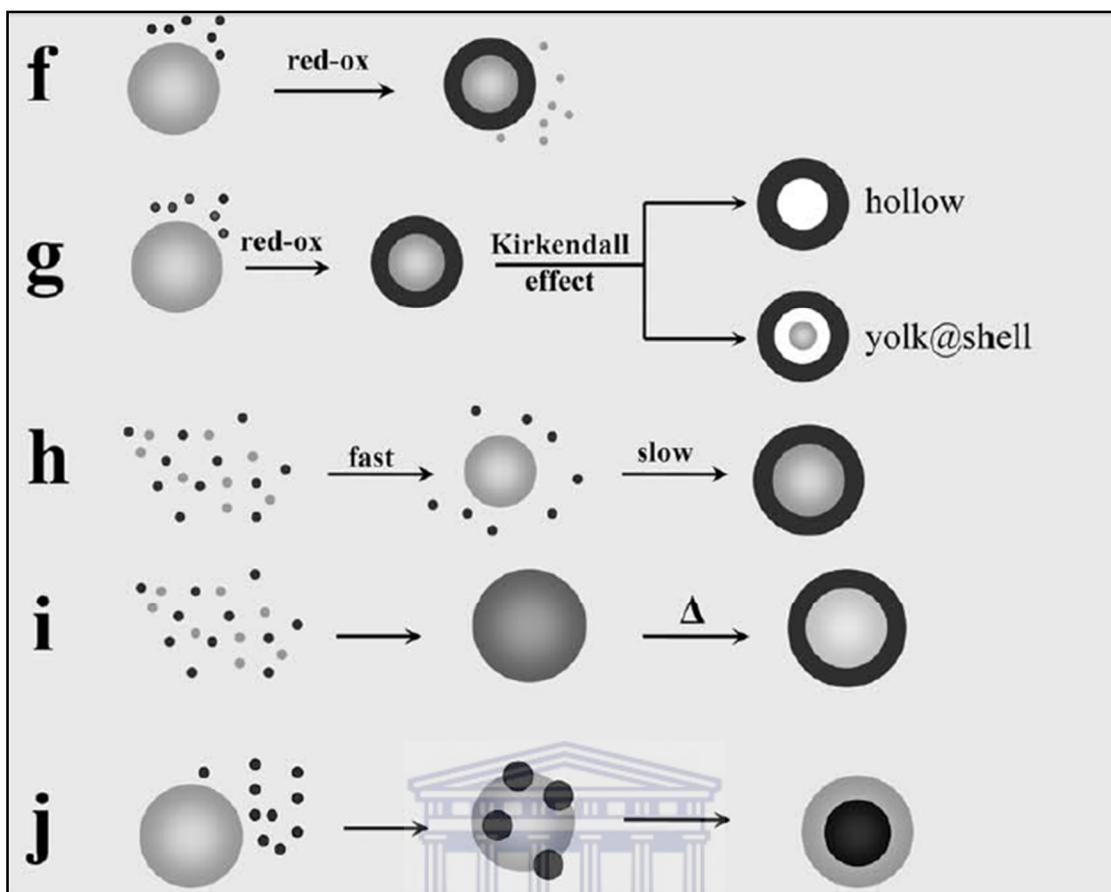
Scheme 10: The mechanisms leading to the formation of core@shell HNCs: **(f)** sacrificial redox replacement of the outer seed layer; **(g)** surface-confined red-ox reaction followed by vacancy coalescence via the Kirkendall effect; **(h)** self-controlled nucleation-growth; **(i)** thermally driven crystal-phase segregation; **(j)** solid-state diffusion and coalescence (obtained from ref **[147]**).

Scheme 10 is a continuation of **Scheme 9**. The mechanism illustrated in **Scheme 10 (f)** shows another way of forming a core@shell structure through sacrificial conversion of some of the outermost exposed layers of a starting nanocrystalline core into a different material by a galvanic replacement reaction. It therefore means that the final core diameter of the core@shell structure is smaller than the starting core diameter because parts of the exposed layers have been removed during a reaction which can be a redox type reaction to allow the incoming deposited material to form a shell layer on top of the inner core **[153, 154]**.

The mechanism shown in **Scheme 10 (g)** occurs through what is known as "Kirkendall effect" which means an atomic diffusion process takes place through vacancy exchange. This take place without having a direct interchange of atoms to form either a core@shell structure with a large gap in between a core and shell as an intermediate structure, or a completely hollow structure which is a final structure obtained when all matter has moved from core to the shell **[155, 156]**. In this type of a mechanism a core@shell structure is firstly formed using a redox or sacrificial reaction. Then, in this core@shell, the inner core region hosts a fast-diffusing species, while the outer region acts as reservoir of slowest diffusing species (e.g., metal cations and oxygen anions in oxide passivated metallic nanoparticle, respectively). A net transport of matter from the core outwards takes place along with coalescence of the generated vacancies into a single large void **[155, 156]**.

Scheme 10 (h) illustrates the self-controlled nucleation-growth mechanism in which the energy activation barriers for the homogeneous nucleation of the individual compounds may diverge to such an extent that: two different materials form at distinct times or temperatures and the shell material is produced most exclusively by heterogeneous nucleation on the *in-situ* formed seeds **[147]**. That is, from two distinct materials, the second material's particles aggregate faster to form the core serve as seeds, whereas the other material aggregates slowly, forming a shell on the *in-situ* formed seeds. The final structural result will be a core@shell structure composing of core represented as lighter particles and a shell made up of dark particles in **Scheme 10 (h)**.

The thermally induced phase segregation and solid-state diffusion mechanism **Scheme 10 (i)** involves the mixing of two different materials forming a solid-state composite particle, which upon heating, diffuse and phase segregate into two completely distinct entities to form core@shell structure **[147]**. The last mechanism in **Scheme 10 (j)** is referred to as solid-state diffusion and coalescence, whereby a core particle combines with other small particles of different materials which initially adsorb and coalesce as they grow on the surface of the core and ultimately form a core@shell structure via diffusion **[146, 147]**.

2.14. Experimental techniques for characterisation of nanoalloys

For optimization of nanoalloy synthetic methods, rapid, quantitative feedback concerning final nanoalloy size, shape, optical properties and their relationship to the countless synthetic variables is necessary [157]. Hence, a variety of experimental techniques, including diffraction, microscopy and numerous spectroscopies, have been applied to characterise and study the properties of mono- and multi-metallic nanoparticles. The following section gives a brief general overview of some of the most commonly applied techniques.

2.14.1. Spectroscopic techniques

2.14.1.1. UV-Visible spectroscopy

UV-Vis is a spectroscopic technique that uses photons in the visible and adjacent ultraviolet (UV) and near infrared (NIR) ranges [143]. However, photons in the UV and visible region do not have sufficient energy to penetrate as deeply into a sample as higher energy photons like X-rays but are absorbed at the surface, thus making UV-Vis spectroscopy relatively surface sensitive. Although UV-Vis spectroscopy provides an easy and cheap means for compositional analysis, it is limited to bulk analysis and some metals are suited more for UV-Vis analysis than others; for example, gold metal exhibits distinct optical plasmon absorbance in the visible range [158]. UV-Vis *in situ* studies can be carried out to monitor the progress of the particle formation or shell deposition in the characterisation of core-shell particles [159,160]. UV-Vis spectroscopy can also be used for particle size measurements since the absorption spectra of metal nanoparticles are dependent on the particle size and wavelength. However, the contribution of the particle size to the absorption spectra becomes less and less significant with decreasing particle size [161]. Furthermore, it is used in the quantitative determination studies. The absorption of light at a specific wavelength is determined by the ratio of transmitted intensity and intensity of the incident light (I_t/I_i). Therefore optical absorbance can be expressed as:

$$Abs = -log_{10}\frac{I_t}{I_i} \tag{35}$$

That is, if a material absorbs UV-Visible light, then its concentration at a particular wavelength can be monitored using the Beer-Lambert relationship:

$$Abs = \varepsilon C_0 l \tag{36}$$

Where ε is the molar extinction coefficient (ε, L.mol^{-1}cm^{-1}), C_0 is the concentration of the absorbing species (C_0, g.L^{-1}) and l is the optical path length (l, cm) of the absorbing medium. The drawback of UV-Vis is that it requires a certain degree of monodispersity and of regular shaped particles in order to achieve accurate measurements [162].

2.14.1.2. Fourier Transform Infra-Red (FTIR) spectroscopy

Infrared (IR) (including Fourier transform IR (FT-IR)) spectroscopy is widely used to study the vibrational spectra of small molecules adsorbed on metallic clusters. For example, by making comparisons with pure metal clusters or surfaces, IR spectroscopy of small molecules (e.g., CO) adsorbed on bimetallic nanoparticles can be used as a probe for the surface composition and structure of the sample [117, 163]. FT-IR is an effective analytical instrument that is able to detect chemical functional groups and characterise covalent bonding information in the sample. The most useful region of infrared lies between 4000 and 625 cm^{-1}. FT-IR depends on transitions between vibrational energy states stretching and bending.

2.14.1.3. Energy Dispersive X-ray (EDX) spectroscopy

This analytical technique is often used in conjunction with SEM and TEM. An electron beam (typically 10-20 keV) strikes the surface of a conducting sample causing X-rays to be emitted, the energies of which depend on the material under examination. The X-rays are generated in a region about 2 µm in depth. The generated X-rays are element specific, because each element in the chosen nanoparticle emits X-rays at their characteristic energies by electron beam irradiation and their intensity is proportional to the concentration of each element in the particle, hence compositional analysis is enabled in scanning electron microscopy and transmission electron microscopy when fitted with EDX microanalysis

detectors **[162]**. Therefore in general, EDX is a high-resolution (with approximately 1.5 nm lateral resolution) variant of X-ray microanalysis that measures and identifies the elements present and concentration inside a single particle. EDX can also do line scans across a particle to show detailed distributions, or carry out 2D mapping thus showing the distribution of the elements over the full particle **[117]**. EDX works very well for heavier elements, as it accomplish analyses down to Boron.

2.14.1.4. Auger Electron Spectroscopy (AES)

AES is a popular technique for determining the composition of the top few layers of a surface and is sensitive to chemical identity because Auger electron energies are element specific. It involves detection of secondary electrons which are ejected upon relaxation of a core hole **[117]**. In Auger electron spectroscopy (AES), electrons emitted after the interaction between primary X-rays or electrons and a sample are detected. The interaction is illustrated in **Figure 3**. The amount of electrons having escaped from the sample without energy loss is typically measured in the range of 20 to 2000 eV. The data is represented as a graph of intensity versus electron energy. Due to the impact of the primary beam, the atoms in the sample are ionised and electrons are liberated from the surface, as a result of the radiationless de-excitation in the Auger electron emission process **[164, 165]**.

Although X-Ray Photoelectron Spectroscopy (XPS) and AES are comparable methods in the sense that both are based on the use of a spectrometer to measure electrons of relatively low energy, the main difference between the two methods is the source of the primary radiation, which is necessary to provoke ionisation of the atoms. AES makes use of an electron gun while XPS relies on soft X-rays. As a consequence of that, one of the main differences is the lateral resolution of the two methods **[164-166]**. The lateral resolution of AES is typically situated in the 10 to 100 nm range, while with XPS only a lateral resolution of a few to 100 μm can be reached. These types of measurements are, out of necessity performed under ultra-high vacuum conditions and only non-volatile samples restricted in size can be analysed **[165]**.
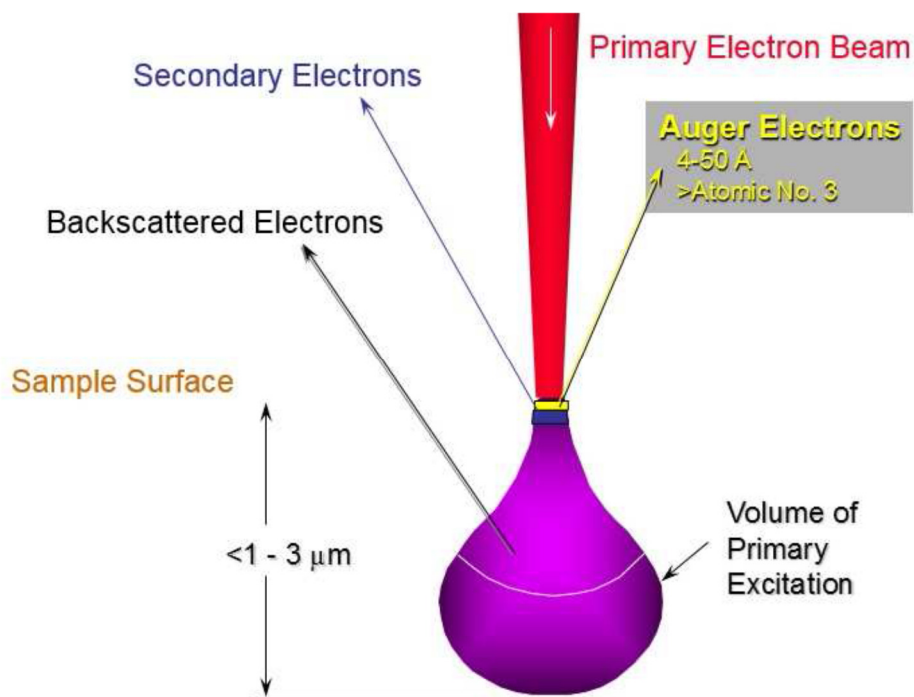
Figure 3: Schematic representation of the primary beam – sample interaction for AES analysis, (reprinted from **[164]**).

AES uses, in contrast to XPS, electrons as primary radiation. The analysed electrons are not the emitted core electrons, but Auger electrons that are ejected as a consequence of the return of the ionized atom to its ground state **[165]**.
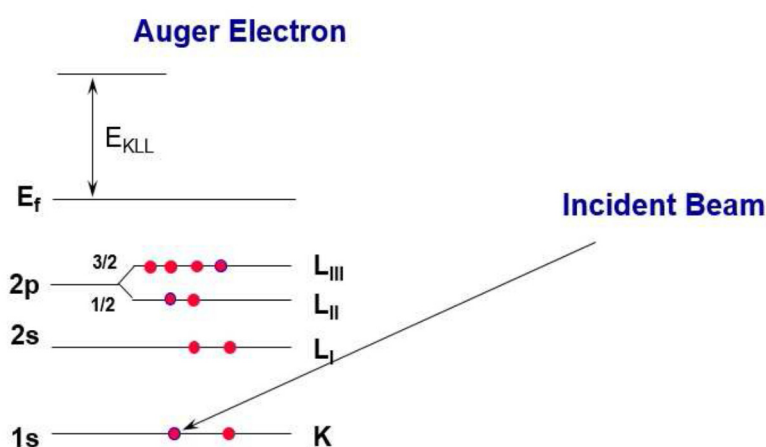
Figure 4: Schematic representation of the Auger electron emission process, (obtained from ref **[167]**).

76

For the AES process shown above (see **Figure 4**), a hole is created on the K level in the initial ionization step. This requires a primary energy greater than the binding energy of the electron in that shell. For the ionization to be efficient, a primary energy of about 5 times the binding energy is taken. In practice, typical primary energies are between 5 and 10 keV. The hole can be produced by either the primary beam, or the backscattered secondary electrons **[165-167]**. **Figure 5** below shows the general set-up of AES, where all the parts are contained within a vacuum chamber. As for most techniques, the system is operated and controlled by a computer.
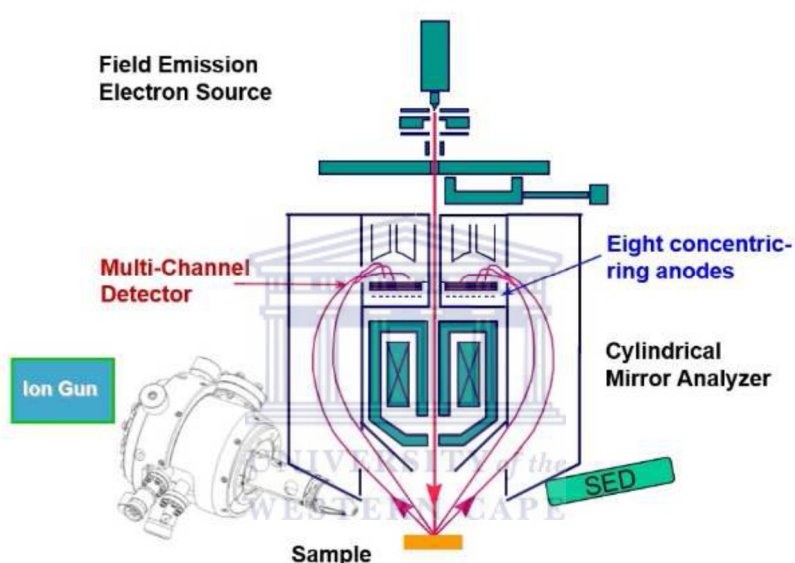
Figure 5: Schematic representation of AES configuration with a cylindrical mirror analyser and a central electron gun, (reprinted from ref **[167]**).

The electron spectrometer and sample room must be operating under true ultra-high vacuum (UHV) conditions typically in the range of 10^{-8} to 10^{-10} torr. The reason being that lowering the vacuum level to e.g. 10^{-6} torr, would immediately result in the formation of a monolayer of residual gas absorbed on the sample surface in less than a second **[167-168]**. A vacuum of 10^{-10} torr allows measurements to be carried out for about an hour before a monofilm is formed thus allowing unambiguous, accurate surface characterisation by preventing sample contamination during analysis **[168]**. Hydrocarbon contamination, is a common interference in poor quality vacuum, but is reduced to insignificant levels on all sample types as with the PHI 700 Scanning Auger Nanoprobe which was used in this study.

2.14.2. Diffraction techniques

2.14.2.1.   X-Ray Diffraction (XRD)

X-ray diffraction (XRD) is a powerful, non-destructive technique that has widely been used for characterizing crystalline nanoparticles. It is used to interrogate crystallinity or grain size, crystal structure, lattice spacing parameters (and hence some information on the degree of mixing or segregation, provided that the lattice spacing of the two metals are distinct) and qualitative chemical composition information [117, 169]. The compounds or elements present in the sample are identified by comparing the fingerprint compiled in the library of XRD with the peaks obtained experimentally. Furthermore, for the analysis of nanoalloys, the diffraction patterns of monometallic and bimetallic alloys are compared to confirm the formation of a nanoalloy structure.

XRD can be used to look at single crystal or polycrystalline materials. A beam of X-rays is allowed to pass through the sample and interact with the electrons inside the matter; the way the beam is scattered by the atoms in the path of the X-ray is studied. The atomic planes of a crystal cause an incident beam of scattered X-rays to constructively interfere with one another as they leave the crystal. This phenomenon is called X-ray diffraction. Therefore, diffraction of these X-rays is observed as patterns or peaks which provide information about size and shape of the crystal unit cell [162, 169, 170]. This interference can be looked at using Bragg's Law to determine various characteristics of the crystal or polycrystalline material. Measurements are made in Angströms, 1 Angström = 0.1 nm.

Therefore Bragg's law is given by the equation below:

$$2d \sin \theta = n\lambda \qquad\qquad (37)$$

This law was developed to explain why the cleavage faces of crystals appear to reflect X-ray beams at certain angles of incidence (theta, θ). The variable d is the distance between atomic layers in a crystal, θ is one half the angle between the incident and scattered X-ray beams and the variable lambda λ is the wavelength of the incident X-ray beam; n is an integer [170].
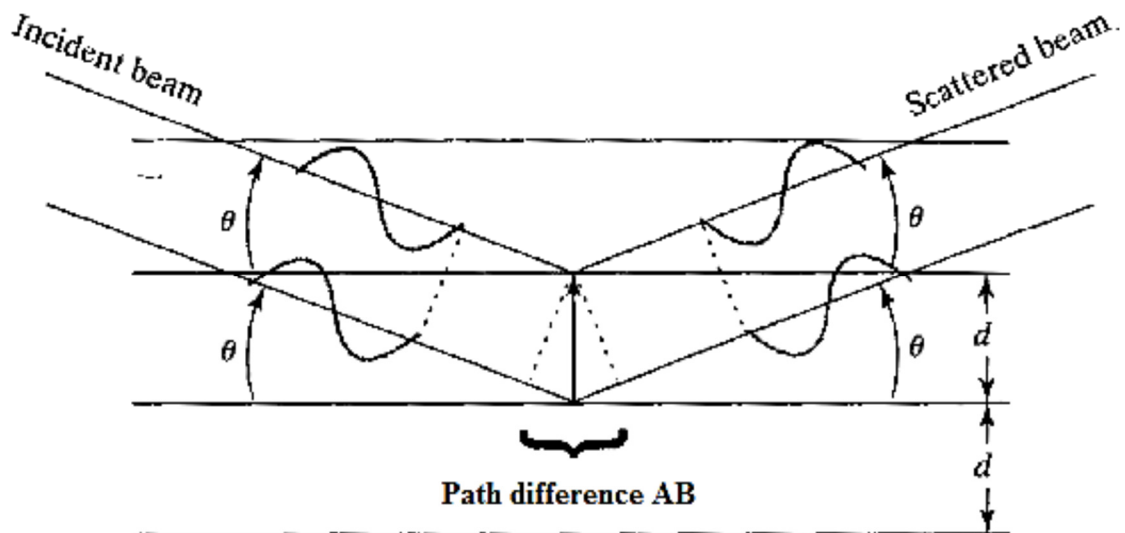
Scheme 11: Illustration of the conditions required for Bragg diffraction to occur, (reprinted from ref **[170]**).

Peak width from the X-ray spectrum is dependent on size of interacting volume that is large single crystalline material to give sharp, narrow peaks, while for smaller crystals the peak width is larger. XRD can be used quantitatively for the determination of average particle size. From the well-known Scherrer's formula the average crystallite size, *L*, can be determined as **[171]**:

$$L = \frac{K\lambda}{\beta.\cos\theta} \tag{38}$$
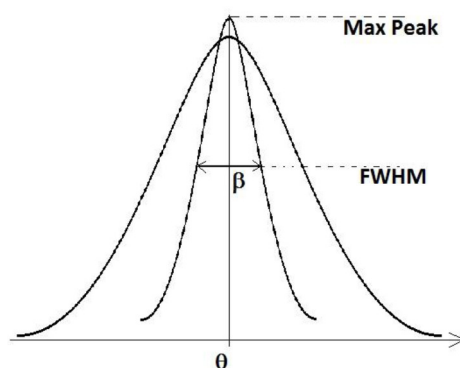
Figure 6: Illustration of the peak width at half maximum on a diffraction peak profile

Where: *L*= diameter,

λ= X-ray wavelength in nanometer (nm),

β= peak width at half maximum (FWHW) resulting from small crystallite size in radians,

θ= the Bragg angle can be in degrees or radians and

K= a shape factor (typical 0.9 for spherical shape)

The lattice parameter (a_o) could also be calculated using the following equation:

$$a_o = d(h^2 + k^2 + l^2)^{\frac{1}{2}} \tag{39}$$

Where h, k and l constitute the reciprocals of the fractional intercepts which the plane makes with crystallographic axes (Miller indices) of a crystal facet and d is the interplanar spacing determined using Bragg's equation [169, 170].

2.14.2.2. Selected Area Electron Diffraction (SAED)

Electron diffraction is a diffraction technique that has been more widely used for molecular beams of clusters [117]. Although interpretation of the electron diffraction results is complex; information on the geometry, average size and temperature of the nanoparticles may be obtained [117]. SAED is a crystallographic experimental technique that can be performed inside a transmission electron microscope (TEM), and is referred to as "selected" because the user can easily choose from which part of the specimen to obtain the diffraction pattern. As a diffraction technique, SAED can be used to identify crystal structures and examine crystal defects. It is similar to X-ray diffraction, but unique in a sense that areas as small as several hundred nanometers in size can be examined, whereas X-ray diffraction typically samples areas several centimeters in size. SAED of nanocrystals gives ring patterns similar to those from X-ray powder diffraction and can be used to distinguish nanocrystalline from amorphous phases [162].

2.14.3. Microscopic techniques

Electron microscopy such as scanning electron microscopy (SEM) and transmission electron microscopy (TEM) are used the most and it is also one of the few techniques that are capable of imaging tiny individual nanoparticles and they are subsequently used to determine their particle size and shape. This is as a result of their high resolution and high imaging speed.

2.14.3.1. High Resolution Transmission Electron Microscopy (HRTEM)

HRTEM is used for imaging nanostructures and is usually equipped with EDX and SAED microanalysis detectors, enabling elemental compositional analysis by energy dispersive X-ray. Crystallinity of the NPs can also be studied using electron diffraction analysis. However, the information obtained from these images cannot always be used to verify the presence of a core@shell structure, thus other techniques like NanoSAM has to be used to support the TEM and TEM-EDX results obtained. The main difference between TEM and SEM is that TEM can achieve a higher lateral resolution than SEM because the electron energies used in TEM is well above 100 keV; hence the purchase and operation costs exceed those of SEM by several times **[162]**.

In TEM the image is generated by detecting primary electrons transmitted through an ultra-thin sliced sample, typically less than 100 nm **[162]**. Hence special sample preparation methods are required. Generally the nanoparticles are dispersed onto an electron-transparent substrate, such as a thin carbon-coated microgrid. TEM is particularly useful because of the high contrast between the metal atoms (especially heavy metals) and any passivating organic molecules or polymers **[117]**. Furthermore, electrons are emitted by a source and focused and magnified by a system of magnetic lenses, while the electron beam is condensed by the two condenser lenses which also control brightness of the beam. After passing through condenser aperture, the beam interacts with sample. The transmitted beam consisting primarily of elastically scattered electrons (i.e. electrons that did not lose energy during electron-sample interaction) passes through objective lens, aperture and magnifying system which comprises of intermediate and a final projector lens. Lastly, the magnified image is displayed on a fluorescent screen or on CCD camera system as observed in **Figure 7** below **[172]**.
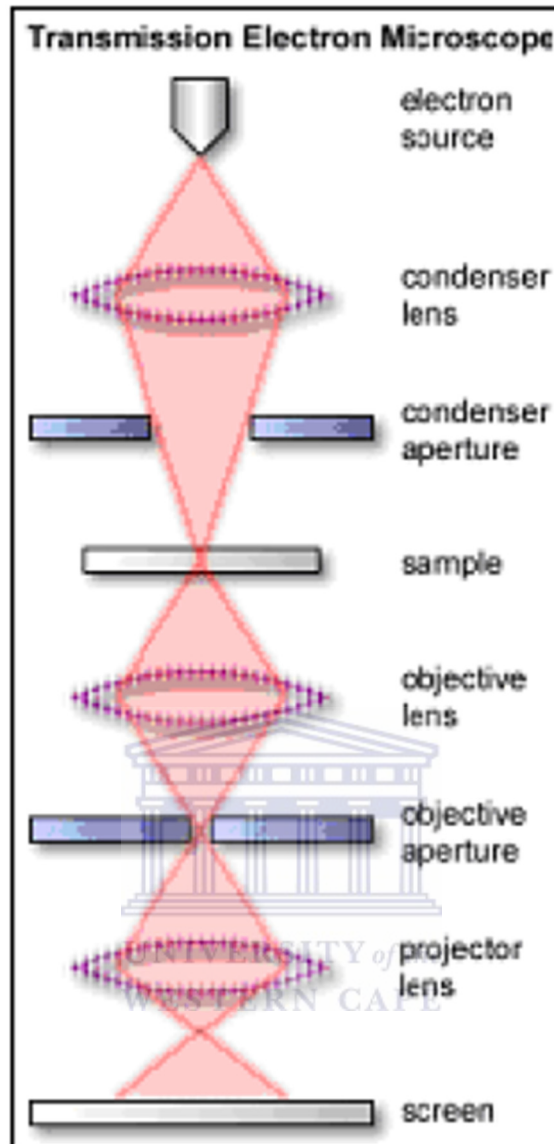
Figure 7: The schematic diagram showing the inside features of TEM, (obtained from ref **[172]**)

In many modern TEMs, there are two high resolution imaging modes: High-Resolution Transmission Electron Microscopy (HRTEM) and Scanning Transmission Electron Microscopy (STEM). HRTEM is essentially a phase contrast technique **[173]**. HRTEM offers resolution down to the Ångstrom level and enables information to be obtained on the structure (atomic packing) rather than just the morphology of the nanoparticles. Particle growth can also be studied using *in situ* TEM **[117]**. It provides information not only on the particle size and shape, but also on the crystallography of the monometallic and multimetallic nanoparticles.

2.14.3.2. High Resolution Scanning Electron Microscopy (HRSEM)

Although, SEM provides a lower lateral resolution than TEM as discussed in the above section, its moderate electron energies of ~ 10 keV are sufficient to transmit particles in the nanometre size range, thus providing nanometre resolution **[174]**. SEM can image nanoparticles distributed over a surface, size and shape and it can offer surface imaging up to resolution < 2 nm. In SEM, electrons are focused in vacuum (10^{-7} and 10^{-9} mbar) into a fine probe that is rastered over the surface of specimen. A beam (2 – 30 kV) passes through the scan coils and an objective lens that deflect the beam horizontally and vertically so that beam scans the surface. As electrons penetrate surface, a number of interactions occur that can result in emission of electrons or photons from, or through, a surface. A fraction of the electrons emitted by surface is the collected by appropriate detectors. The collected electrons are amplified and converted into a digital image by a digital camera system connected to the different detectors. Scanning electron beams across a surface yields topographical representation of surface and three types of images produced by a SEM include: secondary electron, backscattered electron images and elemental X-ray maps **[172]**.

Typically, the image in SEM is due to secondary electrons emitted by the sample surface following excitation by the primary electron beam. Although SEM images have lower resolution than TEM, SEM is better for imaging bulk samples and has a greater depth of view, giving rise to better 3D images of the sample **[117]**. HRSEM is used for better resolution. Below is the schematic illustration of working principles of HRSEM (**Figure 8**).
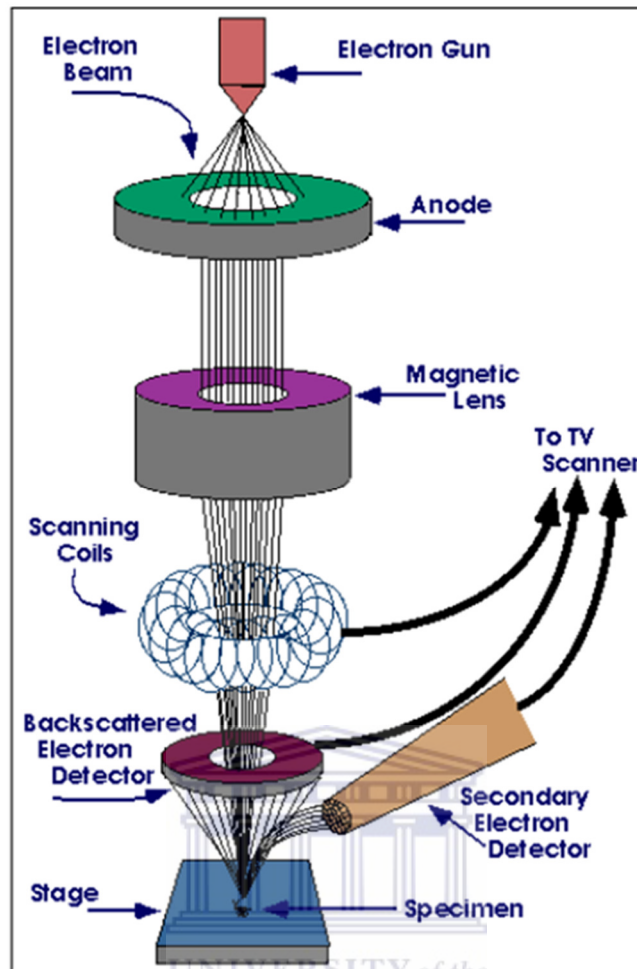
Figure 8: Schematic diagram of HRSEM **[172]**.

2.14.3.3. Scanning Auger Microscopy (SAM)

By combining an electron spectrometer with an ultra-high vacuum (UHV) SEM in a Scanning Auger Nanoprobe microscopy (NanoSAM) it becomes possible to carry out scanning Auger microscopy. Thus in this mode of operation various imaging and chemical mapping procedures become possible. SAM allows surface chemical maps to be collected with lateral resolutions better than 1μm **[168]**. However, the image resolution generally is influenced by some sample-specific effects such as the Auger electron escape depth, the surface topography and the contribution from secondary electrons. For topographical analyses, the imaging of SAM does not reach the same resolution as TEM, but since AES is based on reflection rather than transmission, it does not suffer from the intrinsic problem of

mixed signals from core and shell. **[162]**. Since the Auger electron yield is very sensitive to the electron take-off angle, an image of Auger electron intensities will invariably reflect the surface topography of the specimen, possibly more strongly than the chemical variations **[168]**.

2.14.4. Electrochemistry

The electrochemical techniques are of great importance when it comes to the study of nanoalloys because by investigation of the individual metal components of the trimetallic nanoalloy one can confirm the alloyed structure of the three various metal nanoparticles from their respective reduction-oxidation (REDOX) electrochemical reaction response. Electro-analytical techniques are concerned with the measurements of electrical quantities such as current, potential or charge and their relationship to chemical parameters. Electrochemical processes are distinctive from many other chemical measurements in the sense that they take place at the electrode-solution interface **[175, 176]**.

Both potentiometric and potentiostatic measurements require an electrochemical cell consisting of the electrolyte solution and at least two electrodes. The electrode surface acts as the interface between an ionic conductor and an electronic conductor. One of the electrodes is termed the working electrode; this is the electrode on which the reaction of interest takes place. Based on whether the reaction on the electrode is oxidation or reduction, the working electrode can be called anode or cathode. The working electrode is often used in conjugation with other two electrodes termed the reference electrode and an auxiliary or counter electrode **[175-177]**.

The electrode potential is used to study electron-transfer processes at the electrode-solution interface, while the resultant cell's current is being measured. Consequently, the resulting current is in correspondence with the rate at which electrons move across the electrode-solution interface **[175]**. Unlike the potentiometric technique (e.g., chronopotentiometry), the potentiostatic or controlled-potential techniques (e.g., cyclic voltammetry) have high sensitivity, selectivity towards electro active species, speciation capability, a wide linear range; they are portable and are lower in terms of cost of instrumentation **[175]**.

Compared with UHV and electron-based spectroscopic techniques, electrochemical techniques for surface measurement allow direct investigation of the surfaces of real catalysts under ambient conditions, thereby bridging the so-called "pressure" and "materials" gap between surface science and heterogeneous catalysis [117]. Hence, for particles aimed for applications in heterogeneous catalysis, information about the surface structure is of highest importance. This, in principle, means that the outer-most layer of atoms of the catalyst particle is of particular interest [162].

2.14.4.1. Cyclic Voltammetry (CV)

Cyclic voltammetry (CV) has become the most widely used technique for acquiring qualitative information about electrochemical reactions and is often the first experiment performed in an electroanalytical study [175]. In CV surface redox reactions are probed by letting the potential on the stationary working electrode be swept over a potential range as the current response is being measured by the potentiostat. The resulting plot of current versus potential is termed a cyclic voltammogram [175, 177]. The characteristic peaks in the cyclic voltammogram are caused by the formation of the diffusion layer near the electrode surface. As a result, the potential and kinetics of the redox reactions can be used as material specific fingerprints and be correlated to properties like catalytic activity, electrochemically active surface area, affinity for adsorbates etc. [178]. **Figure 9** below illustrates the expected response of a reversible redox couple during a single potential cycle and the different parameters such as peak potentials (E_{pc}, E_{pa}) and peak currents (I_{pc}, I_{pa}) of the cathodic and anodic peaks, respectively. Initially it is assumed that only the oxidized form O is present. Hence, a negative-going potential scan is chosen for the first half-cycle, starting from a value where no reduction occurs. As the applied potential approaches the characteristic formal electrode potential, E^o for the redox process, a cathodic current starts to increase, until a peak is reached. After traversing the potential region in which the reduction process takes place (at least $90/_{n\ mV}$ beyond the peak), the direction of the potential sweep is reversed. During the reverse scan, R molecules (generated in the forward half cycle and accumulated near the surface) are reoxidized back to O and anodic peak results [175].

86
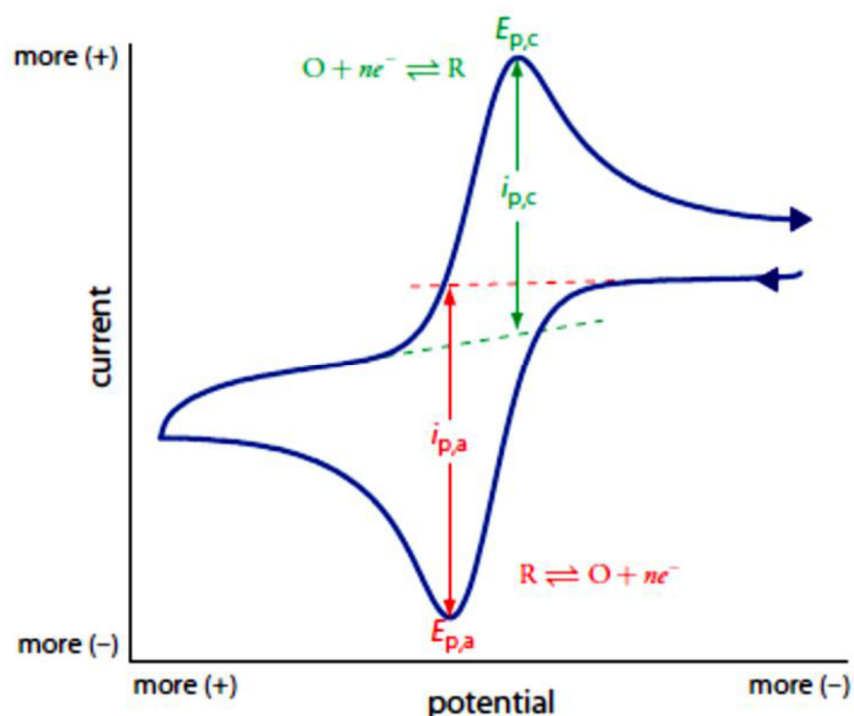
Figure 9: Typical cyclic voltammogram for a reversible $O + ne^- \leftrightarrow R$ redox process showing the basic peak parameters, (reprinted from ref **[179]**).

The potential of CV gives information on redox couple if is fully reversible. By looking at the cyclic voltammogram showed above in **Figure 9** the two peaks are positioned on either side of the formal potential of the analyte redox couple E^o as follows:

$$E^o = \frac{E_{p,a} + E_{p,c}}{2} \tag{40}$$

The formal and standard potentials are conceptually similar as follows:

$$E^o = E^\theta + \frac{RT}{nF} \ln \frac{C_0}{C_R} \tag{41}$$

To fully investigate an electrochemical reaction, it should be run a series of CV experiments with varied experimental parameters such as temperature, potential scan rate etc. Therefore, depending on the outcome of diagnostic test, the redox system can be considered as reversible, irreversible or quasi reversible. Some of these diagnostic tests are tabulated below **[82, 180]**.

Table 5: Potential sweep rate (v) diagnostic for $O + ne^- \leftrightarrow R$ electrode reaction under semi-infinite diffusion condition.

CV parameter	Reversible	Quasi-reversible	Irreversible
E_p	Independent of v	$E_{p,c}$ shifts negatively with increasing v	$E_{p,c}$ shifts by -$30/\alpha_C n_\alpha$ mV per 10-fold increase in v
ΔE_p at 25ºC	=59/n mV	>59/n mV and increases with increasing v	No reverse peak or > 200/n mV
$\lvert I_\text{p,a}/I_\text{p,c}\rvert$	=1	=1 provided $\alpha_C = 0.5$	No reverse scan
$I_\text{p,c}$ vs $v^{1/2}$	Linear	Curved increase	Linear
$\lvert E_\text{p,c} - E_\text{p/2}\rvert$ at 25ºC	= 56.5/n mV	Intermediate values	=48/$\alpha_C n_\alpha$ mV

Data adapted from ref **[179]**.

For a reversible system, the current peak height will increase linearly with the square root of the scan rate. The slope of the resulting line will be proportional to the diffusion coefficient and such a plot is known as Randles-Sevčik plot **[82]**. Furthermore, the peak current for a reversible couple is related to the concentration of the electroactive species as depicted by the Randles-Sevčik equation below:

$$I_\text{p} = 0.4463 nF \left({nF}/{RT} \right)^{1/2} C_0 D^{1/2} v^{1/2} \tag{42}$$

The Randles-Sevčik equation at 25ºC reduces to form:

$$I_\text{p} = (2.69 \times 10^5) n^{3/2} D^{1/2} v^{1/2} C_0 \tag{43}$$

In equation (42) and (43) above, I_p is the peak current density and is in A cm^{-2}, D is the diffusion coefficient and is in cm^{2}s^{-1}, Scan Rate v is in V s^{-1} and C_0 is in mol cm^{-3}. Faraday's constant F = 96485 C mol^{-1}, Gas Constant R = 8.314 J mol^{-1} K^{-1} and absolute Temperature T = 298.15 K.

2.14.4.2. Square Wave voltammetry (SWV)

Square-wave voltammetry is one of the recent techniques by electrochemists for kinetic and mechanistic work. SWV also has become a popular technique for analytical work mainly because its speed and sensitivity **[175-178]**. Square-wave voltammetry is a large-amplitude differential technique in which a waveform composed of a symmetrical square wave, superimposed on a base staircase potential, is applied to the working electrode. During each square-wave cycle the current is sampled twice, once at the end of the forward pulse (at t_1) and once at the end of reverse pulse (at t_2). The difference between the two measurements is plotted versus the base staircase potential. The resulting peak-shaped voltammogram is symmetrical about half-wave potential and the peak current is proportional to the concentration of the electroactive species **[175]**. Since the net current is larger than either the forward or reverse components, the sensitivity is higher than that of differential pulse polarography (in which the reverse current is not used) see **Figure 10** below **[175]**.

One of the drawbacks of fast scanning in CV is that it produces a large capacitive background current. This noise makes it hard to detect the Faradaic current (signal of interest) and severely affects the signal to noise ratio. Since SWV is a pulsed technique, it has an advantage over CV because it can discriminate against the charging current and eliminate this drawback **[181]**. In addition to that, SWV offers high speed measurements for faster reactions as it allows you to program on high scan rates, it further offers high sensitivity as it can detect micromolar concentrations of electroactive species whereas CV can detect only millimolar concentrations and lastly, since SWV effectively removes the background current from a measurement, it has a wide dynamic range (which is ability to respond to both high and low concentration of electroactive species) thus allowing for the use of concentration as an experiment variable **[176, 177, 181]**.
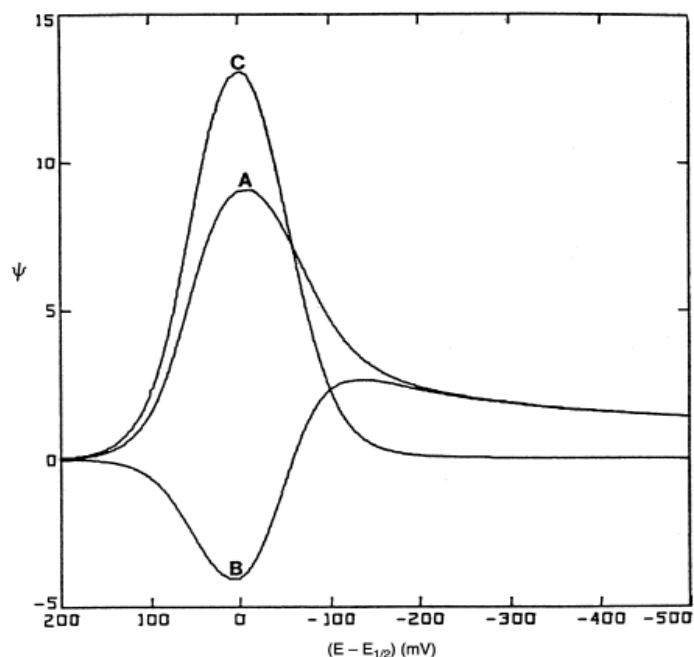
Figure 10: Square-wave voltammograms for reversible electron transfer. Curve **A**: forward current. Curve **B**: reverse current. Curve **C**: net current. (Reproduced from ref **[175]**)

In summary, in this study, the electrochemical studies of the nanoalloys were carried out using CV and SWV. The size, the degree of aggregation and morphology of the nanoalloys were obtained using microscopic techniques such as HRTEM and HRSEM. EDX was used to determine the elemental composition of the nanoalloys while the complete reduction of the metal salts to nanoalloys was investigated using UV-Visible spectroscopy. Furthermore, XRD was used to confirm crystallinity of the synthesised nanoalloys and FTIR was employed to ensure a successful modification of nanoalloys' surface with PVP capping agent. NanoSAM was used for surface analysis of multi-shell nanoalloy.
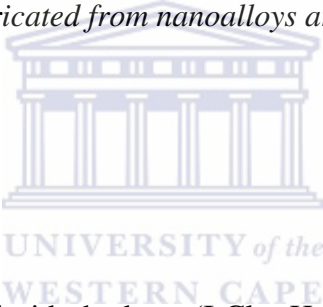
CHAPTER 3

EXPERIMENTAL SECTION

Summary

This chapter discusses the chemicals and instrumentations used. It further presents detailed experimental procedures for the chemical syntheses of Cu, Pt and Ir nanoparticles, Cu@Pt@Ir (multi-shell) and Cu-Pt-Ir (mixed) polyvinylpyrrolidone (PVP) capped nanoalloys obtained by a conventional borohydride reduction method. The description of the necessary sample preparations and parameters used for spectroscopic, microscopic and electrochemical characterisation of the synthesised nanoalloys are outlined. The details of how the electrocatalysts were fabricated from nanoalloys are also described.

3.1.   Reagents and materials

Analytical grade iridium (III) chloride hydrate ($IrCl_3.xH_2O$), hydrogen hexachloroplatinate (IV) hexahydrate ($H_2Cl_6Pt.6H_2O$), copper (II) nitrate hydrate ($Cu(NO_3)_2.xH_2O$), ammonium hydroxide (NH_4OH), polyvinylpyrrolidone (PVP, MW = 10000), lithium perchlorate ($LiClO_4$), potassium hydroxide (KOH) and sodium borohydride ($NaBH_4$) were all purchased from Sigma-Aldrich (Cape Town, South Africa). All chemicals were of analytical reagent grade and were used without further purification. Deionized water (18.2 MΩ cm) purified by a Milli-QTM system (Millipore) was used as reagent water for aqueous solution preparations. Alumina polishing pads and powder (0.05, 0.3 and 1.0 μm) were obtained from Buehler, Illinois, USA. Analytical grade argon gas purchased from Afrox Company, South Africa.

3.2. Instrumentation

Electrochemical measurements (CV and SWV) were performed with an Epsilon electrochemical system from BASi. The system consists of a conventional three-electrode system. A catalyst coated glassy carbon (GC) disc (3-mm diameter) was used as the working electrode; a platinum wire was used as a counter electrode and an Ag/AgCl (3 M NaCl) as the reference electrode. Alumina polishing pads and powder (0.05, 0.3 and 1.0 μm) were used for polishing the GC electrodes. The platinum auxiliary electrode was cleaned by rinsing with acetone and deionised water to remove any contaminants while the Ag/AgCl electrode was just cleaned by rinsing with copious amounts of deionised water. All experimental solutions were purged with high-purified argon gas for at least 20 min prior to each set of experiments. Then the argon environment was maintained over the solutions in the electrochemical cell during the respective measurements. A fresh clean electrolyte solution was used for each set of experiments. The experiments were carried out at room temperature.

The microscopic characterisation of the nanoalloys synthesised was carried out using a high resolution transmission electron microscope (HRTEM) Tecnai G2. F20X-Twin MAT 200 kV HRTEM from FEI (E-indhoven, Netherlands) and the morphology was interrogated using high resolution scanning electron microscope (HRSEM) using a Zeiss Auriga HRSEM analyser. Sometimes, the system (HRTEM) is also equipped with other sources and detectors, so that other techniques such as selected area electron diffraction (SAED) and energy dispersive X-ray spectroscopy (EDX) can be applied simultaneously.

For the spectroscopic characterisation, X-ray diffraction analyses for crystallinity were performed by using a Bruker AXS (Germany) D8 Advance diffractometer (voltage 40 kV; current 40 mA), Fourier transform infrared (FTIR) spectroscopic measurements were done with a PerkinElmer model Spectrum 100- series spectrometer (Perkin Elmer, Walthan, MA, USA) and a Ultra-violet visible (UV-Vis) spectrophotometer Nicolet evolution model 100 (Thermo Electron Corporation, UK) was used for optical measurements. Furthermore, surface analysis of multi-shell nanoalloy was carried out with a PHI 700 Scanning Auger Nanoprobe (electron beam of voltage 25 kV, current 10 nA) and sample measurements were done under true UHV conditions.

3.3. Preparation of nanoalloys

3.3.1. Synthesis of novel PVP-capped ternary nanoalloys

Procedure 1: Cu@Pt@Ir nanoalloys

The chemical synthesis was carried out via a direct heterogeneous nucleation and growth mechanism whereby there is a growth of one or more secondary material layers onto the surface of preformed nano-crystals seeds serving as starting "cores". (In general multi-layered nanostructures were formed by first preparing nanoparticles of one material which were then used as nucleation seeds to deposit other materials on the surface).

In a typical synthesis of a trimetallic Cu@Pt@Ir multi-shell nanoalloy, the metal precursors were reduced successively. Thus firstly, a $Cu(NO_3)_2.xH_2O$ solution (2 mL, 0.102 M) was dissolved in 100 mL of highly purified water in a round bottom flask. The light blue solution was stirred for 5 minutes and then a freshly prepared solution of $NaBH_4$ (3.1 mL, 0.2M) which was aged for 3 hours was added under vigorous magnetic stirring over 10 minutes. To this solution, $H_2Cl_6Pt.6H_2O$ solution (2 mL, 0.096 M) was added, with $NaBH_4$, acting as a reducing agent, was added slowly drop wise (2.8 mL, 0.2 M) to the reaction mixture under vigorous magnetic stirring for further 10 minutes. Lastly, the $IrCl_3.xH_2O$ solution (1.1 mL, 0.188 M) and $NaBH_4$ (1.5 mL, 0.2 M) was added. After a few seconds, PVP (1.5 mL, 5mg/mL) was added drop-wise to the reaction mixture as a capping agent to stabilise and prevent agglomeration of nanoparticles and the reaction mixture was left under vigorous magnetic stirring for continuous 10 minutes. The resultant nanoparticle solution was black in colour after all metal precursors were fully reduced (see **Scheme 12**). The synthesis was carried out at room temperature ~ 25 ºC. More details on how multi-shell nanoalloys are formed via a direct heterogeneous nucleation and growth mechanism has been discussed under subsection of "Mechanisms leading to the formation of core@shell hybrid nano crystals (HNCs)" of the previous chapter.
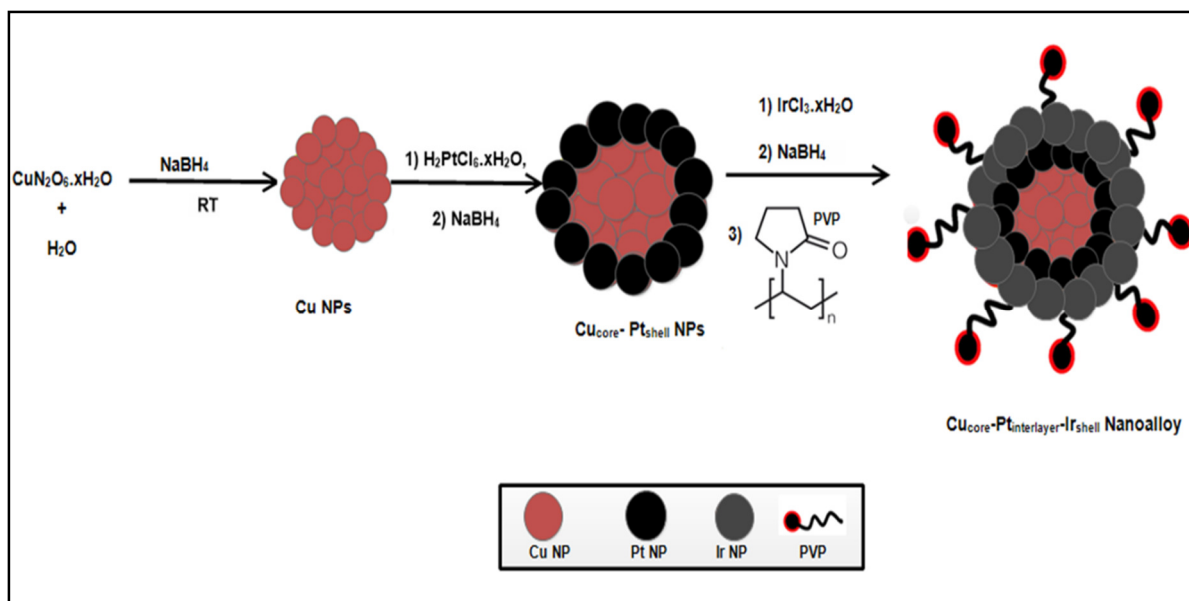
Scheme 12: Methodology used for synthesis of Cu@Pt@Ir nanoalloys via a direct heterogeneous nucleation and growth mechanism.

Procedure 2: Cu, Pt, Ir mono-metallic NPs and Cu-Pt-Ir nanoalloys

Cu, Pt and Ir mono-metallic NPs were prepared in the same way using the appropriate precursors i.e. $Cu(NO_3)_2.xH_2O$, $H_2Cl_6Pt.6H_2O$ and $IrCl_3.xH_2O$ solutions respectively. Similarly, the Cu-Pt-Ir mixed nanoalloys were prepared by one-pot synthesis through co-reduction of $Cu(NO_3)_2.xH_2O/H_2Cl_6Pt.6H_2O/IrCl_3.xH_2O$ solution mixture with a $NaBH_4$ reducing agent in presence of the PVP capping agent. (The quantities used were the same as the one used in **Procedure 1**).

3.3.2. Purification of the novel PVP-capped nanoparticles

The resulting nanoparticle hydrosol was subjected to centrifugation at 14000 rpm for 30 min (and the precipitated NPs product was collected by discarding the colourless supernatant) to remove any remaining impurities such as excess PVP and unreacted metal precursors. The pre-concentrated NPs solution was washed twice with double distilled water and finally with ethanol. Some of the resultant nanoparticles were lyophilized (freeze dried) and analysed by

various techniques such as XRD, AES/SAM, etc. and for the purpose of HRSEM, FTIR, HRTEM and electrochemical characterisation techniques, the resultant NPs were redispersed in ethanol at room temperature.

There are always obstacles when it comes to production of highly purified (that is free of excess starting salt material and ligand) and mono-dispersed nanoalloys; hence the strategies for overcoming this challenge needs to be developed. More specifically, these variables (purity and mono-dispersity) can affect the precise determination of optical and electronic properties [182]. In most cases when synthesised nanoalloys are water-soluble, then the purification process is even more difficult because other impurities also have similar solubility too. In such cases standard purification techniques known like precipitation, extraction, chromatography, centrifugation, or dialysis) becomes inefficient and diafiltration method can be used as a greener alternative to conventional methods [182]. In this study the diafiltration membranes (Vivaspin centrifugal tubes) were used to separate nanoparticles solution which could not be purified by conventional centrifuge systems.

3.3.3. Formation mechanism of CuPtIr alloy nanoclusters in presence of PVP

During this process, Cu (II), Pt (IV) and Ir (III) are reduced successively to their metallic (zero-oxidation) state i.e. Cu^0, Pt^0 and Ir^0 with Cu being reduced prior to Pt and finally reducing Ir, to form the Cu@Pt@Ir. For the formation of the mixed Cu-Pt-Ir nanoalloys, the metal ions are reduced at the same time and their structure is controlled by the order of the respective chemical reduction potentials of their ions. The BH^{4-} plays the role of being the reducing reagent, which is the source of electrons, while PVP acts as the stabilizing reagent for controlling the particle growth or the reduction rate of metal ions. A polymer like PVP, with its high affinity to bind strongly to noble metals, is often used to prevent agglomeration of metal atoms by inhibiting increasing particle size. PVP is the most commonly used polymer for NP stabilization and catalysis, due to the fact that it fulfils both steric and ligand requirements by binding to the NP surface via the heteroatom. The polymer becomes adsorbed to the cluster in aqueous solution, reducing the surface tension during synthesis.

Therefore, an oversimplified scheme of the interactions between the PVP capping agent and metal ions is shown in **Figure 11 [183]**, which illustrates that the Pt (IV), Ir (III) and Cu (II) ions coordinate with the nitrogen (N) and oxygen (O) atoms of the amide group in a PVP polymeric chain by the strong ionic bonds. A covered layer would generate on the surface of the particles and through steric and electrostatic stabilization of the amide groups of the pyrrolidone rings and the methylene groups, this layer stabilises and inhibits the growth and agglomeration of the nanoparticles **[183-185]**. Steric hindrance is a phenomenon that is attributed to the large molecular weight (> 10 000) and the repulsive forces acting among the polyvinyl groups. However, the real mechanism is more complex, due to the presence of hydrogen bonds between water molecules themselves and between the water molecules and the carbonyl polarized groups or positively charged nitrogen from the pyrrolidone rings. Besides, each ion is surrounded with a shell of water molecules.
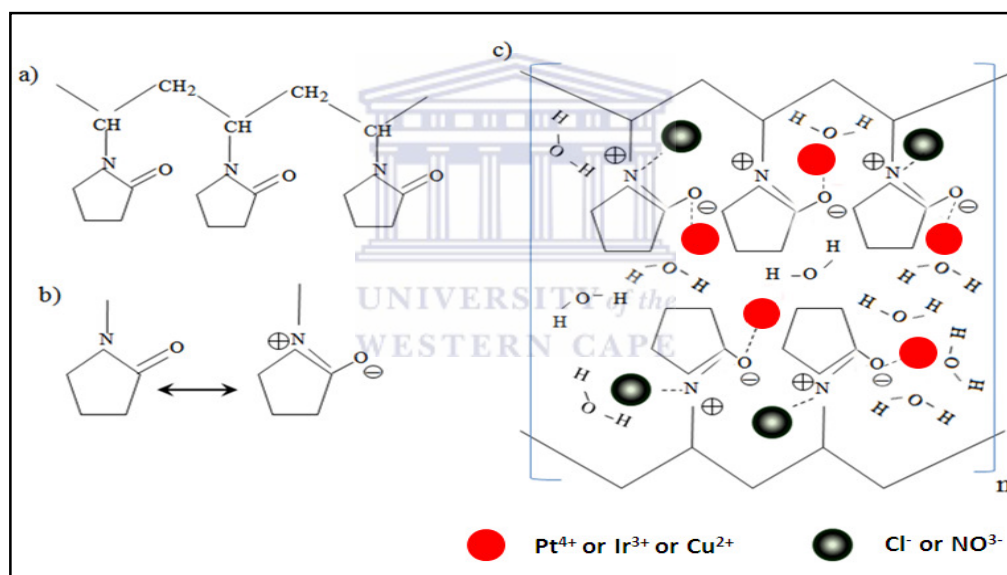
Figure 11: (**a**) A one short chain of PVP polymer; (**b**) resonance structures of a pyrene ring in PVP molecule and (**c**) the proposed oversimplified mechanism of interactions between PVP and metal ions, (adapted from ref **[183]**).

After the successful synthesis of the PVP capped nanoparticles, their surface is protected by a negatively charged protective layer of PVP which is coordinated to the surface of NPs through O atom as illustrated in **Figure 12** below. Owing to the repulsion of negative charges on the surface coating of the NPs, the aggregation of clusters is avoided.
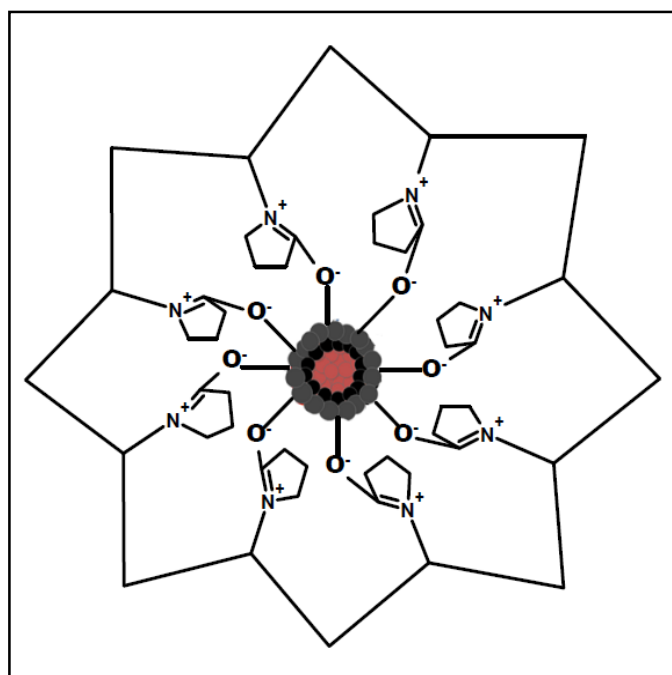
Figure 12: Sketch of nanoparticles protected by the PVP layer.

3.4.   Electrode Preparation

Prior to electrochemical characterisation, the surface of the GC disc electrodes were cleaned by polishing the surface on polishing pads and aqueous slurries of (0.05, 0.3 and 1.0 μm) alumina powder. Eventually, the electrodes were rinsed and thoroughly washed by ultrasonic treatment in ethanol and doubly distilled water, for 5 minutes respectively. The electrodes were thoroughly rinsed and wiped to dry before modification.

3.5.   Fabrication of the GC electrode with nanoalloys

The already prepared pure NPs solutions obtained after purification were used for the electrochemical characterisation and application. Thus, 10 μL solutions of the synthesised nanoalloys were drop-coated and spread evenly onto the surfaces of the GC electrodes to form the nanoalloy modified GC electrodes. Afterwards, the electrodes were allowed to dry overnight at room temperature. Consequently, the completely dried nanoalloy modified

electrodes were rinsed with distilled water prior to electrochemical characterisation and application, to remove weakly adsorbed sample particles. From there, the modified electrodes were ready for electrochemical characterisation and application.

3.6. Characterisation of the nanoalloys and sample preparation

The purpose of the present work is to report in the synthesis of the PVP-capped colloidal Cu-Pt-Ir mixed and multi-shell trimetallic nanoparticles through a conventional borohydride reduction method. The structural and morphological characteristics of the prepared Cu-Pt-Ir trimetallic nanoparticles were studied with various techniques to verify the influence of PVP on the morphology, stability and particle size distribution of the nanoparticles, as well as to explore other parameters of interest. This sub-section presents various characterisation techniques employed to attain the objectives of the study.

3.6.1. Structural characterisation

3.6.1.1. UV-Visible spectroscopy

UV-Visible spectroscopy was used to ensure complete reduction of metal ions to form the nanoparticles. The absorption spectra were collected using a Nicolet evolution model 100 UV-Vis spectrophotometer (Thermo Electron Corporation, UK). The freshly prepared samples (from mother liquor) were measured against distilled water as a reference. All the samples were sufficiently diluted with distilled water in the 3 mL quartz cuvettes for measurements. All the measurements of samples were taken on the visible region ($\lambda = 200$ nm - 800 nm) at scan speed of 1200 nm/min using both D2 (Deuterium) and W (tungsten) lamps.

3.6.1.2. Fourier Transform Infrared (FTIR) Spectroscopy

Fourier transform infrared spectroscopy was used to identify the presence of certain functional groups of the capping agent so as to confirm the surface modification of the synthesised NPs with PVP. The FTIR spectra of pure PVP and PVP capped Cu-Pt-Ir nanoalloy systems were obtained on a PerkinElmer model Spectrum 100 series FTIR Spectrometer. Before recording spectra, the samples were placed on a Universal diamond Attenuated Total Reflectance (ATR) sampling top-plate and pressed by applying pressure and then the spectra were recorded. The ATR crystals were cleaned by using ethanol soaked piece of tissue between sample measurements. PVP was used in its powder form, whereas PVP capped nanoparticles liquid samples from the mother solutions were used. FTIR spectra of all samples were recorded in the range 4000 - 400 cm^{-1}.

3.6.1.3. Auger Electron Spectroscopy (AES)/Scanning Auger Microscopy (SAM)

Surface analysis of a multi-shell nanoalloy sample was carried out with a PHI 700 Scanning Auger Nanoprobe working under (electron beam of 25 kV, 10 nA with Filament current = 2.288 A, Extractor Voltage = 3.58 kV, Extractor current = 226 uA and rate of 1 eV/step; 50 ms/step) to obtain AES surveys on different areas. To perform depth profiling, a "soft etching" process using low energy argon (Ar) ion gun was used for sputtering to remove surface contamination on the samples prior to analysis. The etching parameters for the ion beam energy (2 kV), total ion current (1.5 uA) at sputter rate of 15 nm/min for 1x1 mm raster and sputtering time (30 sec sputter intervals) for 5 sweeps/element were done.

The SAM images on different areas were taken by the secondary electron detector incorporated in the AES system (PHI 700 Scanning Auger Nanoprobe) by passing electron beam of 25 kV 10 nA (same as AES analysis) to achieve a 5 nm The instrument was operating under UHV conditions (upper pressure = 9.9-10 Torr, main chamber pressure = 3.47-10 Torr) and a beam diameter of about 12 nm (10 nA). The primary electron source was a Schottky thermal field emission electron column.

3.6.1.4. X-Ray Diffraction (XRD)

The structure and crystallinity of lyophilized powder samples of PVP capped Cu-Pt-Ir nanoalloys system were analysed using XRD. The XRD patterns were acquired from a Bruker AXS (Germany) D8 Advance diffractometer (voltage 40 KV; current 40 mA). The XRD spectra were recorded in the range 10-100º using X-ray source of Cu Kα (λ=0.154 nm) monochromatic radiation source.

3.6.2. Morphological characterisation

3.6.2.1. High Resolution Transmission Electron Microscopy (HRTEM)

Liquid samples of nanoparticles dispersed in ethanol, which were obtained by washing the pre-concentrated mother solutions with ethanol by centrifuging were used for HRTEM analysis. The size, shape, crystallinity and elemental composition of the nanoalloys were interrogated using High Resolution Transmission Electron Microscopy (HRTEM) coupled with Energy Dispersive X-ray (EDX) spectroscopy and Selected Area Electron Diffraction (SAED). The HRTEM images, EDX data and SAED patterns were obtained from Tecnai G2 F20X-Twin MAT Field Emission Transmission Electron Microscope from FEI (E-indhoven, Netherlands) at an acceleration voltage of 200 kV after placing a small drop of dilute nanoparticles solution on carbon coated copper grids and dried under electric bulb for 20 minutes. As for the copper containing nanoparticles nickel grids were used. Therefore the Cu/C grids were ready to be mounted on a microscope.

3.6.2.2. High Resolution Scanning Electron Microscopy (HRSEM)

The HRSEM was used to study the surface morphology of nanoalloys. The images were recorded using a Zeiss Auriga HRSEM analyser using the secondary electron (SE) mode with accelerating voltages of 25 kV. The HRSEM samples were prepared in a same way as HRTEM samples (**described in section 3.6.2.1 above**), that is catalyst suspensions were

drop-coated on nickel grids surface, allowed to dry and then placed onto a carbon adhesive mounted on aluminium stubs. From there the grids were ready to be mounted on a microscope.

3.6.3. Electrochemical characterisation

3.6.3.1. Cyclic Voltammetry (CV)

For the electrochemical characterisation of the nanoparticles, the nanoalloy modified GC electrodes (**described in section 3.5 above**) were used as working electrodes. The electrochemistry of synthesised nanoparticles was interrogated in each of 3 mL of 0.1 M LiClO$_4$ electrolyte at a potential range of -1.0 V to 1.0 V at different potential scan rates. The electrolyte solutions were degassed with argon gas for about 20 minutes before and blanketed with argon atmosphere during measurements at room temperature using an Epsilon potentiostat.
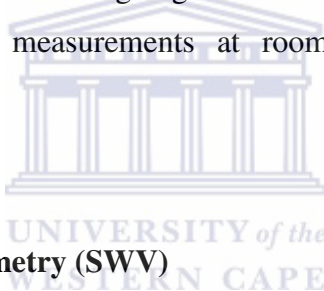
3.6.3.2. Square wave voltammetry (SWV)

Square wave voltammetric studies were done to complement the results obtained from CV as SWV is more sensitive. A conventional three-electrode system from BASi and an Epsilon potentiostat were used to record voltammograms. The same parameters (electrolytes and potential window) used for CV studies were applied for SWV of electrocatalysts and all experiments were carried under argon atmosphere.

3.7. Application of nanoalloys in the electrochemical oxidation of ammonia

Cyclic and square wave voltammetric techniques were used for the oxidation of ammonia at room temperature in a single compartment three-electrode glass cell. This was performed on Epsilon electrochemical analyser with conventional three-electrode system as explained in

section **3.2** above. The glassy carbon electrodes fabricated with Cu, Pt, Ir NPs, mixed Cu-Pt-Ir and multi-shell Cu@Pt@Ir nanoalloys respectively (prepared in experimental procedures section **3.5** above) were used as the working electrodes. Thus the electrocatalytic activity of the GC|Cu, GC|Pt, GC|Ir, GC|Cu-Pt-Ir mixed and GC|Cu@Pt@Ir multi-shell electrodes for ammonia oxidation were tested by CV and SWV studies in an alkaline solution consisting of 1 M KOH and 0.1 M NH$_4$OH supporting electrolyte solutions. The electrolyte solutions were degassed with argon gas for approximately 20 minutes. The potential range of -1.0 V to 0.10 V was applied at a scan rate of 10 mV s^{-1}. Therefore, the voltammetric studies were also done at different scan rates to investigate the processes that occur on the electrode surface. The effect of ammonia concentration was also investigated.

UNIVERSITY *of the*

WESTERN CAPE

CHAPTER 4

RESULTS AND DISCUSSION (I)

Summary

This chapter discusses the results obtained from the study of the novel Cu-Pt-Ir nanoalloys synthesised for the electrochemical oxidation of ammonia. The chapter specifically addresses the characterisation of Cu, Pt, Ir, Cu@Pt@Ir (multi-shell) and Cu-Pt-Ir (mixed) nanoalloys prior to their application in the electrochemical oxidation of ammonia. These polyvinylpyrrolidone (PVP) capped nanoalloys were successfully synthesised by the conventional borohydride reduction of metal precursors at room temperature. The optical, structural, morphological and electrochemical properties of these nanoalloys were characterised using UV-Vis, FTIR, XRD, NanoSAM, HRSEM, HRTEM, CV and SWV and are also discussed.
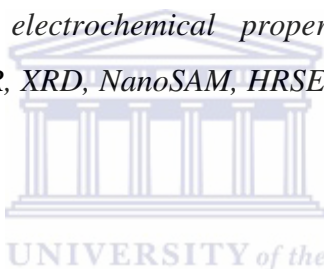
4.1. Spectroscopic and microscopic characterisation of nanoalloys

4.1.1. UV-Visible spectroscopy

UV-Visible spectroscopy was used to show the complete reduction of the metal ions, which confirmed that Cu^{2+}, Pt^{4+} and Ir^{3+} were fully reduced to form the nanoparticles. **Figure 13A** illustrates the UV-Visible spectra of the solutions of the starting materials $H_2Cl_6Pt.6H_2O$, $IrCl_3.xH_2O$ and $Cu(NO_3)_2.xH_2O$, whereas **Figure 13B** shows the changes observed in UV-Visible spectra for the Cu, Pt, Ir, Cu@Pt@Ir and Cu-Pt-Ir nanoparticles formed. The reaction mixture before reduction was pale yellow to colourless with the $Cu(NO_3)_2.xH_2O$ showing absorption peaks at 302 nm, 780 nm whereas the $H_2Cl_6Pt.6H_2O$ solution showed an absorption peak at 262 nm, while the $IrCl_3.xH_2O$ solution showed absorption bands at 400 nm, 490 nm, 606 nm, all of which are a result of the ligand to metal charge transfer transitions between filled and unfilled d-orbitals of the Cu, Pt and Ir metal ions ($Cu(NO_3)_2$, $PtCl_6^{2-}$, $IrCl_3$). The colour of reaction mixture turned dark brown, grey and finally black after

the reaction. The absorption peaks observed from the individual pure metal pre$_{cu}$rsors solutions were no longer visible after the reduction process, signifying that the metal precursors were fully reduced to their respective zero-valent nanoparticles **[143]**.
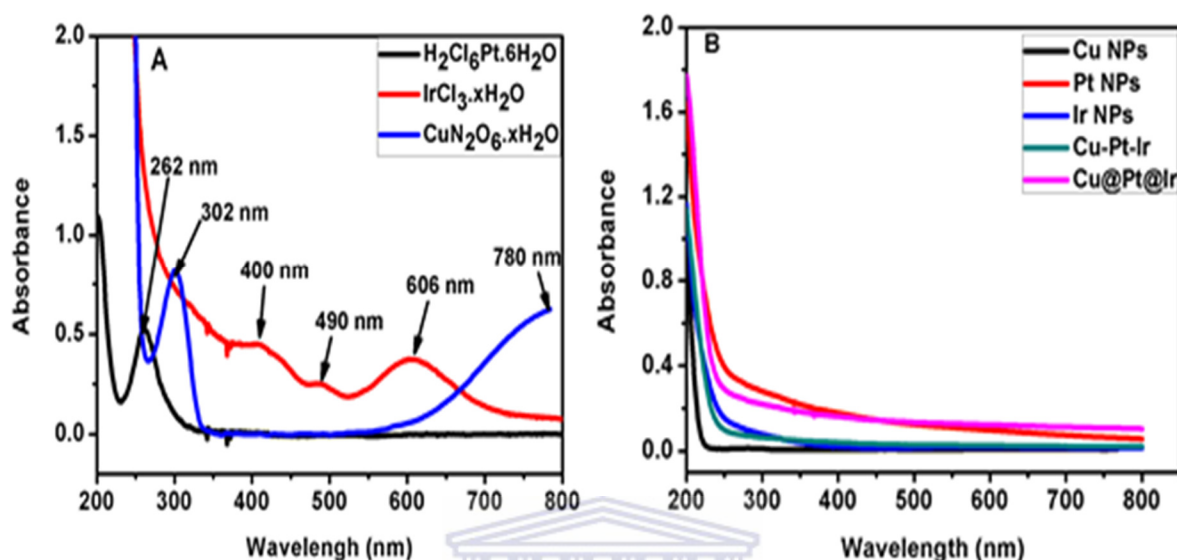
Figure 13: UV-Vis spectra of plain metal salts: Copper (II) nitrate hydrate, Iridium (III) chloride hydrate and Hydrogen hexachloroplatinate (IV) hexahydrate solutions (**A**) and UV-Vis spectra of Cu, Pt, Ir mono-metallic NPs and Cu-Pt-Ir and Cu@Pt@Ir trimetallic nanoalloys (**B**). All spectra were measured in water.

4.1.2. Fourier transform infra-red (FTIR) spectroscopy analysis

FT-IR spectroscopy was used to ensure that the synthesised nanoalloys were PVP (**Figure 14**) capped. A strong broad peak in the range of 3500 to 3200 cm^{-1} was observed due to the presence of hydroxyl groups from the water adsorbed onto the surface of NPs. Pure PVP also showed a similar but very weak absorption peak which may also be due to some moisture (**Figure 15**). The vibrational peak of carbonyl group in PVP was observed at around 1650 cm^{-1} while that for the NPs (at 1644 cm^{-1}) shows a slight red shift in the position of the peak (**Figure 15**). The peak shift of C = O absorption band reveals the strong interaction between NPs (Cu, Pt, Ir, Cu-Pt-Ir and Cu@Pt@Ir) and PVP. The other peaks which appear at 1285 cm^{-1}, 2860 cm^{-1} and 2941 cm^{-1} (**Figure 15**) corresponding to the C-N stretch of PVP monomer, the CH$_2$ stretch modes of pyrrolidone ring and the polymer backbone and the

tertiary C-H stretch of the pure PVP respectively were weakened greatly on adsorption to the NPs [185]. These changes, including the shift in the peaks (**Figure 15**) indicate that there was some interaction/coordination between oxygen atom in the amide group of the PVP and the NPs [183, 185].
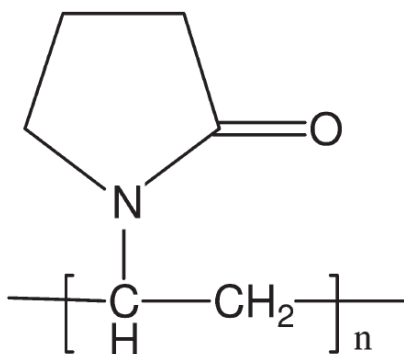
Figure 14: The structure of polyvinylpyrrolidone (PVP).
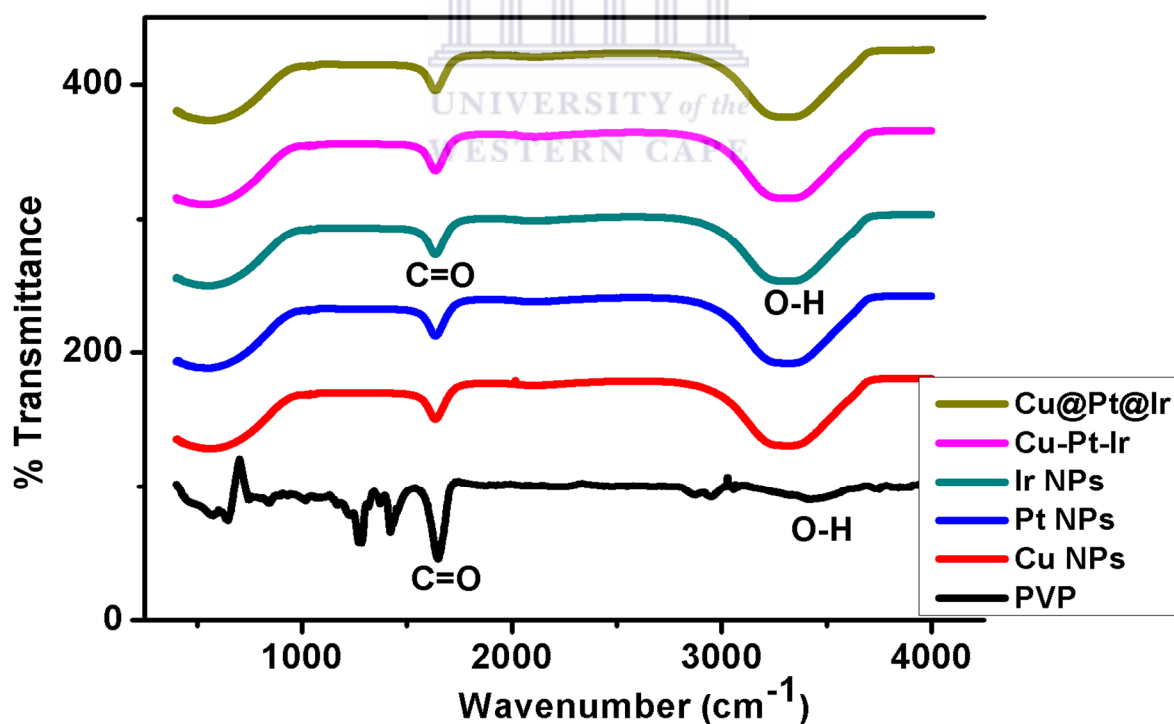
Figure 15: Typical FTIR spectra of PVP capped Cu@Pt@Ir, Cu-Pt-Ir, Pt, Ir and Cu NPs in comparison with pure PVP.

4.1.3. High resolution transmission electron microscopy (HRTEM) analysis
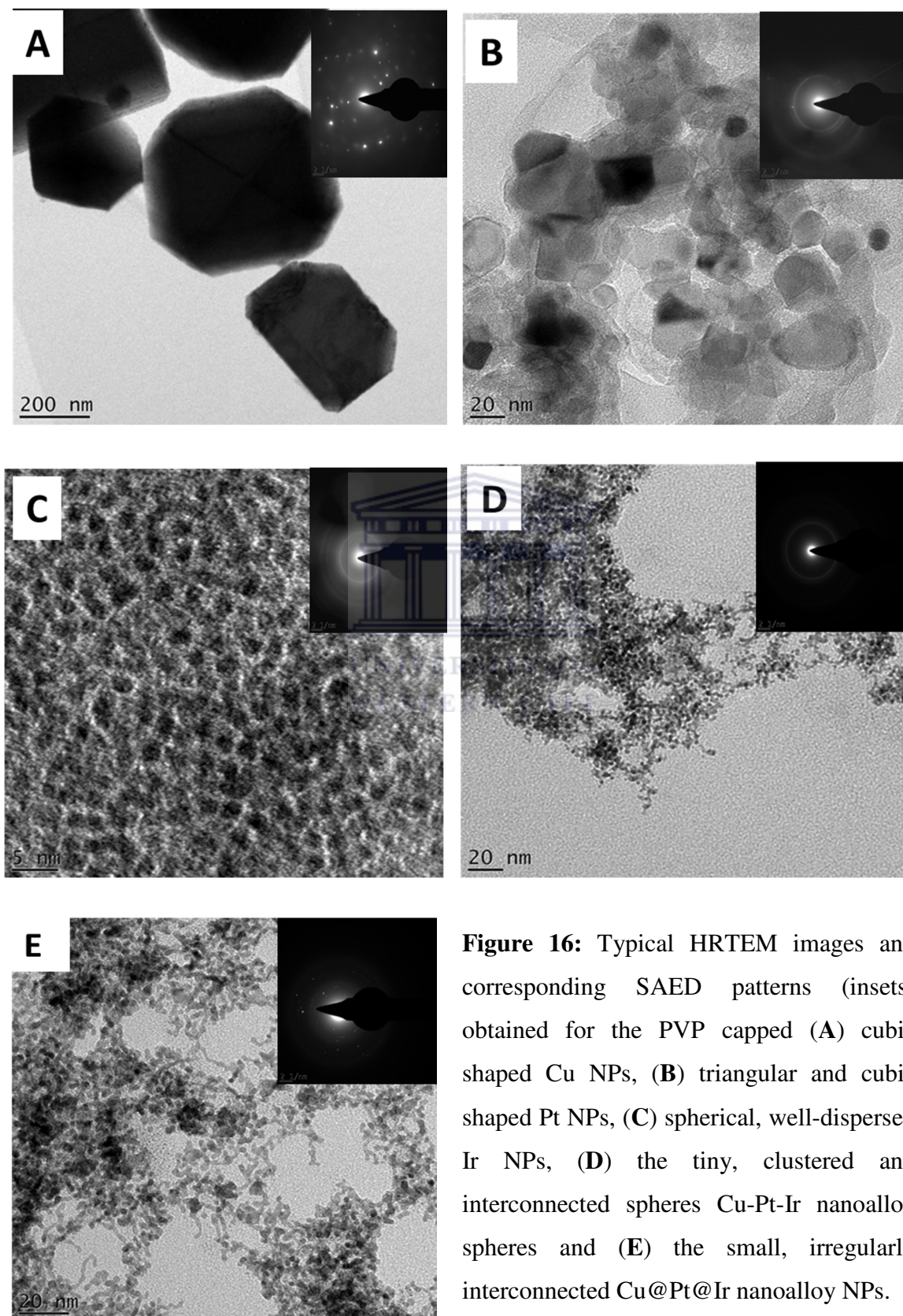
Figure 16: Typical HRTEM images and corresponding SAED patterns (insets) obtained for the PVP capped (**A**) cubic shaped Cu NPs, (**B**) triangular and cubic shaped Pt NPs, (**C**) spherical, well-dispersed Ir NPs, (**D**) the tiny, clustered and interconnected spheres Cu-Pt-Ir nanoalloy spheres and (**E**) the small, irregularly interconnected Cu@Pt@Ir nanoalloy NPs.

106

The particle size, shape and crystallinity of the NPs were investigated using High Resolution Transmission Microscopy. **Figure 16A** shows HRTEM image obtained for the PVP capped Cu nanoparticles. The nanoparticles produced were found to be well dispersed, cubic shaped with an average diameter of 400 nm. The disadvantage of Cu NPs is that their size and shape are difficult to control as they undergo very rapid growth, coupled with rapid colour changes. Spherical, cubic and triangular shaped (poly-oriented) 20-30 nm sized Pt nanoparticles were obtained (**Figure 16B**). The presence of cubic shaped nanoparticles is a characteristic feature of (100) oriented nanoparticles **[143]**. The spherical, well dispersed Ir NPs ~ 2-5 nm sized was observed as shown in **Figure 16C**. For the nanoalloys, dense agglomerates of interconnected Cu-Pt-Ir nanoalloy NPs with average particle size of ~ 3-10 nm (**Figure 16D**) and small interconnected irregular shaped Cu@Pt@Ir nanoalloy NPs with a ~ 5-10 nm size (**Figure 16E)** were observed. Upon close inspection of **Figure 16E**, one can observe that the Cu@Pt@Ir nanoalloy comprises spherical, as well as non – spherical, NPs. The spherical NPs are called the primary particles, while the non - spherical ones are referred to as the secondary NPs. The secondary nanoparticles grow at the expense of the primary nanoparticles via intraparticle Ostwald ripening which occurs during heterogeneous nucleation followed by ripening or coalescence **[147]**. The nanoalloys were found to be smaller (<10 nm) in size and aggregated compared to the individual NP counterparts, making measurement of exact particle size difficult. The non-aggregation observed in Cu, Pt and Ir nanoclusters is assumed to have resulted from the electrostatic, partial negatively charged oxygen atom, present in the PVP amide functional group **[143]**. Whereas aggregation of the produced nanoalloys may be due to insufficient PVP capping agent present as this would cause an increase in the surface area to volume ratio, with a concomitant increase in the attractive forces between the nanocrystals causing them to agglomerate **[179]**. Due to the very small size of NPs, HRTEM could not reveal nanoalloy structure was a multi-shell structure or not. The only observation that could be made was the difference in contrast between the structures, whereby black spots and grey spots can be detected, but not much else could be concluded. Hence, the multi-layered structures were probed with the NanoSAM technique. However, when it comes to catalysis, noble metal NPs of sizes of less than 10 or 20 nm are of particular interest due to their excellent high surface area effects and increased catalytic active sites **[86]**. On the other hand, HRTEM coupled to EDX is more restricted when it comes to confirming multi-layered structures of small systems due to the possibility of sample preparation damage and analytical artefacts which are related to the thin sample

preparation methods used for electron transparency and the utilization of high primary beam energy [186].

The selected area diffraction (SAED) data presented as insets showed a distinct pattern of very bright but diffuse spots for Cu NPs (**Figure 16A**), which is a characteristic of crystalline defects showing some degree of amorphousness. As for Ir NPs (**Figure 16C**) and Cu-Pt-Ir nanoalloy (**Figure 16D**), their SAED patterns resemble that of crystalline particles owing to the bright rings observed. On the other hand, the SAED pattern obtained for the Pt NPs (**Figure 16B**) and Cu@Pt@Ir nanoalloys (**Figure 16E**) exhibited polynanocrystalline diffraction rings from the few pronounced spots corresponding to their characteristic reflections [187]. High magnification HRTEM images (not shown) of the NPs showed lattice fringes associated with the crystallinity of the NPs. To further validate the crystallinity of the nanoalloy systems, XRD was used, which showed both the individual NPs and the nanoalloys to be crystalline (see **Figure 19A-E**), thus supporting the obtained SAED results.
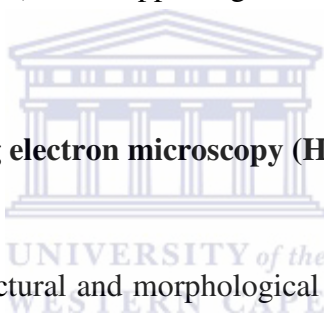
4.1.4. High resolution scanning electron microscopy (HRSEM) analysis

HRSEM was utilized for the structural and morphological studies of the PVP-capped mono-metallic NPs and nanoalloys, and the obtained HRSEM images are presented in **Figure 17A-E** below. The Cu NPs possess well defined sharp faces and corners. The surfaces of the ~ 200-350 nm sized Cu NPs are smooth and dispersed. Unfortunately, attempts to obtain HRSEM images for the particles did not yield clear images due oxidation of the Ir NPs surface (**Figure 17C**) resulting in a non-conducting iridium oxide. This caused charging of the specimen when it was scanned by the electron beam, resulting in scanning faults and other image artefacts. Nonetheless, the HRSEM images obtained (**Figure 17**) showed that only the image of Cu NPs (**Figure 17A**) was the most clear due to the size of the big particles, whereas the Pt NPs, Cu-Pt-Ir and Cu@Pt@Ir nanoalloys had their HRSEM images which exhibited particles with smooth shaped morphologies, but owing to their small size, the shapes were not quite clear. Furthermore, just as for HRTEM, the HRSEM data obtained was not sufficient to provide chemical information on the multi-shell structure because of the scale of the excitation volume [186].
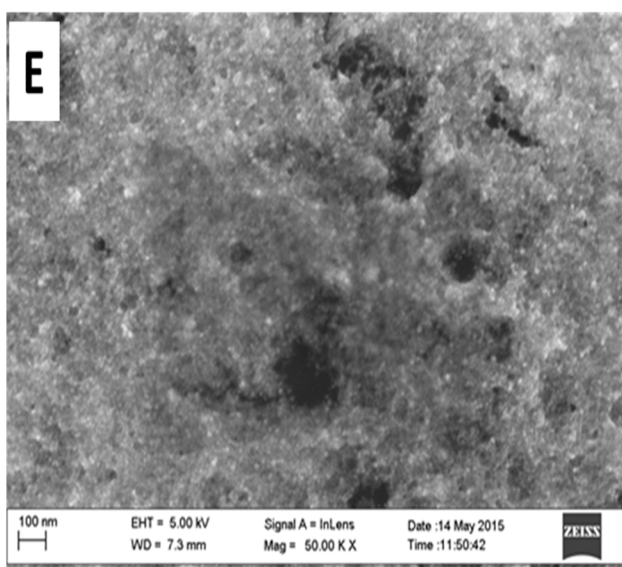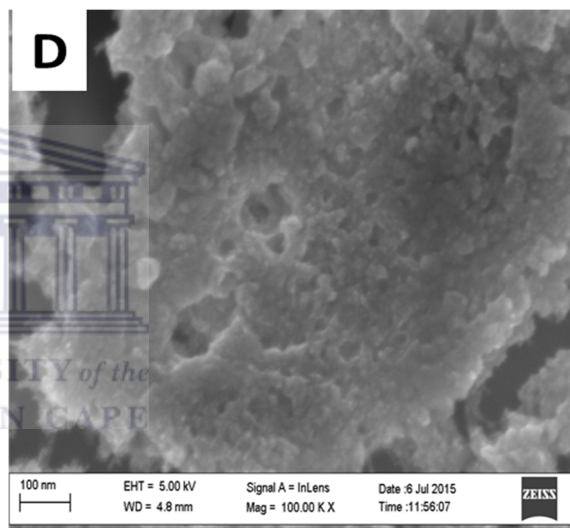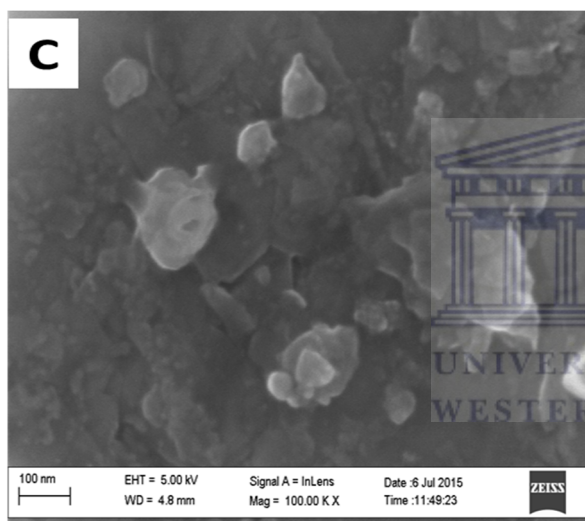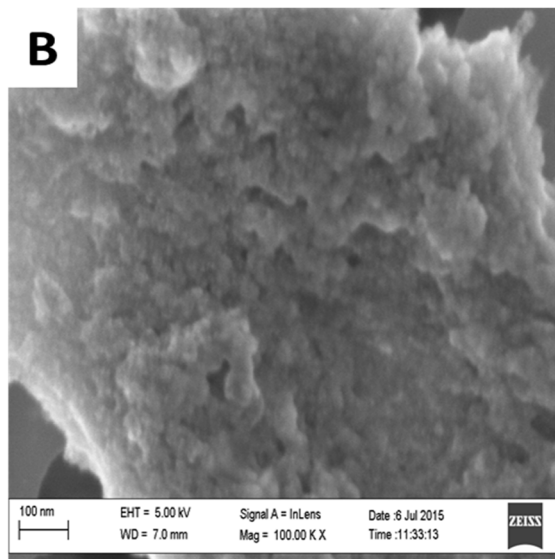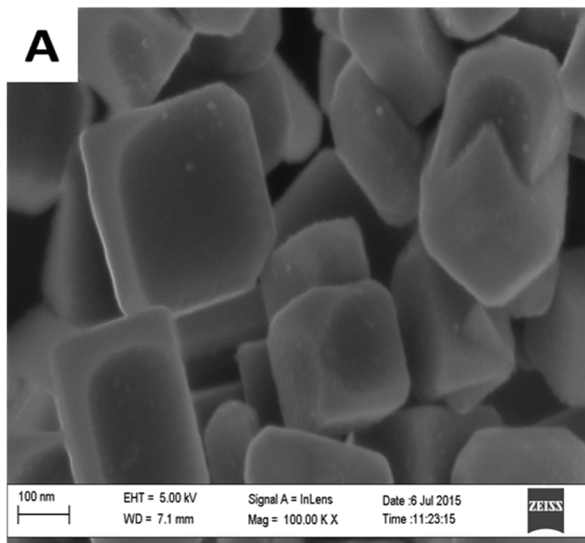
Figure 17: HRSEM micrographs of PVP capped (**A**) cubic shaped Cu NPs, (**B**) Pt NPs, (**C**) Ir NPs, (**D**) Cu-Pt-Ir nanoalloy and (**E**) Cu@Pt@Ir nanoalloy.

109

4.1.5. Energy dispersive X-ray spectroscopy (EDX) analysis

EDX was used to investigate the elemental composition of the synthesised nanoalloys. **Figure 18** (**A**), (**B**), (**C**), (**D**) and (**E**) illustrate the EDX spectra of Cu, Pt, Ir, Cu-Pt-Ir and Cu@Pt@Ir nanoparticles, respectively. The analyses confirmed the elemental composition of nanoalloy systems to be that of Cu, Pt and Ir. However, other impurities were also detected and these include: carbon, oxygen, copper, nickel and chlorine. The presence of copper and nickel in non-copper and non-nickel containing nanoparticles is due to the copper and nickel grids which were used as substrates for HRTEM analyses. The presence of oxygen is likely to be from the stabilizing agent (PVP) used, while carbon could be from the sample grids which were carbon coated and the PVP, while chlorine may be the result of unreacted metal chloride precursors. The absence of Ir in both the mixed and multi-shell Cu-Pt-Ir nanoalloy may be attributed to the overlapping of the Pt and Ir signals; hence EDX could not determine the atomic composition of the sample **[12]**. Due to time constraints inductively coupled plasma optical emission spectroscopy (ICP-OES) analyses which could have indicated the Ir presence/content could not be carried out. When certain elements are present in small quantity in the sample, other elements which have close K-alpha, L-alpha or M-line energy values may be more dominant and hinder such elements and are therefore not detected.
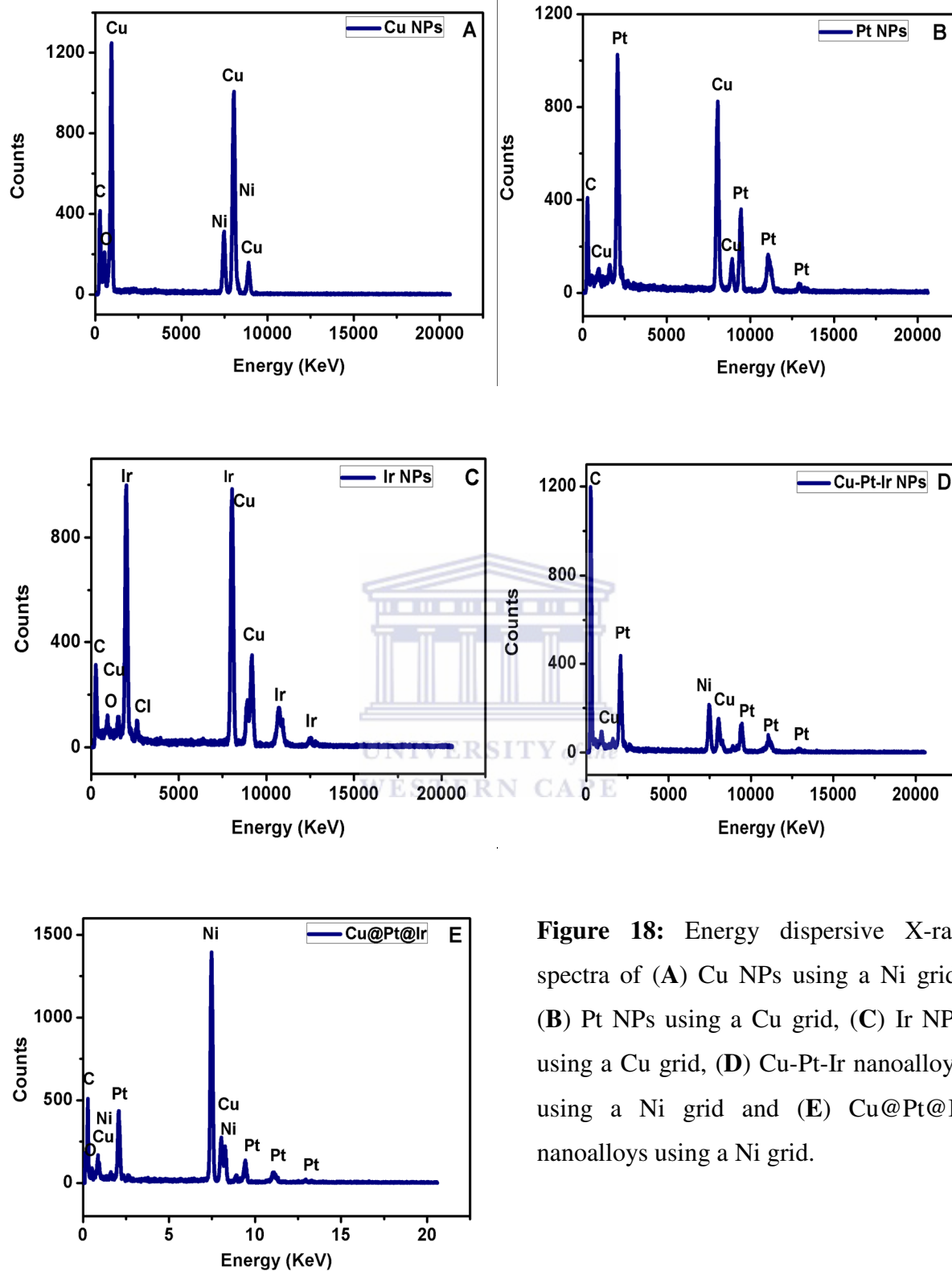
Figure 18: Energy dispersive X-ray spectra of (**A**) Cu NPs using a Ni grid, (**B**) Pt NPs using a Cu grid, (**C**) Ir NPs using a Cu grid, (**D**) Cu-Pt-Ir nanoalloys using a Ni grid and (**E**) Cu@Pt@Ir nanoalloys using a Ni grid.

111

4.1.6. X-ray Diffraction (XRD) spectroscopic analysis
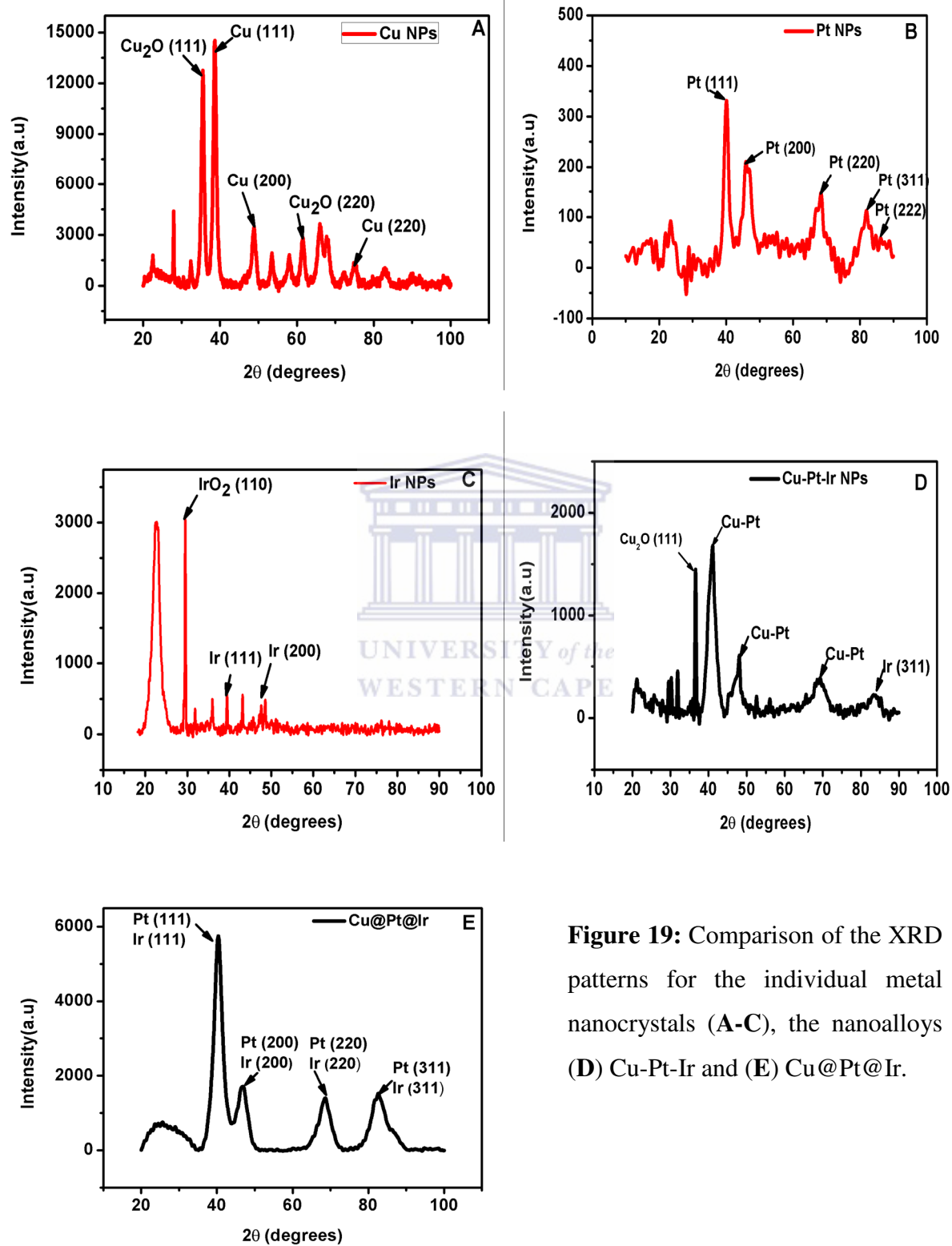
Figure 19: Comparison of the XRD patterns for the individual metal nanocrystals (**A-C**), the nanoalloys (**D**) Cu-Pt-Ir and (**E**) Cu@Pt@Ir.

The diffraction patterns obtained from XRD gives information on the estimated nano crystallite size and the unit cell shape or structure from the peak positions observed as well as the electron density information from peak intensities. The XRD pattern of the mono-metallic NPs and nanoalloys showed that they are crystalline and it also showed successful reduction of metal salts, confirming the UV-Vis spectroscopy and HRTEM results. The diffraction patterns of the pure metallic NPs can be indexed to the (111), (200), (220), (311) and (222) planes of the face centered cubic (FCC) crystal structures **[28]**. In both the co- and successively reduced nanoalloys, the lines for Pt are shifted to higher 2θ values due to the incorporation of Cu and Ir. This is sometimes due to a solid solution of other atoms that modify the unit cell slightly to larger or smaller values. Thus a solid solution of Cu-Pt (Hongshiite) in Cu-Pt-Ir and solid solution of Pt-Ir in Cu@Pt@Ir could be the origin of the slight Pt peak shift to higher 2θ values. Again, as observed in the EDX spectra for both mixed Cu-Pt-Ir and multi-shell Cu@Pt@Ir nanoalloy the peaks of Pt and Ir were overlapping. Therefore, in general these observations suggest the formation of a solid solution corresponding to the specific nanoalloy, indicating that binary and ternary nucleation has been the major nucleation process involved in the formation of these nanoalloys **[28]**. The absence of Cu peaks in the XRD pattern of multi-shell Cu@Pt@Ir nanoalloy can be attributed to the coincidence that the signal peaks of all three elements (Pt, Ir and Cu) appear at almost the same positions. The Pt and Ir elements having much larger atomic size therefore exhibit more pronounced signals than that of the small Cu atom counterpart. The EDX analysis results however showed that the Cu@Pt@Ir nanoalloy has Cu. The Pt and Ir were observed to have crystallized with the same FCC crystallographic structure, with lattice constants in very good approximation i.e. Pt (a = 3.92310 Å) Ir (a = 3.83940 Å). Thus, the NPs may be successfully employed as metal catalysts for catalysis applications. The oxidation forms of Cu and Ir may have resulted from a slight, inevitable, surface oxidation during the process of PVP-capping, NP washing, or drying. However, it is a well-known fact that it is not easy to prepare pure Cu NPs without oxygen contamination from air **[183]**. This result is in good agreement with the EDX results of samples. The observed extra diffraction peaks are due to the presence of the impurity phases. The average particle size for the NPs were determined from the FWHM of the XRD signal patterns, using the well-known Scherrer formula cited in equation (38).

From the calculations made, the crystalline particle sizes were found to be 4.4 nm, 4.5 nm, 12.3 nm, 3.5 nm and 3.4 nm for Cu NPs, Pt NPs, Ir NPs, Cu-Pt-Ir and Cu@Pt@Ir nanoalloys respectively. In comparing the average particle sizes estimated by powder XRD and HRTEM techniques, the average particles sizes estimated form XRD Scherrer equation were considerably smaller than the ones estimated from HRTEM images which were found to be 400 nm, 20-30 nm, 2-5 nm, 3-10 nm and 5-10 nm for Cu NPs, Pt NPs, Ir NPs, Cu-Pt-Ir and Cu@Pt@Ir nanoalloys respectively. This may be because HRTEM images show the total size of a nanoparticle, whereas XRD provides the average size of the single crystalline domain inside the nanocrystal **[188]**.

4.1.7. Auger Electron Spectroscopy (AES)/Scanning Auger Microscopy (SAM)

Auger electron spectroscopy (AES) provides spatially resolved surface elemental information analysis and is complementary to XPS results. Surface analysis of the multi-shell Cu@Pt@Ir nanoalloy was carried out with AES as the NanoSAM system analyses the top 10 nm of the samples. However there was a problem of excessive charging from the sample of interest which required the adjustment of Auger experimental settings to control the charging effect and the related drift parameter during the analysis. The suitable excitation conditions which give high sensitivity with the reduced beam current of 25 kV 1 nA was used as a strategy to reduce charging effects and the following results SAM images (**Figure 20)** from which AES surveys tests were conducted on different areas 3, 5, 9, 13-15spe (**Figure 21)**, were obtained under these conditions. The % atomic concentrations of elements obtained from AES spectra are tabulated in **Table 6.**
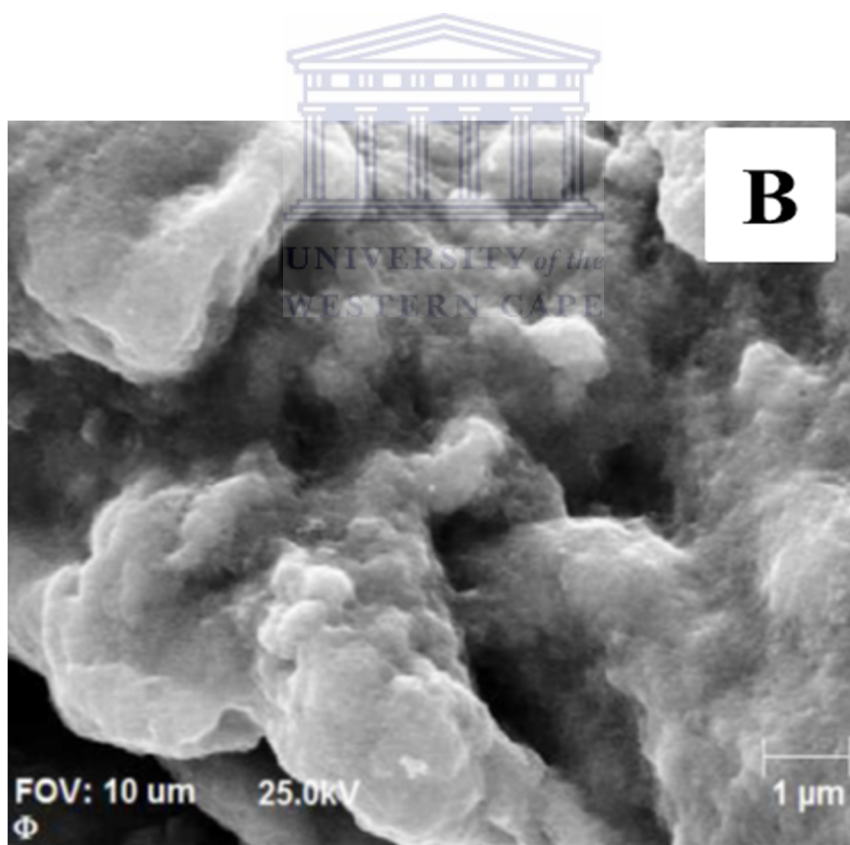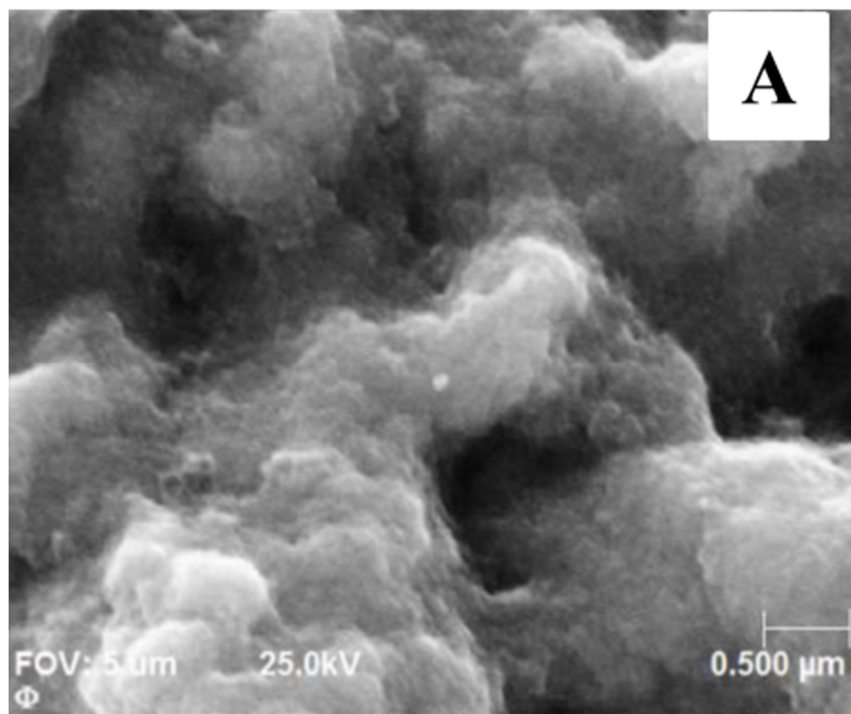
Figure 20: SAM images of multi-shell Cu@Pt@Ir nanoalloy at different magnification (**A**) 0.500 µm and (**B**) 1 µm scale view.
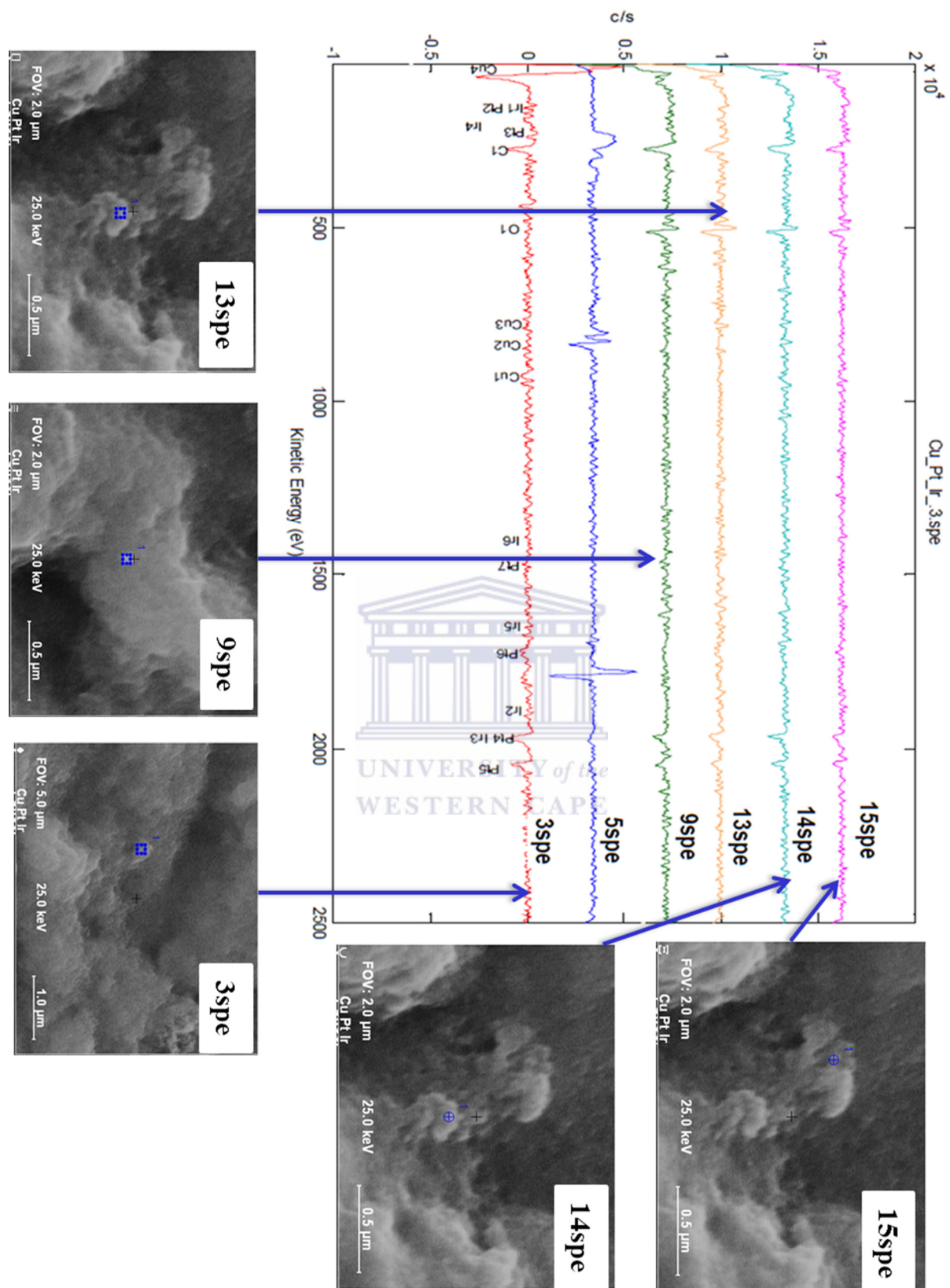
Figure 21: The full AES survey spectra for Cu@Pt@Ir is shown, along with the SAM maps (insets) for the location of various spots chosen for survey analysis.

Since the Auger peaks are small and exhibit some overlap, the spectrum is usually presented in derivative form for interpretation as in **Figure 21** above. It is evident that sample requirements (conductive) play a significant role in surface analysis by AES. The SAM images obtained (**Figure 20**) are a true reflection of the HRSEM image obtained for the Cu@Pt@Ir nanoalloy. Thus a sample can give good results and be analysed using AES if one can obtain good SEM pictures from it without coating.

Table 6: Atomic Concentration

Spots	C1	O1	Cu1	Ir2	Pt4
3spe	35.51	3.07	4.13	14.50	42.79
5spe	55.94	5.19	4.89	8.25	25.73
9spe	46.75	16.46	2.97	3.46	30.37
13spe	33.94	18.76	2.09	10.57	34.64
14spe	35.26	14.37	3.47	10.97	35.93
15spe	41.14	13.24	3.71	11.45	30.45
Mean	41.42	11.85	3.54	9.87	33.32

Analysis of all the points analysed showed element transitions for C1, O1, Cu1, Ir2 and Pt4 which attests to the presence of all three metals with mixed boundaries. Thus according to this results, Cu@Pt@Ir which was assumed to be a multi-shell nanoalloy based on the mechanism of its chemical synthesis, was indeed proved to be a mixed nanoalloy of Cu, Pt and Ir, confirming that the Cu and Ir signals in the XRD and EDX were indeed obscured by overlap, and not due to the absence of Cu and Ir. All the surveys tests showed that Cu@Pt@Ir nanoalloy is composed of high concentration of Pt, with lower concentration for Cu. Any sample exposed to ambient atmospheric conditions will have C and O on the surface due to adsorption of hydrocarbons and water and surface oxidation. It could be that the sample had already decomposed and was no longer in its original state by the time of analysis. Hence the

structure was more for that of a mixed nanoalloy. Owing to charging effect of the specimen, AES elemental mapping and AES line profile experiments could not be carried out to validate the obtained AES survey results. If it were possible to accomplish profile spectra on some areas where there is no mixing of layers, it could have been detected. Again it could have been better if the AES results for both mixed Cu-Pt-It and multi-shell Cu@Pt@Ir were obtained for comparison, however due to limited time and accessibility of the instrument this could not be achieved. In the future it will be advisable to use classically effective methods such as charge neutralization, tilting and sample thickness reduction (cross polisher) to prevent the charging effect during AES experiments of non-conductive nanomaterials **[186]**. In addition, the combined use of both AES and XPS techniques can be very useful for the analysis of complex multi-shell structure.

4.2. Electrochemical characteristics of the nanoalloys

In order to gain a clear understanding of electrochemistry of the chemically synthesised nanoparticles, their redox studies were evaluated using CV. **Figure 22** shows a series of characteristic voltammetric profiles of the Cu-Pt-Ir, Cu@Pt@Ir and their corresponding mono-metallic NPs counterparts in 0.1 M $LiClO_4$ electrolyte. These were measured at a scan rate of 50 mV s^{-1} in a potential range of -1000 mV to 1000 mV.
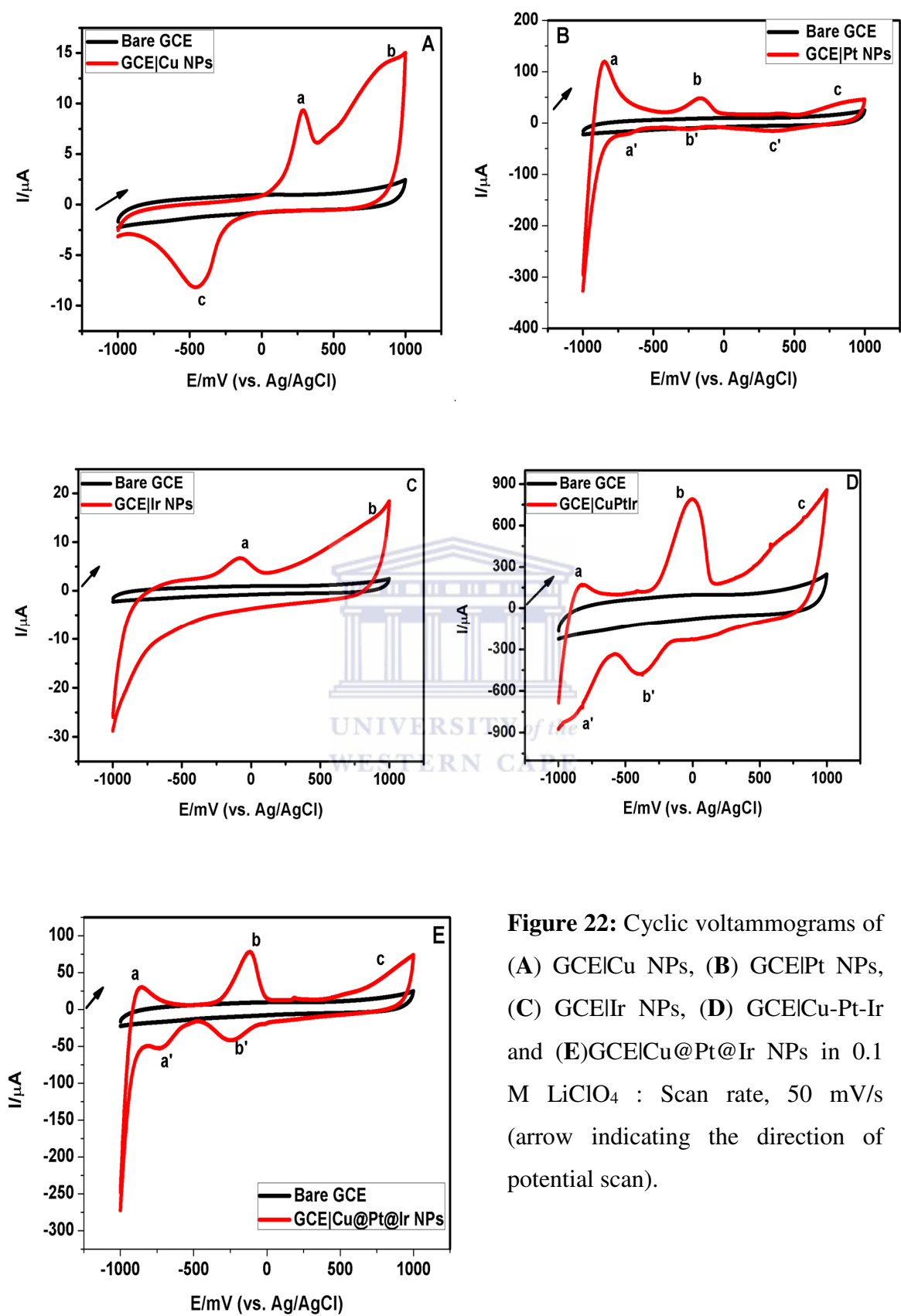
Figure 22: Cyclic voltammograms of (**A**) GCE|Cu NPs, (**B**) GCE|Pt NPs, (**C**) GCE|Ir NPs, (**D**) GCE|Cu-Pt-Ir and (**E**)GCE|Cu@Pt@Ir NPs in 0.1 M LiClO$_4$: Scan rate, 50 mV/s (arrow indicating the direction of potential scan).

119

Figure 22A showed two anodic peaks designated a and b for the oxidation of Cu(0) to Cu(I) ($E_{p,a}$ = 283 mV) and Cu(I) to Cu(II) ($E_{p,a}$ = 980 mV) respectively. The peak c ($E_{p,c}$ = -443 mV) represent the reduction of Cu(II) to Cu(I) or Cu(0) **[189]**. The three set of redox peaks were observed in **Figure 22B**, wherein peak a at $E_{p,a}$ = -859 mV s and peak b at $E_{p,a}$ = -166 mV were attributed to the oxidation of adsorbed and absorbed hydrogen atoms on the surface of platinum, respectively. On the cathodic scan, peaks a′ ($E_{p,c}$ = -677 mV) and b′ ($E_{p,c}$ = -254 mV) are due to the reduction of adsorbed and absorbed hydrogen atoms on the platinum surface. During the anodic scanning, the Pt^0 nanoparticles deposited on the GCE surface were oxidised to Pt^{4+} and formed a platinum oxide layer (peak c $E_{p,a}$ = 920 mV). The Pt oxides are reduced on the reverse negative-going scans to Pt metal (peak c′ $E_{p,c}$ = 350 mV) **[143, 190]**. In case of GCE|Ir NPs **Figure 22C**, only two anodic peaks denoted (peak a $E_{p,a}$ = -85 mV) and (peak b $E_{p,a}$ = 960 mV) corresponding to oxidation of Ir(III) to Ir(IV) and formation of Ir(OH)$_3$ or IrOOH layer on Ir surface **[191]**.

From the cyclic voltammogram of the mixed Cu-Pt-Ir nanoalloy (**Figure 22D**) a distinct broad anodic peak (peak b) around -4 mV was due to the combination of Cu, Pt and Ir confirming the formation of the nanoalloy. It was also notable that the characteristic of cathodic peak for Cu(II)/Cu(0) denoted peak c in **Figure 22A** was also noted in **Figure 22D** as peak b' with a considerable shift to more negative potentials. The pair of peaks for hydrogen adsorption/desorption (a/a') in **Figure 22D** were shifted to more cathodic potentials if compared to GCE|Pt NPs in **Figure 22B**. Additionally, the peak at about $E_{p,a}$ = 900 - 980 mV which is a characteristic of Pt and Ir oxides formation was still observed at the same potential region in both GCE|Cu-Pt-Ir and GCE|Cu@Pt@Ir NPs systems.

The two pairs of redox couple peaks for hydrogen adsorption/desorption (a/a') and hydrogen absorption/desorption (b/b') were also depicted in **Figure 22E** at almost the same potential range as in GCE|Pt. Thus the electrochemical behaviour of Pt and Ir were more dominant in GCE|Cu@Pt@Ir NPs because they were deposited on a surface of Cu NPs during synthesis so they are the on the outermost surface exposed to the reaction. These observations indicate a successful incorporation of Pt and Ir into Cu in nanoalloy systems. Furthermore the shifting of peaks for GCE|Cu-Pt-Ir system confirms the presence of Cu, Pt and Ir as a solid solution (mixed alloy) whereas the segregated individual characteristics of Pt and Ir NPs (with very slight shifting in peaks) observed for GCE|Cu@Pt@Ir system shows that the surface of the nanoalloy consists mostly of Cu, Pt and Ir in layered multi-shell structural form with some

mixing between Pt and Ir layers. The higher current peak values showed higher electrochemical activity for nanoalloys electrode systems in comparison to the mono-metallic NPs modified electrodes, which is due to the synergistic effect of the combination of Cu, Pt and Ir in the nanoalloy systems.

CHAPTER 5

RESULTS AND DISCUSSION (II)

Summary

This chapter is the discussion of the results acquired from a comparative study of the Cu, Pt, Ir monometallic NPs, Cu-Pt-Ir (mixed) and Cu@Pt@Ir (multi-shell) trimetallic NPs for their potential application as electrocatalysts in ammonia electro-oxidation. In addition to the application, the effect of different ammonia concentrations and potential scan rates were further investigated.

5.1. The catalytic performance of Cu, Pt, Ir monometallic NPs and CuPtIr nanoalloys

5.1.1. Electrocatalytic oxidation of ammonia

The supporting electrolyte is usually comprised of ions that have a high mobility and are non-reactive in the operating potential. Hence, the catalytic activity of the synthesised nanoalloys towards the electro-oxidation of ammonia was carried out in a strong alkaline solution (1 M KOH) and ammonium hydroxide. The KOH in the electrolyte acts as a source for the OH$^-$ ions for the anodic reaction. The CV was carried out in the presence and absence of ammonia.
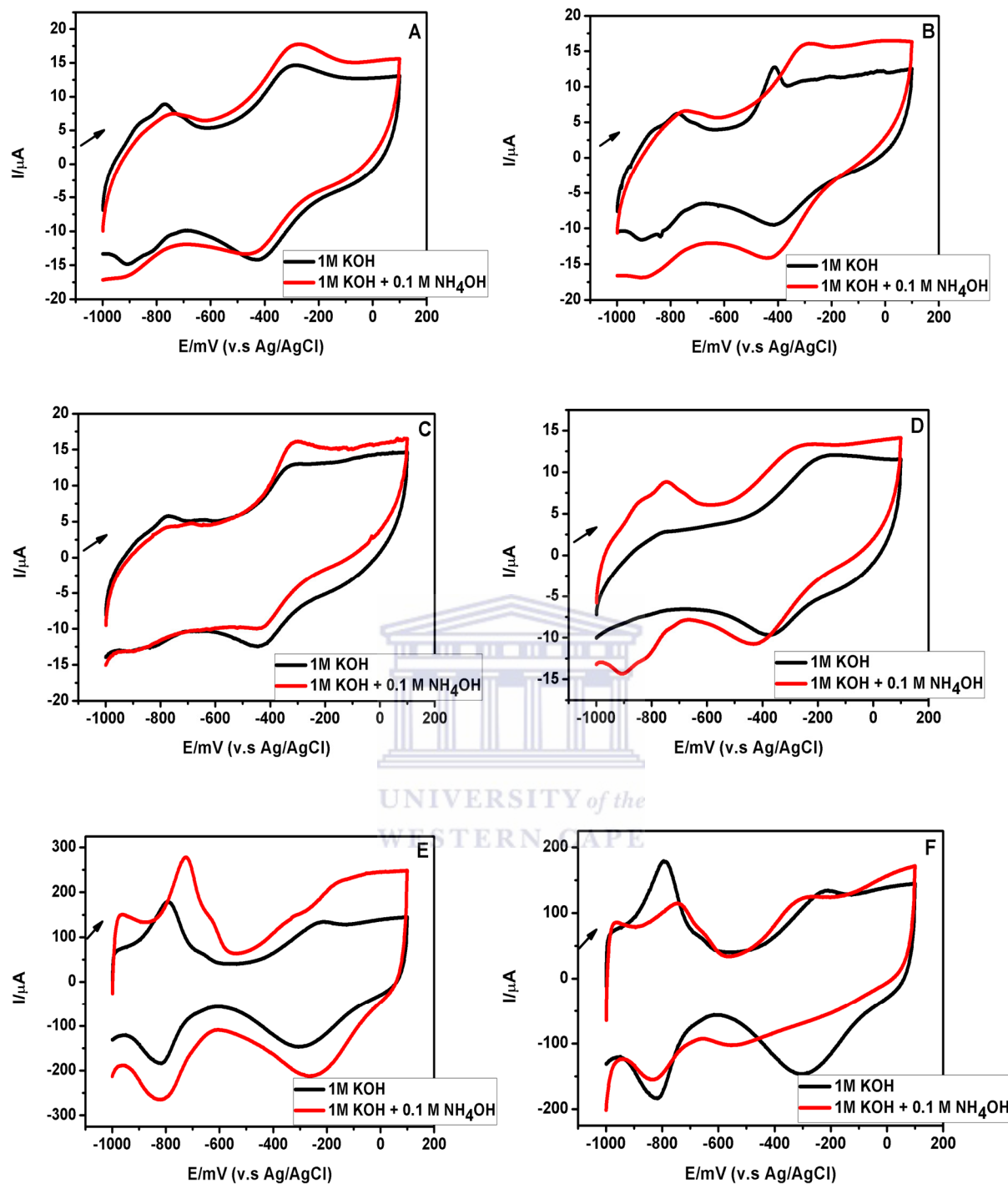
Figure 23: Cyclic voltammograms of CGE|Cu NPs (**B**), GCE|Pt NPs (**C**), GCE|Ir NPs (**D**) GCE|Cu-Pt-Ir NPs (**E**) and GCE|Cu@Pt@Ir NPs (**F**) electrodes before (**red curve**) and after (**black curve**) addition of 0.1 M NH₄OH into 1 M KOH aqueous solution: Scan rate, 50 mV/s (arrow indicating the direction of potential scan).

Figures 23 above shows the cyclic voltammograms of Cu, Pt, Ir, Cu-Pt-Ir (mixed) and Cu@Pt@Ir (multi-shell) nanoparticles modified GC electrodes in 1 M KOH aqueous solution with and without 0.1 M ammonia hydroxide. Ammonia oxidation (between -400 mV and -250 mV) was observed on all of the tested electrodes. However, both the potential and the peak currents of the oxidation peaks were dependent on the electrode material. The voltammograms in the presence of ammonia displayed less distinctive features as the same electrochemistry was observed for all electrodes in presence and absence of ammonia with an exception for nanoalloys modified electrodes which displayed current enhancement for additional peaks at (-900 to -600 mV). The slight increase in $I_{p,a}$ for ammonia oxidation was observed for all tested electrodes. The nanoalloy of Cu-Pt-Ir was found to give slightly higher peak currents coupled with lower overpotential than bare GCE and monometallic NPs as well as Cu@Pt@Ir multi-shell nanoalloy (see **Table 7**), which can be explained by cooperative effects between Cu and PGMs metals, Pt and Ir. This showed that CuPtIr nanoalloys were suitable electrocatalysts for the oxidation of ammonia based on their reduced overpotential and increased current properties. An overlay of the different modified electrodes is shown in **Figure 24**.
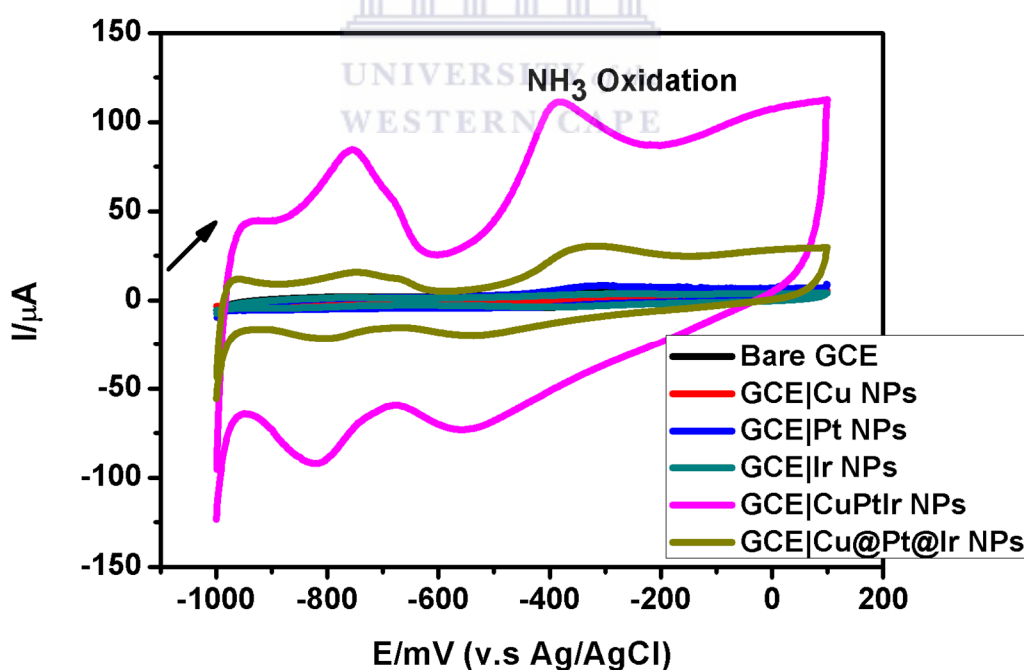
Figure 24: Overlay CVs of GCE, GCE|Cu NPs, GCE|Pt NPs, GCE|Ir NPs, GCE|Cu-Pt-Ir NPs and GCE|Cu@Pt@Ir NPs electrodes in 0.1 M ammonium hydroxide and 1 M KOH aqueous solution: Scan rate 10 mV/s (arrow indicating the direction of potential scan).

The catalysis of ammonia oxidation by CuPtIr electrocatalysts was validated with square wave voltammetry techniques under the same conditions used for CV studies. Therefore the data obtained from the cyclic voltammograms results in **Figure 24** and anodic scans of square wave voltammetric experiments are summarised in **Table 7**. The cyclic voltammetric studies on PVP capped CuPtIr nanoalloy systems in 0.1 M NH₄OH + 1 M KOH solution showed a well-defined peak around -298 mV (vs. Ag/AgCl), confirming the activity of the electrocatalyst for ammonia electro-oxidation. This anodic peak observed was attributed to the oxidation of NH_3 to N_2. Other oxidation products such as nitrite and nitrogen oxide form at above -200 mV [143]. Whereas, the cathodic peak at -500 mV was related either to the reduction or desorption of oxidised species of ammonia such as NH_{ads} and NH_{2ads}. The cathodic peak at -839 mV corresponds to the reduction of other oxidised species such as nitrite anions. These cathodic peaks are dependent on the upper sweep limit of the preceding anodic scan [91]. The electrochemical activity of mixed Cu-Pt-Ir nanoalloy towards ammonia electro-oxidation was similar to that witnessed for a multi-shell Cu@Pt@Ir nanoalloy, although Cu-Pt-Ir exhibited much higher oxidation current.

Table 7: CV parameters of Cu-Pt-Ir nanoalloy systems in 0.1 M ammonium hydroxide and 1 M KOH (experimental conditions as in **Figure 24**)

Electrode	$E_{p,a}$ (mV)	$I_{p,a}$ (A)	E_{Onset}^{ox} (mV)
GCE	-322	5.652×10^{-6}	-427
GC|Cu NPs	-419	2.001×10^{-6}	-460
GC|Pt NPs	-310	8.316×10^{-6}	-445
GC|Ir NPs	-298	3.597×10^{-6}	-384
GC|Cu-Pt-Ir NPs	-382	110.615×10^{-6}	-536
GC|Cu@Pt@Ir NPs	-337	29.805×10^{-6}	-509

In comparing the electro-catalytic activity of the various GCE modified electrocatalysts towards NH_3 oxidation, it was observed that the nanoalloys have high current values as well as reduced on-set potentials than mono-metallic NPs (see **Table 7** above), with the mixed Cu-

Pt-Ir nanoalloys exhibiting enhanced properties compared to the multi-shell nanoalloy. The high catalytic activity of Cu-Pt-Ir mixed nanoalloys can be attributed to the very small particle size of this nanoalloy as evidenced from the HRTEM images obtained, since noble metal NPs of sizes of less than 10 or 20 nm are known to exhibit excellent catalytic properties owing to their high surface area effects and increased catalytic active sites **[86]**. The observed behaviour may also be due to the properties evolved from synergistic effect between Cu, Pt and Ir. Since, for the Cu@Pt@Ir NPs are likely to experience segregation between layers of core, interlayer and shell, thus the catalytic behaviour observed might be due to Ir only. This means that the structure of the synthesised Cu@Pt@Ir NPs did not have nano porosity which has resulted in difficulties for guest species to access the Pt interlayer. The obtained results are controversial in a sense that according to the literature **[15, 91]**, Cu was expected to have a low affinity for N_{ads}, however based on the results obtained Cu showed the highest affinity for N_{ads}, hence ammonia was dehydrogenated at significantly lower potentials than on Pt, Ir and nanoalloys, leading to the formation of surface poisonous N_{ads} at much lower potentials than on the Pt, Ir and nanoalloys. This may be ascribed to the surface oxidation of the synthesised Ir NPs which formed iridium foams (IrO_2) as well as the morphology of Cu NPs synthesised. For example, the cyclic voltammetric study by Endo *et al.* **[91]** reported that the main ammonia oxidation peak on Ir was located at a lower potential (and hence lower overpotential) than that on Pt. However, the peak current density on Ir was much lower than that on Pt, thus based on their results the addition of inactive Cu to Pt has lowered the activity of Pt. Therefore the results obtained for Ir and Pt in this study, were in disagreement with the study conducted by Endo *et al* **[91]**. In this work, Pt NPs showed lower overpotential as well as higher anodic peak current than Ir NPs and the combination of Cu with PGMs (Pt and Ir) resulted in higher activity than individual Pt and Ir NPs towards ammonia oxidation with a good dehydrogenation capacity and sufficiently low affinity for the formation of N_{ads}, leading to a steady-state production of the active intermediates needed to form N_2.

5.1.2. Effects of potential scan rates

To investigate the effect of potential scan rates, the ternary Cu-Pt-Ir and Cu@Pt@Ir nanoalloy electrocatalysts which showed the highest ammonia oxidation current density and lower overpotential were used.

Figure 25: Cyclic voltammograms of GCE|Cu-Pt-Ir NPs in the presence of 0.1 M ammonium hydroxide and 1 M KOH aqueous solution at different scan rates: (**A**) 1 - 10 mV/s and (**B**) 50 - 300 mV/s (arrow indicating the direction of potential scan).

In order to study the nature of the oxidation of ammonia on ternary CuPtIr nanoalloys, the CVs measured on GCE|Cu-Pt-Ir NPs (**Figure 25**) and GCE|Cu@Pt@Ir NPs (**Figure 26**) in 0.1 M ammonia and 1 M KOH solution were performed at different scan rates. The anodic peak currents at about -298 mV increased significantly with the increasing potential scan rate (see **Figure 25A**) but at higher potential scan rates the main oxidation peak of ammonia started weakening (see **Figure 25B**). Furthermore, the additional anodic peak observed at approximately -760 mV and the two cathodic peaks observed at about -500 mV and -839 mV in all the curves turned out to be more pronounced (high peak currents) at higher scan rates and deactivated the ammonia oxidation peak (-298 mV) as presented in **Figure 25B**. This could be due to the intermediates (NH_{ads} and NH_{2ads}) generated during NH_3 oxidation blocking the ammonia adsorption hence a degradation in anodic peak current (-298 mV) of NH_3 oxidation was witnessed. The peak currents followed a linear $v^{1/2}$ (v: potential scan rate) dependence as shown in **Figure 27**, indicating a diffusion controlled rather than a surface controlled electron transfer kinetics. Information pertaining to the reversibility of an

127

electrochemical process can be obtained from the values of the peak separation, ΔE_p, the anodic current $I_{p,a}$ and the peak cathodic current $I_{p,c}$ for the redox species (see **Table 5**). The peak potential shifted positively with increasing scan rates indicative of an irreversible process of the oxidation of ammonia **[189]**. **Figure 27** below show the same CV experiment for GCE|Cu@Pt@Ir NPs.
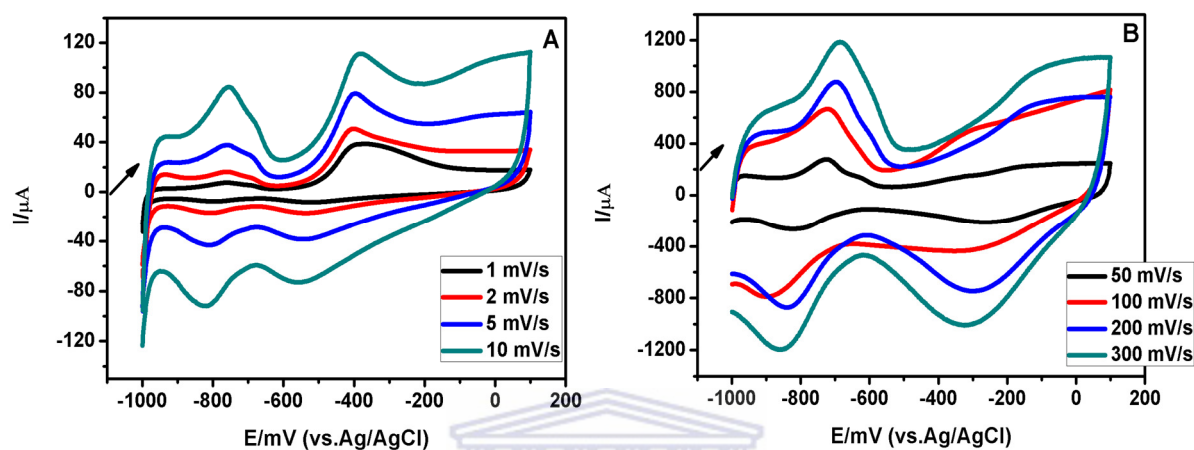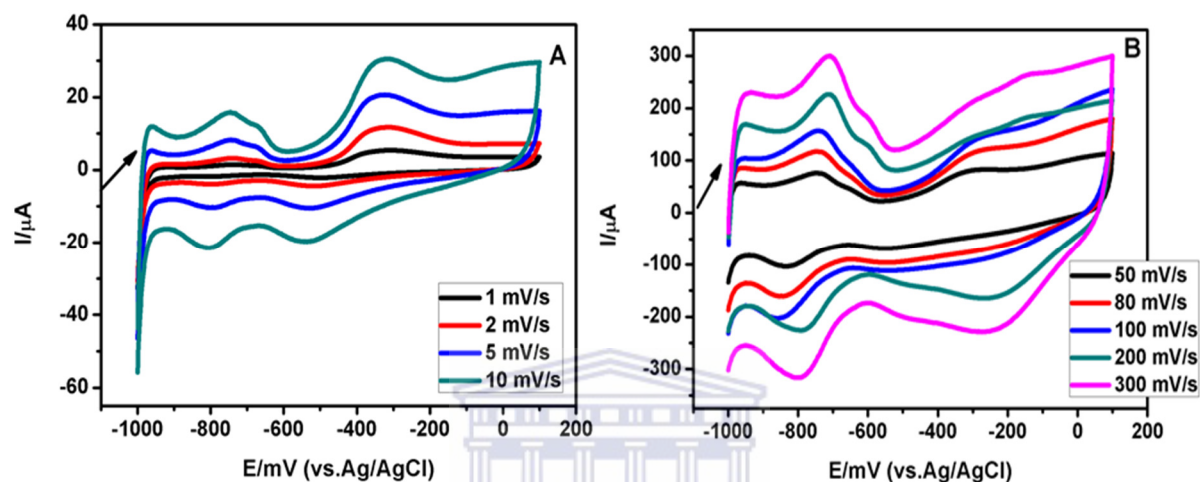

Figure 26: Cyclic voltammograms of GCE|Cu@Pt@Ir NPs electrode in the presence of 0.1 M ammonium hydroxide and 1 M KOH aqueous solution at different scan rates: (**A**) 1 - 10 mV/s and (**B**) 50 - 300 mV/s (arrow indicating the direction of potential scan).

The behaviour witnessed for the GCE|Cu-Pt-Ir NPs was also observed for the GCE|Cu@Pt@Ir NPs. The anodic peak currents at about -298 mV increased significantly with the increasing potential scan rate (**Figure 26A**). The process of ammonia oxidation got deactivated at higher scan rates where the anodic peak of interest started fading with the positive shift in peak potential (**Figure 26B**). This behaviour can be attributed to the instability of the electrocatalyst after numerous cycling scans which is caused by Cu metal being easily oxidised to form oxide compounds in the alkaline medium **[192]**. Randles-Sevčik plots in **Figure 27** below were plotted from the data obtained from cyclic voltammograms presented in **Figure 25** and **Figure 26** above to study the relationship of peak current (I_p) with square root of scan rate ($v^{1/2}$) so as to confirm the irreversibility of this systems.
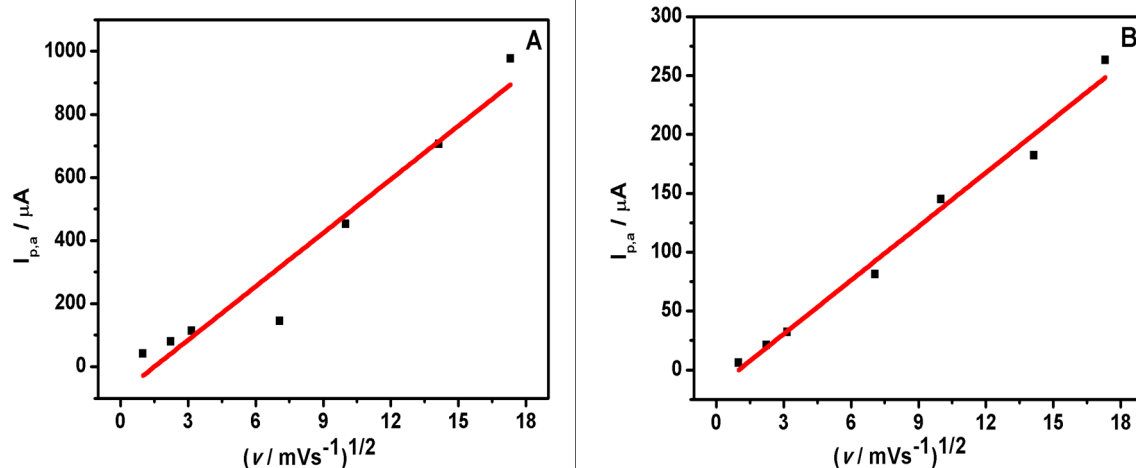
Figure 27: Randles-Sevčik plot, square root of scan rate versus anodic peak current for ammonia oxidation reaction on GCE|Cu-Pt-Ir NPs (**A**) and GCE|Cu@Pt@Ir NPs (**B**) electrodes in the presence of 0.1 M NH₄OH and 1 M KOH aqueous solution mixture over a range of 1 - 300 mV/s.

To obtain additional information on the process of electrochemical oxidation of ammonia on GCE|Cu-Pt-Ir and GCE|Cu@Pt@Ir surfaces, the I_p values calculated from the anodic peak at about -298 mV of the CVs in **Figure 25** and **26** at the scan rate range of 1 - 300 mV/s were plotted. Therefore, a linear relationship between $I_{p,a}$ versus $v^{1/2}$ was observed since the linear correlation coefficients (R^2) was 0.95 and 0.98 for GCE|Cu-Pt-Ir and GCE|Cu@Pt@Ir respectively. The slope of 1.79×10^{-3} A (V s^{-1})$^{-1/2}$ and 4.82×10^{-4} A (V s^{-1})$^{-1/2}$ for GCE|Cu-Pt-Ir and GCE|Cu@Pt@Ir respectively were obtained from the Randles-Sevčik plot. These results indicate that the electron transfer reaction anodic peak current was diffusion controlled in 1M KOH and 0.1 M NH₄OH solutions.

5.1.3. Effects of ammonia concentration

To investigate the effect of ammonia concentration, ternary Cu-Pt-Ir and Cu@Pt@Ir nanoalloy electrocatalysts which showed the highest ammonia oxidation current density and lower overpotential were used. **Figure 28** shows cyclic voltammograms measured on GCE|Cu-Pt-Ir NPs in 1 M KOH solution with various ammonia concentrations. It can be seen that two anodic current peaks were observed at approximately $E_{p,a}$ = -760 mV and $E_{p,a}$ = -298

mV in all the curves, respectively. With an increase in ammonia concentration, the peak current at -298 mV increased continuously. This can be attributed to the adsorption of more ammonia on the electrode surface resulting in increased oxidation of the ammonia [148]. Thus, the anodic current increases continuously with the ammonia concentration. In particular, there was a significant increase in peak current when the ammonia concentration increased from 0.1 M to 3 M. With respect to the influence of the ammonia concentration on peak current at -760 mV, there was also a significant increase in peak current at lower ammonia concentration resulting in inhibition of peak current of interest at -298 mV (see **Figure 28A**). However, the opposite was observed at higher concentrations of ammonia presented in **Figure 28B** where the ammonia oxidation peak started increasing with a shift to more positive potentials.
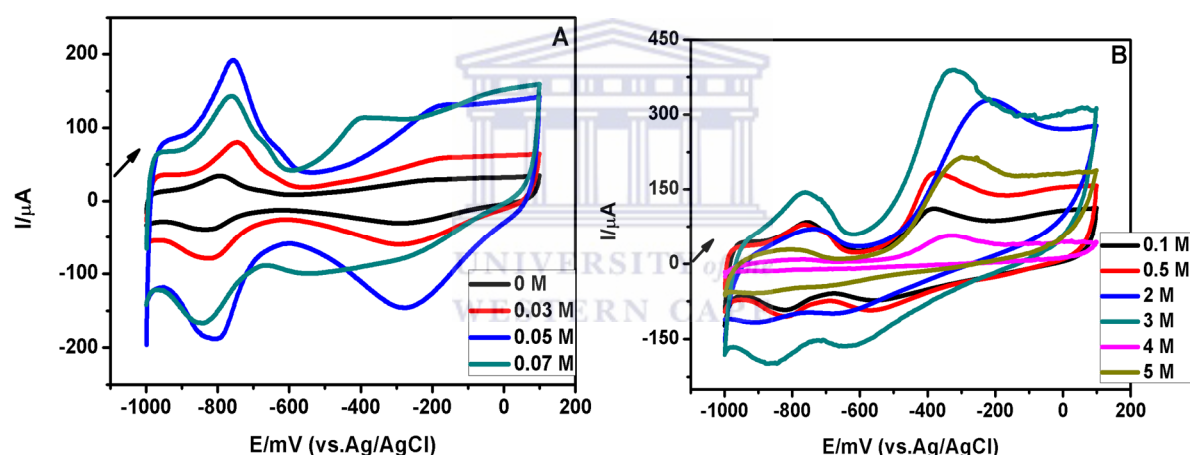
Figure 28: Ammonia oxidation reaction activity on GCE|Cu-Pt-Ir NPs in 1 M KOH solutions with various concentrations of ammonia: (**A**) 0 - 0.07 M NH$_4$OH and (**B**) 0.1 - 5 M NH$_4$OH: Scan rate 10 mV/s (arrow indicating the direction of potential scan).

When the ammonia concentration reached a certain level, i.e. 3 M in this work, the adsorption of ammonia on GCE|Cu-Pt-Ir NPs achieved a relatively saturated status. The intermediates generated during ammonia oxidation, such as NH$_{2,ads}$ and NH$_{ads}$, could remain on the electrode surface and block the ammonia adsorption [148]. Therefore it is reasonable to assume that the blocking effect was significant when the solution contains too high, and too low, concentrations of ammonia. However, 0.1 M was chosen as an optimum concentration due to the fact that even though, 0.5 M, 2 M and 3 M show higher peak current values, they

also have high overpotentials. Whereas oxidation of ammonia on GCE|Cu-Pt-Ir electrocatalyst in 1 M KOH and 1 M NH$_4$OH occurs at lower potentials with high peak current. Therefore, an increase of the ammonia concentration beyond 3 M resulted in a sudden decrease in anodic peak current which increased again when the concentration was further increased showing some instability of ammonia oxidation at higher ammonia concentrations (**Figure 28B**). The present results showed that ammonia can be oxidised effectively on GCE|Cu-Pt-IrNPs electrode from -1000 mV to 100 mV at a concentration range of 0.1 – 3 M.
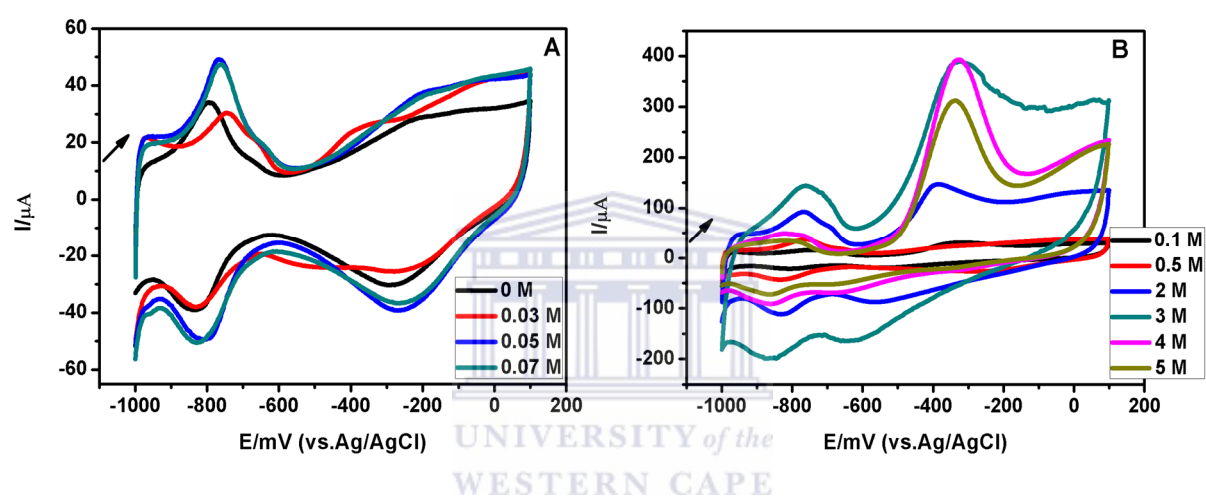
Figure 29: Ammonia oxidation reaction activity on GCE|Cu@Pt@Ir NPs in 1 M KOH solutions with various concentrations of ammonia: (**A**) 0 - 0.07 M NH$_4$OH and (**B**) 0.1 – 5 M NH$_4$OH: Scan rate 10 mV/s (arrow indicating the direction of potential scan).

Figure 29 shows cyclic voltammograms measured on GCE|Cu@Pt@Ir NPs in 1 M KOH solution with various ammonia concentrations. It can be seen that two anodic current peaks were observed at approximately $E_{p,a}$ = -760 mV and $E_{p,a}$ = -292 mV in all the curves, respectively. The catalytic cyclic voltammograms presented above are characterised by a steady increase of the anodic current with increasing concentration, this behaviour continues up to a concentration of 3 M where the adsorption of ammonia on GCECu@Pt@Ir NPs electrode has achieved a relatively saturated status as presented in **Figure 29B**. However, a similar behaviour observed for GCE|Cu-Pt-Ir NPs **Figure 28A** was also witnessed at lower concentrations (see **Figure 29A**) where there was a significant increase in peak current for anodic peak at -760 mV at lower ammonia concentration resulting in inhibition of peak

current of interest at -298 mV. Then suddenly, there was a sharp rise of peak current coupled with a significant shift of ammonia oxidation peak to more positive potentials when the concentration was increased from 0.5 M to 3 M as seen in **Figure 29B**. Therefore, an increase of the ammonia concentration beyond 3 M resulted in slight decrease in anodic peak current due to ammonia saturation on the electrode surface. It is reasonable to assume that the blocking effect was significant when the solution contains too high and too low concentrations of ammonia. Therefore, in this work the optimum ammonia concentration was chosen to be 0.1 M due to reasonable lower overpotential and high peak current achieved at this concentration.

5.2.   Sub conclusion

According to the comparative CVs, which were illustrated in **Figure 24**, the height of the peak current observed for each electrocatalyst presented in **Table 7**, the tested electro-catalysts can be classified as: GCE|Cu-Pt-Ir NPs > GCE|Cu@Pt@Ir NPs > GCE|Pt NPs > GCE|Ir NPs > GCE|Cu NPs in terms of maximising the peak current while the overpotential of ammonia oxidation decreases as follows: GCE|Ir NPs > GCE|Pt NPs > GCE|Cu@Pt@Ir NPs > GCE|Cu-Pt-Ir NPs > GCE|Cu NPs. The increased electrochemically active surface area of the nanoalloys and electronic effect generated by the core and existing synergism among three metals in the trimetallic nanoparticles might be responsible for increase in the catalytic activity of Pt-containing catalysts. Thus, increasing the stability of nanoalloys against adsorption of poisonous N_{ads} intermediate that suppresses reaction (29) in the Gerischer–Mauerer mechanism which was the main problem for monometallic NPs. Ammonia electro-oxidation on both Cu-Pt-Ir and Cu@Pt@Ir nanoalloy modified GC electrodes is controlled by mass-transfer process of ammonia towards the electrode surface. The concentration of NH_4OH and potential scan rates were found to significantly affect the performance of the electrocatalysts and the optimal concentration was found to be 0.1 M at lower potential scan rates of 1 – 20 mV/s. Cu-Pt-Ir trimetallic nanoalloy is a promising, high performing catalyst for future large-scale application in ammonia electro-oxidation.

CHAPTER 6

CONCLUSION AND RECOMMENDATIONS

Summary

This chapter gives brief overview of the results obtained in correlation with the conceptual framework of the research and specific objectives of the study to validate whether the aims of this study were achieved or not. The success, challenges encountered and shortcomings of the study are further discussed. Also outlined here, are the perspectives on future developments for enhancing the performance of the non-noble@PGMs multi-shell nanoalloys based electrocatalysts at the end.

6.1. Conclusion
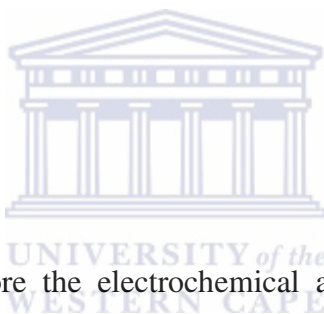
The study was set out to explore the electrochemical activity of mixed and multi-shell structured nanoalloys of CuPtIr for the oxidation of ammonia. We have reported for the first time according to our knowledge, the successful synthesis of small irregular, interconnected PVP stabilised Cu-Pt-Ir (3 - 10 nm) and Cu@Pt@Ir (5 - 10 nm) nanoalloys, which was achieved by a simultaneous or successive reduction of their respective metal salts in a mixture of PVP, NaBH$_4$ and water at room temperature under vigorous magnetic stirring. The high surface sensitivity of AES surveys revealed the presence of Pt, Ir and Cu elements in all probed spots suggesting some mixing between the layers of the nanoalloy. The tested electro-catalysts can be classified as: GCE|Cu-Pt-Ir NPs > GCE|Cu@Pt@Ir NPs > GCE|Pt NPs > GCE|Ir NPs > GCE|Cu NPs in terms of maximising the peak current while overpotential of ammonia oxidation decreases as follows: GCE|Ir NPs > GCE|Pt NPs > GCE|Cu@Pt@Ir NPs > GCE|Cu-Pt-Ir NPs > GCE|Cu NPs. Moreover, it was evident that both mixed and multi-shell CuPtIr electrocatalysts showed enhanced catalytic activity than mono-metallic based electrocatalysts owing to their high electro-active surface area and synergistic effects arising from combined properties of Cu, Pt and Ir. Thus in revisiting the aims, objectives, research

questions and literature gap stated earlier on this work, one could say that this was a successful study, although is incomplete as research is continuous and never ending. However, progress was made by focusing on novel electrocatalysts development and successful characterisation of the nanoalloys.

Based on the results obtained, the Cu-Pt-Ir electrocatalytic material can be considered as a promising candidate for anode electrode materials in hydrogen production from electro-oxidation of ammonia. Moreover the knowledge acquired from this research would potentially aid in guiding future research to improve the efficiency of ammonia electro-oxidation. However, they were few challenges encountered during the process of this study such as not being able to get a cross-sectional composition profile of Cu@Pt@Ir due to the charging effects from the sample and not achieving nanoporous Cu@Pt@Ir architectures to take the advantage of synergistic role of the three metals involved. These problems can be avoided by taking into consideration various factors influencing segregation, mixing and ordering of nanoalloys as well as the mechanism of their synthesis. The cross sectional composition profile characterisation can be obtained with AES depth profiling, however it will be advisable to use classically effective methods such as charge neutralization, tilting and sample thickness reduction (cross polisher) to prevent the charging effects of non-conductive nanomaterials or to use synthesis methods that will preferentially yield conductive nanomaterials or rather use XPS. Unfortunately, due to the time constraints the characterisation of related binary core-shell nanoalloys such as Cu@Pt, Cu@It and Pt@Ir could not be completed for proper comparison to obtain a tangible conclusion that the synthesised ternary nanoalloys can perform better than both their binary and monometallic counterparts, hence the conclusion in this study was only based on comparison of mono-metallic and mixed and multi-shell ternary nanoalloys.

6.2. Future work and recommendations

Although this study may be considered to be successful, it still leaves a knowledge gap that can be further explored and interrogated. As the major requirements for practical application of the catalytic decomposition to develop efficient, economical and easily recyclable catalysts

still remains a major challenge. Consequently, the following improvements are recommended for future research activities:

- The green synthesis of nanoalloys is recommended because when it comes to catalysis application purposes pure metallic NPs are of significance and capping agents that are used in conventional synthetic methods are not easy to be completely removed on the surface of NPs. Following that, inductively coupled plasma atomic emission spectroscopy (ICP-AES) measurements can be carried out to ensure purity of metal catalysts and also to quantify its real metallic loadings.

- Interrogation of the electrocatalytic behaviour of iridium based multi-shell ternary nanoalloy systems anchored on graphene with controlled morphology and size ranges of approximately 10–30 nm to enhance catalytic activity, conductivity, stability and durability can be explored.

- Thus the use of graphene as substrates of catalysts can provide an innovative opportunity for designing and fabrication of next-generation catalysts due to its unique nanostructure properties, such as the high strength, high thermal conductivity and high specific surface area, etc.

- It is suggested that the role of crystallinity of the core in a novel multi-shell nanoalloy (e.g., Fe@Pt@Ir) and its use as electrocatalyst for ammonia oxidation can be of importance in producing magnetically recyclable anode materials.

- It is proposed that the analysis of multi-shell nanostructures with grazing incidence small-angle X-ray scattering and grazing incidence X-ray diffraction (GISAXS/GIXRD) measurements by examining the internal structure and core and shell sizes of the multi-layered nanoalloys will be helpful for confirming core@shell structures.

- In addition to NanoSAM, further characterisation of multi-shell nanostructures with X-ray photoelectron spectroscopy (XPS) might be useful in complementing NanoSAM results.

- The mappings from high angle annular dark field (HAADF) in conjugation with scanning transmission electron microscopy (STEM) mode and X-ray energy

135

dispersive spectroscopy (XEDS) can also be employed to reveal the multi-shell nature of nanoalloys using elemental mappings and imaging.

- The application and turnover rate studies of the fabricated electrocatalysts as next generation anode materials in a direct ammonia fuel cell prototype is worth investigating.

In particular, future work should pay more attention to the evaluation of the stability and durability of the electrocatalysts during ammonia electro-oxidation reaction. It is anticipated that such an integrated approach will assist in understanding the degradation mechanisms and fabrication of electrocatalysts with both long term performance and high activity for ammonia electro-oxidation. Further research on the alloying strategies and synthesis of novel unique nanostructures is also expected to enhance the development of active and low-cost electrocatalysts for large-scale applications of ammonia electro-oxidation technologies, contributing to solving some of the challenging energy and environmental problems.
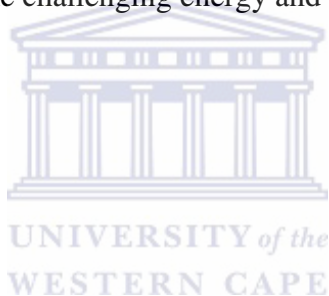
REFERENCES

[1].   Winter, M. & Brodd, R.J. 2005, "What Are Batteries, Fuel Cells and Supercapacitors? (Chem. Rev. 2003, 104, 4245-4269. Published on the Web 09/28/2004.)", *Chemical reviews,* vol. 105, no. 3, pp. 1021-1021.

[2].   Lan, R., Irvine, J.T. & Tao, S. 2012, "Ammonia and related chemicals as potential indirect hydrogen storage materials", *International Journal of Hydrogen Energy,* vol. 37, no. 2, pp. 1482-1494.

[3].   Wang, L. & Yamauchi, Y. 2011, "Strategic synthesis of trimetallic Au@ Pd@ Pt core− shell Nanoparticles from poly(vinylpyrrolidone)-based aqueous solution toward highly active electrocatalysts", *Chemistry of Materials,* vol. 23, no. 9, pp. 2457-2465.

[4].   Barbir, F. 2009, "Transition to renewable energy systems with hydrogen as an energy carrier", *Energy,* vol. 34, no. 3, pp. 308-312.

[5].   Bhattacharyya, S.C. 2012, "Energy access programmes and sustainable development: A critical review and analysis", *Energy for sustainable development,* vol. 16, no. 3, pp. 260-271.

[6].   Song, C. 2002, "Fuel processing for low-temperature and high-temperature fuel cells: Challenges and opportunities for sustainable development in the 21st century", *Catalysis today,* vol. 77, no. 1, pp. 17-49.

[7].   Alcaide, F., Cabot, P. & Brillas, E. 2006, "Fuel cells for chemicals and energy cogeneration", *Journal of Power Sources,* vol. 153, no. 1, pp. 47-60.

[8].   Rees, N.V. & Compton, R.G. 2011, "Carbon-free energy: a review of ammonia- and hydrazine-based electrochemical fuel cells", *Energy & Environmental Science,* vol. 4, no. 4, pp. 1255-1260.

[9].   Hamann, R. 2004, "Corporate social responsibility, partnerships and institutional change: The case of mining companies in South Africa", *Natural Resources Forum* Wiley Online Library, pp. 278.

[10].   Vitse, F., Cooper, M. & Botte, G.G. 2005, "On the use of ammonia electrolysis for hydrogen production", *Journal of Power Sources,* vol. 142, no. 1, pp. 18-26.

[11]. Vidal-Iglesias, F., Garcıa-Aráez, N., Montiel, V., Feliu, J. & Aldaz, A. 2003, "Selective electrocatalysis of ammonia oxidation on Pt (100) sites in alkaline medium", *Electrochemistry communications,* vol. 5, no. 1, pp. 22-26.

[12]. Vidal-Iglesias, F., Solla-Gullón, J., Montiel, V., Feliu, J. & Aldaz, A. 2007, "Screening of electrocatalysts for direct ammonia fuel cell: Ammonia oxidation on PtMe (Me: Ir, Rh, Pd, Ru) and preferentially oriented Pt (100) nanoparticles", *Journal of Power Sources,* vol. 171, no. 2, pp. 448-456.

[13]. Lomocso, T.L., & Baranova, E.A. 2011, "Electrochemical oxidation of ammonia on carbon-supported bi-metallic PtM (M= Ir, Pd, SnO$_x$) nanoparticles", *Electrochimica Acta,* vol. 56, no. 24, pp. 8551-8558.

[14]. Ghosh Chaudhuri, R. & Paria, S. 2011, "Core/shell nanoparticles: classes, properties, synthesis mechanisms, characterization and applications", *Chemical reviews,* vol. 112, no. 4, pp. 2373-2433.

[15]. Zhong, C., Hu, W., & Cheng, Y. 2013, "Recent advances in electrocatalysts for electro-oxidation of ammonia", *Journal of Materials Chemistry A,* vol. 1, no. 10, pp. 3216-3238.

[16]. Jones, R.T. 2005, "An overview of Southern African PGM Smelting", *Nickel and Cobalt 2005: Challenges in Extraction and Production*, 44th Annual Conference of Metallurgists, Calgary, pp. 147-178.

[17]. Hung, C. 2012, "Complex PtPdRh nanoparticles: Synthesis, characterization and performance in the electrocatalytic oxidation of ammonia", *Powder Technology,* vol. 232, pp. 18-23.

[18]. Boggs, B.K. & Botte, G.G. 2010, "Optimization of Pt–Ir on carbon fiber paper for the electro-oxidation of ammonia in alkaline media", *Electrochimica Acta,* vol. 55, no. 19, pp. 5287-5293.

[19]. Allagui, A., Oudah, M., Tuaev, X., Ntais, S., Almomani, F. & Baranova, E.A. 2013, "Ammonia electro-oxidation on alloyed PtIr nanoparticles of well-defined size", *International Journal of Hydrogen Energy,* vol. 38, no. 5, pp. 2455-2463.

[20]. DME (Department of Minerals and Energy). 1998, "White Paper on Energy Policy for South Africa". Pretoria, DME.

[21]. DME (Department of Minerals and Energy). 2003, "White Paper on Renewable Energy".

[22]. Harald Winkler, 2005, "Renewable energy policy in South Africa: policy options for renewable electricity", *Energy Policy,* Vol. 33, pp. 27–38.

[23]. DMR (Department of Mineral Resources). 2011, "A beneficiation strategy for the minerals industry of South Africa"

[24]. Ibrahim Dincer. 2000, "Renewable energy and sustainable development: a crucial review" *Renewable and Sustainable Energy Reviews,* vol.4, pp. 157-175.

[25]. Shahriar Shafiee & Erkan Topal, 2009, "When will fossil fuel reserves be diminished?" *Energy Policy,* vol.37, pp. 181–189.

[26]. European Communities (EUR 20719 EN). 2003, "Hydrogen Energy and Fuel Cells – A vision of our future", ISBN 92-894-5589-6

[27]. Elena Serrano, Guillermo Rus, Javier Garcı´a-Martı´nez. 2009, "Nanotechnology for sustainable energy", *Renewable and Sustainable Energy Reviews,* vol.13, pp. 2373–2384.

[28]. Madhivanan Mathuvel & Gerardine G.Botte. 2009, "Trends in Ammonia Electrolysis", in Modern Aspects of Electrochemistry No. 45, edited by Ralph E. White, pp. 207-245. ISBN: 978-1-4419-0655-7, Available from: Springer E-Book. [20 November 2015].

[29]. Catherine Lepiller, PhD in electrochemistry and chief scientist at Pragma Industries. Fuel Cell Basics: Origins and principle, Available from < http://www.pragma-industries.com/reports/fuel-cell-explained/#origin> [19 March 2015].

[30]. Perry M. L. & Fuller T. F., 2002, "A Historical Perspective of Fuel Cell Technology in the 20th Century", *Journal of The Electrochemical Society,* vol.149, S59-S67.

[31]. Jacob Brouwer. 2010, "On the role of fuel cells and hydrogen in a more sustainable and renewable energy future", *Current Applied Physics,* vol.10, S9–S17.

[32]. Grigorii L. Soloveichik. 2014, "Liquid fuel cells" *Beilstein Journal of Nanotechnology,* vol. 5, pp.1399–1418.

[33]. Kirubakaran, A., Jain, S., Nema, R.K. 2009, "A review on fuel cell technologies and power electronic interface", *Renewable and Sustainable Energy Reviews,* vol.13, pp. 2430–2440.

[34]. Garcia BL, Sethuraman VA, Weidner JW, White RE, Dougal R. 2004, "Mathematical model of a direct methanol fuel cell", *Journal of Fuel Cell Science Technology,* 43–48.

[35]. Farooque, M,. & Maru HC. 2001, "Fuel cells—the clean and efficient power generators", *IEEE Proc,* vol.89, pp.1819–1829.

[36]. Holladay J.D., Hu, J., King, D.L., Wang Y. 2009, "An overview of hydrogen production technologies", *Catalysis Today,* vol.139, pp.244–260.

[37]. Rostrup-Nielsen, J. 2003, 'Encyclopedia of Catalysis', vol.4, I.T. Horvath (ed), *Wiley Interscience.*

[38]. Turner, J., Sverdrup, G., Mann, M.K., Maness, P.-C., Kroposki, B., Ghirardi, M., Evans, R.J., Blake, D. 2008, *International Journal of Hydrogen Energy,* vol.32, pp.379–407.

[39]. Pettersson, J., Ramsey, B., Harrison, D. 2006, *Journal of Power Sources,* vol. 157, pp.28–34.

[40]. Grigoriev, S.A., Porembsky, V.I., Fateev, V.N. 2006, *International Journal of Hydrogen Energy,* vol. 31, pp.171–175.

[41]. Utgikar, V., Thiesen, T. 2006, *International Journal of Hydrogen Energy,* vol.31, pp.939–944.

[42]. Tao, G., Bandopadhyay, S. anderson, H., Brow, R., Virkar, A. 2007, "Development of a novel efficient solid-oxide hybrid for co-generation of hydrogen and electricity using nearby resources for local applications", in *Annual DOE Hydrogen Program Progress Report, U.S. Department of Energy,* Washington, DC, J. Milliken (ed), pp. 82–86.

[43]. Holladay, J.D., Wang, Y., Jones, E. 2004, *Chemical Reviews,* vol.104, pp. 4767–4789.

[44]. Wojcik, A., Middleton, H., Damopoulos, I., Van Herle, J. 2003, *Journal of Power Sources,* vol.118, pp. 342–348.

[45]. Chachuat, B., Mitsos, A., Barton, P.I. 2005, *Chemical Engineering Science,* vol.60 pp.4535–4556.

[46]. Denver Cheddie. 2012, "Ammonia as a Hydrogen Source for Fuel Cells: A Review", in Hydrogen Energy - Challenges and Perspectives, edited by Prof. Dragica Minic, pp.334-362, ISBN: 978-953-51-0812-2, InTech, Available from: <http://www.intechopen.com/books/hydrogen-energy-challenges-and

perspectives/ammonia-as-a-hydrogen-source-for-fuel-cells-a-review>. [19 March 2015].

[47].   Zamfirescu, C., & Dincer, I. 2009, "Ammonia as a green fuel and hydrogen source for vehicular applications", *Fuel Processing Technology,* vol.90, pp.729–737.

[48].   Schlapbach, L., Zütel, A. 2001, "Hydrogen-storage materials for mobile applications", *Nature,* vol.114, pp. 353–358.

[49].   Zamfirescu, C., & Dincer, I. 2008, "Using ammonia as a sustainable fuel", *Journal of Power Sources,* vol.185, pp.459–465.

[50].   Kimihiko Sugiura, Yudai Yamamoto and Mika Tsumura. 2010, "Optimization of Hydrogen Production by Ammonia Electrolysis", *ECS Trans,* vol. 26, no.1, pp. 485-491.

[51].   Daniel J., Little, Milto R., Smith Thomas W. Haman. 2015, "Electrolysis of liquid ammonia for hydrogen generation", *Energy Environ. Sci.,* vol.8, pp.2775-2781.

[52].   Xie, K., Ma, Q., Jiang, Y., Gao, J., Liu, X., Meng, G. 2007, *Journal of Power Sources,* vol.170, pp. 38–41.

[53].   Cairns, E., & Simons, A. 1968, "Ammonia–oxygen fuel cell", *Nature,* vol.217, pp. 780–781.

[54].   Ganley, J.C. 2008, "An intermediate-temperature direct ammonia fuel cell with a molten alkaline hydroxide electrolyte", *Journal of Power Sources,* vol.178, pp.44-47.

[55].   Hejze, T., Besenhard, J.O., Kordesch, K., Cifrain, M., Aronsson, R.R. 2008, "Current status of combined systems using alkaline fuel cells and ammonia as hydrogen carrier", *Journal of Power Sources,* vol.176, pp.490-493.

[56].   Lan, R., & Tao, S.W. 2010, "Direct ammonia alkaline anion-exchange membrane fuel cells", *Electrochem. Solid State Lett.,* vol.13, pp. B83-B86.

[57].   Boggs, B.K., & Botte, G.G., 2009, "On-board hydrogen storage and production: an application of ammonia electrolysis", *Journal of Power Sources,* vol.92, pp. 573-581.

[58].   Lan Ran & Tao S. 2014, "Ammonia as a suitable fuel for fuel cells", *Frontiers in Energy Research,* vol. 2, pp.1-4.

[59].   Vayenas, C. G., & Farr, R. D. 1980, "Co-generation of electric energy and nitric-oxide", *Science,* vol.208, pp.593-594.

141

[60]. Sigal, C.T., & Vayenas, C.G. 1981, "Ammonia oxidation to nitric-oxide in a solid electrolyte fuel-cell", *Solid State Ionics,* vol.5, pp.567-570.

[61]. Suzuki, S., Muroyama, H., Matsui, t., Eguchi, K., 2012, *Journal of Power Sources*, vol.208, pp.257-262.

[62]. Botte, G.G., Vitse, F., Cooper, M. 2004, "Carbon fiber-electrocatalysts for the Oxidation of Ammonia, Ethanol and Coal and their Application to Hydrogen Production, Fuel Cells and Purification Processes", Pending Patent.

[63]. Gerardine G., Botte and Carl A. Feickert. 2012, "Electro Decomposition of Ammonia into Hydrogen for Fuel Cell Use",

[64]. Diaz, L.A., Valenzuela-Muñiz, A., Muthuvel, M., Botte, G.G. 2013, "Analysis of ammonia electro-oxidation kinetics using a rotating disk electrode". *Electrochimica Acta,* vol.89, pp.413-421.

[65]. Zhou, L., Cheng, Y.F. 2008, "Catalytic electrolysis of ammonia on platinum in alkaline solution for hydrogen generation", *International Journal of Hydrogen Energy,* vol. 33, pp.5897-5904.

[66]. Oswin, H.G., Salomon, M., Can. 1963, *J. Chem,* vol.41, pp.1686–1694.

[67]. Katan, T., Galiotto, R.J. 1963, *J. Electrochem. Soc,* vol.110, pp.1022–1023.

[68]. Gerischer, H., Mauerer, A. 1970, *J. Electroanal. Chem,* vol.25, pp. 421–443.

[69]. De Vooys, A.C.A., Koper, M.T.M., van Santen, R.A. J.A.R. van Veen, 2001, *J. Electroanal. Chem,* vol.506, pp.127–137.

[70]. Endo, K., Nakamura, K., Miura, T. 2004, "Pt-Me (Me = Ir, Ru, Ni) binary alloys as an ammonia oxidation anode", *Electrochim. Acta*, vol.49, pp.2503–2509.

[71]. Jisheng, G., Dennis, C.J. 1995, "Electrocatalysis of Anodic Oxygen-Transfer Reactions: Oxidation of Ammonia at Anodized Ag-Pb Eutectic Alloy Electrodes", *Journal of Electrochemical Society,* vol.142, pp. 3420-3423.

[72]. Mikołaj, D., Wojciech, H., Małgorzata, C., Zbigniew, S. 1997, "Electrooxidation of ammonia and simple amines at titanium electrodes modified with a mixture of ruthenium and titanium dioxides", *Electroanalysis,* vol.9, pp.751-754.

[73]. Steven Le Vot, Lionel Roué, Daniel Bélanger. 2013, "Study of the electrochemical oxidation of ammonia on platinum in alkaline solution: Effect of electrodeposition potential on the activity of platinum", *Journal of Electroanalytical Chemistry*, vol.69, pp.18–27.

[74].   Gonzalez-Gonzalez, I., Hernandez-Lebron, Y., Nicolau, E., Cabrera, C.R. 2010, "Ammonia oxidation enhancement at square-wave treated platinum particle modified boron-doped diamond electrodes", *ECS Transactions,* vol.3, pp. 201–209.

[75].   Rosca, V., & Koper, M.T.M. 2006, "Electrocatalytic oxidation of ammonia on Pt (111) and Pt (100) surfaces", *Physical Chemistry Chemical Physics,* vol.8, pp.2513–2524.

[76].   Vidal-Iglesias, F.J., Solla-Gullon, J., Rodriguez, P., Herrero, E., Montiel, V., Feliu, J.M., Aldaz, A. 2004, "Shape-dependent electrocatalysis: ammonia oxidation on platinum nanoparticles with preferential (100) surfaces", *Electrochemistry Communications,* vol.6, pp.1080–1084.

[77].   Vidal-Iglesias, F.J., Solla-Gullon, J., Montiel, V., Feliu, J.M., Aldaz, A. 2005, "Ammonia selective oxidation on Pt (100) sites in an alkaline medium", *Journal of Physical Chemistry,* B 109, pp.12914–12919.

[78].   Vidal-Iglesias, F.J., Solla-Gullon, J., Feliu, J.M., Baltruschat, H., Aldaz, A. 2006, "DEMS study of ammonia oxidation on platinum basal planes", *Journal of Electroanalytical Chemistry,* vol.588, pp.331–338.

[79].   Zeng, Y.F., & Imbihl, R. 2009, "Structure sensitivity of ammonia oxidation over platinum", *Journal of Catalysis,* vol.261, pp.129–136.

[80].   Hai-Long Jiang & Qiang Xu. 2011, "Recent progress in synergistic catalysis over heterometallic nanoparticles", *Journal of Materials Chemistry,* vol.21, pp.13705-13725.

[81].   Carlos F. Zinola., Maria E.Martins., Elena Pastor Tejera., Newton Pimenta Neves Jr. 2012, "Electrocatalysis: Fundamentals and Applications", *International Journal of Electrochemistry,* vol.2012, pp.1-2.

[82].   Bard, A.J., & Faulkner, L.R. 2001, "Electrochemical methods: Fundamentals and Applications", *John Wiley & Sons,* New York

[83].   Knözinger, H., & Kochloefl, K. 2002, "Heterogeneous Catalysis and Solid Catalysts", in Ullmann's Encyclopedia of Industrial Chemistry, 6th (edn), *Wiley-VCH Verlag GmbH & Co KGaA,* Weinheim, Germany, vol.17, pp.5-13.

[84].   Mkhulu K Mathe, Tumaini Mkwizu, Mmalewane Modibedi. 2012, "Electrocatalysis research for fuel cells and hydrogen production", *Energy Procedia,* vol.29, pp. 401 – 408.

[85]. Nguyen Viet Long, Michitaka Ohtaki, Tong Duy Hien, Jalem Randy, Masayuki Nogami. 2011, "A comparative study of Pt and Pt–Pd core–shell nanocatalysts", *Electrochimica Acta,* vol.56, pp.9133– 9143.

[86]. Nguyen Viet Long, Yong Yang, Cao Minh Thi, Nguyen Van Minh, Yanqin Cao, Masayuki Nogami. 2013, "The development of mixture, alloy and core-shell nanocatalysts with nanomaterial supports for energy conversion in low-temperature fuel cells", *Nano Energy,* vol.2, pp.636-676.

[87]. Yao K. and Cheng, Y. F. 2007, Journal of Power Sources, vol.173, pp.96–101.

[88]. Deng, X. H., Wu, Y. T., He, M. F., Dan, C. Y., Chen, Y. J., Deng, Y. D., Jiang D. H., Zhong C. 2011, Acta Chim. Sin., vol.69, pp.1041–1046.

[89]. Cooper, M. & Botte, G. G. *Abstract, 206th Meeting,* The Electrochemical Society, Inc., 2004, p. 517.

[90]. Van Santen R. A. & Niemantsverdriet, J. M. 1995, *Chemical Kinetics and Catalysis,* Plenum, New York, pp. 251.

[91]. Endo, K. Katayama Y., Miura, T. 2004, "Pt-Ir and Pt-Cu binary alloys as the electrocatalyst for ammonia oxidation" *Electrochim. Acta,* Vol.49, pp.1635–1638.

[92]. Markoviˊc, N. M., & Ross Jr, P. N. 2002, *Surf. Sci. Rep.,* vol.45, pp.121–229.

[93]. Jalan, V. and Taylor, E. J. 1983, *J. Electrochem. Soc.,* vol.130, pp.2299–2302.

[94]. Toda, T., Igarashi, H., Uchida H., Watanabe, M. 1999, *J. Electrochem. Soc.,* vol.146, pp.3750–3756.

[95]. L´opez de Mishima, B.A., Lescano, D., Molina Holgado T., Mishima, H. T. 1998, *Electrochim. Acta,* vol. 43, pp.395–404.

[96]. Moran, E., Cattaneo, C., Mishima, H., L´opez de Mishima, B. A., Silvetti, S. P., Rodriguez J. L., Pastor, E. 2008, J. *Solid State Electrochem.,* vol. 12, pp.583–589.

[97]. Bonnin, E. P., Biddinger E. J., Botte, G. G. 2008, J. Power Sources, 182, 284-290.

[98]. Bunce, N. J. & Bejan, D. 2011, *Electrochim. Act*a, vol.56, pp.8085–8093.

[99]. Ge, J., & Johnson, D. C. 1995, *J. Electrochem. Soc.,* vol.142, pp.3420–3423.

[100]. Kim, K. W., Lee, E. H., Kim, J. S., Shin K. H., Kim, K. H. 2001, *Electrochim. Acta,* vol.46, pp.915–921.

[101]. Kim, K. W., Lee, E. H., Kim, J. S., Shin K. H., Jung, B. I. 2002, *J. Electrochem. Soc.,* vol.149, D187–D192.

[102]. Donten, M., Hyk, W., Ciszkowska M., Stojek, Z. 1997, Electroanalysis, vol.9, pp.751–754.

[103]. Kim, K. W., Kim, Y. J., Kim, I. T., Park G. I., Lee, E. H. 2005, *Electrochim. Acta,* vol.50, pp.4356–4364.

[104]. Kim, K. W., Kim, I. T., Park, G. I., Lee, E. H. J. 2006, *Appl. Electrochem.,* vol.36, pp.1415–1426.

[105]. Guo, S., & Wang, E.2011, "Noble metal nanomaterials: controllable synthesis and application in fuel cells and analytical sensors", *Nano Today*, vol.6, pp.240–264.

[106]. Murray, R. 2008, "Nanoelectrochemistry: Metal nanoparticeles, nanoelectrodes and nanopores", *Chemical Review,* vol108, pp.2688–2720.

[107]. Vidal-Iglesias, F. J., Garc´ıa-Ar´aez, N., Montiel, V., Feliu J. M., Aldaz, A. 2003, *Electrochem. Commun,* vol.5, pp..22–26.

[108]. Solla-Gull´on, J., Vidal-Iglesias, F. J., Feliu, J. M. 2011, *Annu. Rep. Prog. Chem., Sect. C,* vol.107, pp.263–297.

[109]. Solla-Gull´on, J., Vidal-Iglesias, F. J., Rodr´ıguez, P., Herrero, E., Feliu, J. M., Clavilier, J., Aldaz, A. 2004, *J. Phys. Chem. B,* vol.108, pp.13573–13575.

[110]. Zhong, C., Hu, W. B., Cheng, Y. F., 2011, *J. Power Sources,* vol.196, pp.8064–8072.

[111]. Liu, J., Zhong, C., Yang, Y., Wu, Y. T., Jiang, A. K., Deng, Y. D., Zhang, Z., Hu, W. B. 2012, *Int. J. Hydrogen Energy,* vol.37, pp.8981–8987.

[112]. Liu, J., Hu, W. B., Zhong C., Cheng, Y. F. 2013, *J. Power Sources,* vol.223, pp.165–174.

[113]. Antolini E. & Perez, J. 2011, *J. Mater. Sci,* vol.46, pp.4435–4457.

[114]. Antolini, E. 2003, *Mater. Chem. Phys,* vol.78, pp.563–573.

[115]. Takasu, Y., Kawaguchi, T., Sugimoto W., Murakami, Y. 2003, *Electrochim. Acta,* vol.48, pp.3861–3868.

[116]. Le Vot, S., Reyter, D., Rou´e L., B´elanger, D. 2012, *J. Electrochem. Soc,* vol.159, F91–F96.

[117]. Ferrando, R., Jellinek, J., Johnston, R. L. 2008, "Nanoalloys: From Theory to Applications of Alloy Clusters and Nanoparticles", *Chemical Reviews,* vol.108, pp.846-910.

[118]. Mu~noz-Flores, B.M., Kharisov, B.I., Jimenez-Perez, V.M., Martínez, P.E., Lopez, S.T. 2011, "Recent Advances in the Synthesis and Main Applications of Metallic Nanoalloys", *Industrial & Engineering Chemistry Research,* vol.50, pp.7705–7721.

145

[119]. Patrice Mélinona, Sylvie Begin-Colin, Jean Luc Duvail, Fabienne Gauffre, Nathalie Herlin Boime, Gilles Ledoux, Jérôme Plain, Peter Reiss, Fabien Silly, Bénédicte Warot-Fonrose. 2014, "Engineered inorganic core/shell nanoparticles", *Physics Reports,* vol.543, pp.163–197.

[120]. Arash Dehghan Banadaki & Amir Kajbafvala. 2014, "Recent Advances in Facile Synthesis of Bimetallic Nanostructures: An Overview", Journal of Nanomaterials, pp.1-28.

[121]. Jin Luo, Lingyan Wang, Derrick Mott, Peter N. Njoki, Yan Lin, Ting He, Zhichuan Xu, Bridgid N. Wanjana, I.-Im S. Lim and Chuan-Jian Zhong. 2008, "Core/Shell Nanoparticles as Electrocatalysts for Fuel Cell Reactions" *Advanced Materials,* vol.20, pp. 4342–4347.

[122]. Johnston, R.L. 2012, "Metal Nanoparticles and Nanoalloys", *Frontiers of Nanoscience*, vol.3, pp.1-42.

[123]. Bonnemann, H., Richards, R. M. 2001, "Nanoscopic Metal Particles Synthetic Methods and Potential Applications", *Eur. J. Inorg. Chem. pp.*2455–2480.

[124]. Bilecka, I., & Niederberger, M. 2010, *Nanoscale,* vol.2, pp.1358–1374.

[125]. Chen, W., Zhao, J., Lee, J. Y., Liu, Z. 2005, "Microwave heated polyol synthesis of carbon nanotubes supported Pt nanoparticles for methanol Electrooxidation". *Mater. Chem. Phys,* vol.91, pp.124–129.

[126]. Doudna, C.M., Bertino, M.F., Tokuhiro, A.T. 2002, "Structural investigation of Ag-Pd clusters synthesized with the radiolysis method", *Langmuir,* vol.18, pp. 2434–2435.

[127]. Mattei, G.C, Maurizio, P., Mazzoldi, F., D'Acapito, G., Battaglin, E., Cattaruzza, C., de Julián Fernández, C., Sada, C. 2005, "Dynamics of compositional evolution of Pd-Cu alloy nanoclusters upon heating in selected atmospheres", *Physical Review B,* vol.71, pp.195418.

[128]. Thakkar, K.N., Mhatre, S.S., Parikh, R.Y. 2010, "Biological synthesis of metallic nanoparticles", *Nanomedicine: Nanotechnology, Biology and Medicine,* vol.6, pp.257–262.

[129]. Kevin Deplanche, Mohamed L. Merroun,, Merixtell Casadesus, Dung T. Tran, Iryna P. Mikheenko, James A. Bennett, Ju Zhu, Ian P. Jones, Gary A. Attard, J. Wood, Sonja Selenska-Pobell, Lynne E. Macaskie. 2012, "Microbial synthesis of

core/shell gold/palladium nanoparticles for applications in green chemistry", *Journal of the Royal Society Interface,* vol.9, pp. 1705–1712.

[130]. Mabbett, A.N., Sanyahumbi, D., Yong, P. Macaskie, L.E. 2006, "Biorecovered precious metals from industrial wastes: single-step conversion of a mixed metal liquid waste to inorganic catalysts with environmental application", *Environ. Sci. Technol,* vol.40, pp.1015–1021.

[131]. Nair, B., Pradeep, T. 2002, "Coalescence of nanoclusters and formation of submicron crystallites assisted by Lactobacillus strains", *Cryst Growth Des,* vol.2, pp.293-8.

[132]. Sweeney, RY., Mao, C., Gao, X., Burt, JL., Belcher, AM., Georgiou, G., et al. 2004, "Bacterial biosynthesis of cadmium sulfide nanocrystals", *Chem Biol,* vol.11, pp.1553-9.

[133]. Rao, C. N. R., Ramakrishna Matte, H. S. S., Rakesh Voggu, Govindaraj, A. 2012, "Recent progress in the synthesis of inorganic nanoparticles", Dalton Transactions, vol.41, pp.5089-5120.

[134]. M. Niederberger, 2007, *Acc. Chem. Res,* vol.40, pp.793–800.

[135]. Liu, Y. C., Chen, Y. W. 2006, "Hydrogenation of p-Chloronitrobenzene on Lanthanum-Promoted NiB Nanometal Catalysts", *Ind. Eng. Chem. Res,* vol.45, pp.2973–2980.

[136]. Aradi, A.A.; Esche, C.K., Jr., McIntosh, K., Jao, T.-C. 2008, "Nanoalloy fuel additives", *Eur. Patent Application EP 1889895*, vol. 23 pp.

[137]. Luo, X., Morrin, A., Killard, A.J., Smyth, M.R. 2006, "Application of Nanoparticles in Electrochemical Sensors and Biosensors", *Electroanalysis,* vol.18, pp.319-326.

[138]. Tominaga, M., Shimazoe, T., Nagashima, M., Taniguchi, I. 2008, "Composition–activity relationships of carbon electrode-supported bimetallic gold–silver nanoparticles in electrocatalytic oxidation of glucose", *Journal of Electroanalytical Chemistry*, vol. 615, pp.51-61.

[139]. Liu, T., Zhong, J., Gan, X., Fan, C., Li, G., Matsuda, N. 2003, "Wiring Electrons of Cytochrome c with Silver Nanoparticles in Layered Films", *ChemPhysChem*, vol. 4, pp.1364-1366.

[140]. Johnston, R.L., Ferrando, R. 2008, "Nanoalloys: from theory to application. Faraday Discuss Faraday Discuss" vol.138, pp.1-442.

147

[141]. Alivisatos, P. 2004, "The use of nanocrystals in biological detection", *Nature Biotechnology*, vol.22, pp.47-52.

[142]. Cao, Y. W., Jin, R. C., Mirkin, C. A. 2001, *J. Am. Chem. Soc,* vol.123, pp.7961.

[143]. Mailu Stephen, 2013, "Electrochemical responses of novel preferentially oriented platinum (100) nanoalloys for ammonia and hydrazine catalysis", Ph.D thesis, Department of Chemistry, University of Western Cape.

[144]. Xu, C., Wang, R., Chen, M., Zhang, Y., Ding, Y. 2010, "Dealloying to nanoporous Au/Pt alloys and their structure sensitive electrocatalytic properties", *Physical Chemistry Chemical Physics*, vol.12, pp.239-246.

[145]. Manlan, T., Zaisheng, W., Meng, W., Mei, H., Yunhui, Y. 2011, "The preparation of label-free electrochemical immunosensor based on the Pt–Au alloy nanotube array for detection of human chorionic gonadotrophin", *Clinica Chimica Acta*, vol.412, pp.550–555.

[146]. Prof Ashok K Ganguli 2014, "Nano structured Materials-Synthesis, Properties, Self Assembly and Applications" (video file). Available from: <https://m.youtube.com/watch?v=k50nf5VonDw>. [4 November 2015].

[147]. Luigi Carbone, & P. Davide Cozzoli. 2010, "Colloidal heterostructured nanocrystals: Synthesis and growth mechanisms", *Nano Today,* vol. 5, pp.449-493.

[148]. Zhang, J., Tang, Y., Weng, L., Ouyang, M. 2009, *Nano Lett,* vol.9, pp.4061.

[149]. Guerrero-Martínez, A., Pérez-Juste, J., Liz-Marzán, L.M. 2010, Adv. Mater. Vol.22, pp.1182.

[150]. Pastoriza-Santos, I., Pérez-Juste, J., Liz-Marzán, L.M. 2006, *Chem. Mater,* vol.18, pp.2465.

[151]. Liz-Marzán, L.M., Langmuir 2006, vol.22.

[152]. Burns, A., Ow, H., Wiesner, U. 2006, "Fluorescent core-shell silica nanoparticles towards", *Chemical Society Reviews*, vol.35, pp. 1028-1042.

[153]. Tracy, J.B., Weiss, D.N., Dinega, D.P., Bawendi, M.G. 2005, *Phys. Rev. B,* vol.72, 064404.

[154]. Sheng Peng, S.S. 2007, *Angew. Chem. Int. Ed,* vol.46, pp.4155.

[155]. Casavola, M., Buonsanti, R., Caputo, G., Cozzoli. P. D. 2008, "Colloidal Strategies for Preparing Oxide-Based Hybrid Nanocrystals", *Eur. J. Inorg. Chem.* pp. 837–854.

[156]. An, K., Hyeon, T. 2009, *Nano Today*, vol.4, pp. 359.

[157]. Wilcoxon, J. P., Abrams B. L. 2006, "Synthesis, structure and properties of metal nanoclusters", *Chem. Soc. Rev.,* vol.35, pp.1162–1194.

[158]. Cookson, N.J. "Preparation and Characterisation of Bimetallic Core-Shell Particles". Master Thesis, University of Birmingham, Birmingham, UK, September 2009.

[159]. Yu, Y.-T., & Dutta, P. 2011, "Synthesis of Au/SnO2 core–shell structure nanoparticles by a microwave-assisted method and their optical properties", *J. Solid State,* vol.184, pp.312–316.

[160]. Li, C., & Yamauchi, Y. 2013, "Facile solution synthesis of Ag@Pt core-shell nanoparticles with dendritic Pt shells", *Phys. Chem. Chem. Phys,* vol.15, pp.3490–3496.

[161]. Creighton, J.A., & Eadon, D.G. 1991, "Ultraviolet Visible Absorption-Spectra of the Colloidal Metallic Elements", J. *Chem. Soc,* vol.87, pp.3881–3891.

[162]. Westsson, E., & Koper, Ger J.M. 2014, "How to Determine the Core-Shell Nature in Bimetallic Catalyst Particles?", *Catalysts,* vol.4, pp.375-396.

[163]. Toshima, N., & Yonezawa, T. 1998, "Bimetallic nanoparticles-novel materials for chemical and physical applications", *New Journal of Chemistry,* vol.22, pp.1179-1201.

[164]. Briggs, D. & Seah, M.P. 1990, 'Practical Surface Analysis. Auger and X-ray Photoelectron Spectroscopy', 2nd edn, vol.1, *John Wiley and Sons,* Chichester

[165]. Watts, J.F. 1990, 'An Introduction to Surface Analysis by Electron Spectroscopy', *Oxford University Press,* Oxford

[166]. Thompson, M., Baker, M.D., Christie, A., Tyson, J.F. 1985, 'Auger Electron Spectroscopy', *John Wiley and Sons,* New York

[167]. Childs, K.D., Carlson, B.A., LaVanier, L.A., Moulder, J.F., Paul, D.F., Stickle, W.F., Watson, D.G.1995, 'Handbook of Auger Electron Spectroscopy', 3rd edn, *C.L. Hedberg, Physical Electronics,* USA

[168]. Watts, J.F., & John Wolstenholme. 2003, 'An introduction to surface analysis by XPS and AES', *John Wiley and Sons,* England

[169]. Tadano, S. & Giri, B. 2011, "X-ray diffraction as a promising tool to characterize bone nanocomposites", *Science and Technology of Advanced Materials,* vol.12, pp.11.

149

[170]. Moram, M.A. & Vickers, M.E. 2009, "X-ray diffraction of III-nitrides", *Reports on Progress in Physics,* vol.72, pp.40.

[171]. Monshi, A., Foroughi, M.R., Monshi, M.R. 2012, "Modified Scherrer Equation to Estimate More Accurately Nano-Crystallite Size Using XRD", *World Journal of Nano Science and Engineering,* vol.2, pp.154-160.

[172]. Dr Cummings F. 2014, Overview of Electron Microscopy, lecture notes distributed in Foundation of Nanophysics NSS 833 at the University of the Western Cape, Bellville, November 2015.

[173]. Barcari, G. 2012, 'Metal. Nanoparticles and Nanoalloys', Wilcoxon, J., Johnston, R.L. (eds) Elsevier: Amsterdam, the Netherland, pp. 213–247.

[174]. Buhr, E., Senftleben, N., Klein, T., Bergmann, D., Gnieser, D., Frase, C.G. 2009, "Characterization of nanoparticles by scanning electron microscopy in transmission mode", Measurements Science and Technology, vol.20, pp.1-9.

[175]. Wang, J. 2000, 'Analytical Electrochemistry', 2nd edn, New York, NY 10158-0012, *John Wiley and Sons,* Inc. 31-32.USA

[176]. Kisssinger, P.T., & Heineman, W.R. 1984, 'Laboratory Techniques in Electroanalytical Chemistry', *Marcel Dekker,* New York

[177]. Bard, A.J., & Faulkner, L.R. 1980, 'Electrochemical Methods', *John Wiley and Sons,* New York

[178]. Pletcher, D. 2001, 'Instrumental Methods in Electrochemistry'; *Horwood Publishing: Cambridge,* UK

[179]. Douman Samantha, 2013, "The Response Dynamics of Indium Telluride Quantum Dots Impedimetric Genosensor for Telomerase Cancer Biomarker", MSc thesis, Department of Chemistry, University of Western Cape.

[180]. Zanello, P. 2003, "Inorganic electrochemistry-theory, practice and application", *Royal Society of Chemistry,* pp.7-155.

[181]. Osteryoung, J. & O'Dea, J.J. 1986, 'Electroanalytical Chemistry', vol.14, pp.212, Bard, A.J., (ed), *Marcel Dekker,* New York

[182]. Scott, F., Sweeney, Woehrle, G.H., Hutchison, J.E. 2006, "Rapid purification and size separation of gold nanoparticles via diafiltration", J. AM. CHEM. SOC, vol.128, pp. 3190-3197.

[183]. Abedini, A., Saion, E., Larki, F., Zakaria, A., Noroozi, M., Soltani, N. 2012, "Room Temperature Radiolytic Synthesized $Cu@CuAlO_2$-Al_2O_3 Nanoparticles", *International Jounal of Molecular Science,* vol.13, pp.11941-11953.

[184]. Kamari, H.M., Naseri, M.G., Saion, E.B. 2014, "A Novel Research on Behavior of Zinc Ferrite Nanoparticles in Different Concentration of Poly(vinyl pyrrolidone) (PVP)" *Metals,* vol.4, pp.118-129.

[185]. Wang, H., Qiao, X., Chena, J., Wang, X., Ding, S. 2005, "Mechanisms of PVP in the preparation of silver nanoparticles", *Materials Chemistry and Physics,* vol.94, pp.449–453.

[186]. Ledeuil, J. B., Uhart, A., Soul´e, S., Allouche, J., Dupin, J. C., Martinez, H. 2014, "New insights into micro/nanoscale combined probes (nanoAuger, µXPS) to characterize Ag/Au@SiO_2 core–shell assemblies", *Nanoscale,* vol.6, pp. 11130-11140.

[187]. Nessrin Kattan, N., David, B.H., Fermín, J., David Cherns, D. 2015, "Crystal structure and defects visualization of Cu_2ZnSnS_4 nanoparticles employing transmission electron microscopy and electron diffraction", *Applied Materials Today,* vol.1, pp.52–59.

[188]. Bradley J.S., Schmid, G., Talapin, D.V., Shevchenko E.V., Weller, H. 2005, "Syntheses and Characterizations: 3.2 Synthesis of Metal Nanoparticles", in Nanoparticles: From Theory to Application, Edited by Günter Schmid, pp.185-238. John Wiley and Sons, ISBN: 9783527602391 Available online from: Wiley Online Library [10 January 2015].

[189]. Othman, M.R., Riyanto, 2012, "Electrochemical Stability of Cu, Ni, Co, Pt and Ir Metals Sheet and Their Composite Electrodes in Potassium Hydroxide Solution", *International Journal of Electrochemical Science,* vol.7, pp.8408-8419.

[190]. Daubinger, P., Kieninger, J., Unmussig, T., Urban, G. A. 2014, "Electrochemical characteristics of nanostructured platinum electrodes – a cyclic voltammetry study", *Phys.Chem.Chem.Phys,* vol.16, pp.8392-8399.

[191]. Allagui, A., Oudah, M., Tuaev, X., Ntais, S., Almomani, F., Baranova, E.A. 2013, "Ammonia electro-oxidation on alloyed PtIr nanoparticles of well-defined size", *International Journal of Hydrogen Energy,* vol.38, pp.2455-2463.

[192]. Haijiang, Z., Jianshe, H., Haoqing, H., Tianyan, Y. 2009, "Electrochemical Detection of Hydrazine Based on Electrospun Palladium Nanoparticle/Carbon Nanofibers", *Electroanalysis,* vol., pp.1869–1874.